Master Thesis

Multichannel Ultra-Wideband Systems with Noncoherent Autocorrelation Detection

Paul Meissner, Bakk. techn.

Signal Processing and Speech Communication Laboratory
Graz University of Technology
Head: Univ.-Prof. DI Dr. techn. Gernot Kubin

Supervisor: DI Dr. Univ.-Doz. Klaus Witrisal

Graz, April 2009

Abstract

This thesis provides an in-depth analysis of a previously introduced noncoherent ultra-wideband (UWB) receiver that uses a parallel autocorrelation frontend to separate a transmitted multichannel signal. The frontend calculates samples of the autocorrelation function of the received signal. Despite this nonlinear operation, a linear multiple-input multiple-output (MIMO) model can be found for the relation between the transmitted data symbols and the receiver outputs. According to the MIMO model, the subchannel data can be separated using well-known combiner structures.

The nonlinear receiver frontend causes crossterms among the subchannel signals and the noise. It is shown that the MIMO model only holds if certain conditions for the mutual crosscorrelation of the subchannel signals are met. Violating this condition leads to a considerable number of performance-degrading crossterms. This thesis focuses on an analysis of the influence of these terms as well as on the introduction of several measures for the general invertibility of the problem. Simulation results for the performance of the originally proposed orthogonal frequency-division multiplexing (OFDM) transmission scheme are provided, which show that the impact of the nonlinear crossterms on the receiver performance is negligible. Another issue is the influence of the linear multipath channel on the subchannel signals' orthogonality, which is shown to be benign.

Furthermore, alternative signaling schemes are introduced. To exploit the increased fading resistance of higher bandwidth signals, these signaling schemes use signal waveforms where each subchannel uses the full signal bandwidth. This implies that the subchannel orthogonality can not be provided by frequency separation as in the OFDM scheme. The investigated schemes include Discrete Prolate Spheroidal Sequences, an orthogonal pulse amplitude modulation (OPAM) scheme based on code-division multiple access (CDMA) spreading codes, shift-added noise waveforms and signals obtained by genetic optimization. Their performance is analyzed and compared with the original OFDM scheme. It is shown that the OFDM scheme is the favourable signaling scheme concerning performance and robustness with respect to the transmission over the multipath channel for the proposed multichannel receiver.

Kurzfassung

Diese Masterarbeit beschäftigt sich mit einer detaillierten Analyse eines zuvor vorgestellten nicht-kohärenten Ultra-Breitband Empfängers. Dieser Empfänger verwendet ein paralleles Autokorrelations-Frontend um ein mehrkanaliges Signal zu trennen. Das Frontend berechnet diskrete Werte der Autokorrelationsfunktion des empfangenen Signals. Trotz dieser nichtlinearen Operation kann ein lineares *multiple-input multiple-output* (MIMO) Modell für den Zusammenhang zwischen übertragenen Datensymbolen und den Ausgangswerten des Empfänger-Frontends formuliert werden. Aufgrund dieses MIMO Modells können die Datensignale mit bekannten Verarbeitungsverfahren getrennt werden.

Die nichtlinearen Verarbeitungsschritte des Frontends haben Kreuzterme zwischen Daten- und Rauschsignalen zur Folge. Es wird gezeigt, dass das MIMO Modell nur dann gültig ist, wenn spezielle Bedingungen betreffend der Korrelationseigenschaften der Subträger-Signale erfüllt sind. Eine Verletzung dieser Bedingungen hat eine große Anzahl von Kreuztermen zur Folge, welche die Bitfehlerrate des Empfängers stark beeinträchtigen. Eine Diskussion der Bedingungen, unter welchen dieses Modell gültig ist, ist ebenso Gegenstand dieser Arbeit, wie generelle Maße für die Invertierbarkeit des Problems. Es werden Simulationsergebnisse für das ursprünglich vorgestellte OFDM Übertragungsverfahren präsentiert, welche zeigen, dass der Einfluss der Kreuzterme zwischen den Kanälen auf die Bitfehlerrate des Empfängers für dieses Verfahren vernachlässigbar ist. Der Einfluss des linearen Mehrwegekanals auf die Orthogonalität der Subträger-Signale ist ebenfalls Gegenstand der Untersuchungen. Dieser Einfluss ist vorhanden, aber gering.

Ein weiterer Teil der Arbeit beschäftigt sich mit der Suche nach alternativen Signalschemas. Bei diesen soll jeder Kanal die volle Signalbandbreite verwenden. Die Motivation hierfür ist eine bessere Auflösbarkeit der Kanalimpulsantwort bei breitbandigen Signalen. Die Überlagerung aller Kanäle im selben Frequenzbereich erschwert jedoch den Entwurf von Signalen, welche Kreuzterme unter den Kanälen vermeiden. Vorgestellt werden Signalschemas auf der Basis von discrete prolate spheroidal sequences, ein OPAM Schema mit binären CDMA Spreizcodes, verschobene und addierte Rauschsequenzen sowie Sequenzen welche auf genetischer Optimierung basieren. Es wird gezeigt, dass das OFDM Verfahren für diesen Empfänger die beste Bitfehlerrate sowie auch die beste Robustheit gegenüber dem Mehrwege-Kanal bietet.

STATUTORY DECLARATION

I declare that I have authored this thesis independently, that I have not used other than the declared sources / resources, and that I have explicitly marked all material which has been quoted either literally or by content from the used sources.

.....	.....
Date	Paul Meissner, Bakk. techn.

Danksagung

Diese Masterarbeit wurde von Juli 2008 bis April 2009 am Institut für Signalverarbeitung und Sprachkommunikation an der Technischen Universität Graz durchgeführt.

Zuerst möchte ich meinem Betreuer Klaus Witrisal danken. Einerseits für die Möglichkeit an einem hochinteressanten Thema arbeiten zu können und andererseits für die außergewöhnliche Betreuung, ohne welche diese Arbeit wohl noch nicht abgeschlossen wäre. Ebenso möchte ich mich für die Möglichkeit, als Studienassistent Erfahrungen sammeln zu können, bedanken.

Mein großer persönlicher Dank geht an meine Eltern, die mir eine sorgenfreie und schöne Studienzeit ermöglicht haben.

Das schönste an dieser Zeit war, dass ich meine Freundin Silvia kennengelernt habe. Ihr gehört der größte Dank, weil sie mich auch während dieser Diplomarbeit ausgehalten hat. Aber eigentlich hauptsächlich deswegen, weil sie einfach so ist, wie sie ist.

Graz, im April 2009 Paul Meissner

Inside the museums, infinity goes up on trial
Voices echo this is what salvation must be like after a while

Bob Dylan, "*Visions of Johanna*"

He probably performed some indoor non line-of-sight channel measurements at an ultra-wide bandwidth before writing that.

Notation and list of symbols

Notation used in this thesis

$\mathbf{A}$	Matrix A (uppercase and boldfaced)
$(N \times L)$	Matrix dimensions, N rows and L columns
$A_{i,j}$	The element in the i-th row and j-th column of the matrix $\mathbf{A}$
$\mathbf{A}^T$	Transpose of the matrix $\mathbf{A}$
$\mathbf{A}^*$	Hermitian transpose of the matrix $\mathbf{A}$
$\mathbf{A}^\dagger$	Pseudoinverse of the matrix $\mathbf{A}$
$\mathbf{a}$	Column vector $\mathbf{a}$ (lowercase and boldfaced)
a	Scalar a
$x(t)$	Continuous-time signal $x(t)$
$x[m]$	Discrete-time sequence $x[m]$
$\langle x(t); y(t) \rangle$	Inner product of the functions $x(t)$ and $y(t)$
$\Phi_{xy}[d]$	Crosscorrelation function of two discrete-time sequences $x[m]$ and $y[m]$ at delay lag d
$\Phi_{xy}(\tau)$	Crosscorrelation function of two continuous-time signals $x(t)$ and $y(t)$ at delay lag τ
$\tilde{\Phi}_{xy}[d]$	Periodic crosscorrelation function of two discrete-time sequences $x[m]$ and $y[m]$ at delay lag d
$*$	Convolution operator

Symbols used in this thesis

N	Number of transmit signal subchannels
L	Number of receiver autocorrelation channels
D_l	One specific receiver delay lag
$\{D_l\}$	Set of receiver delay lags
T_I	Receiver integration interval
$\mathbf{H}$	MIMO channel matrix
$\mathbf{G}$	Matrix of crosscorrelation-induces crossterms
$\mathbf{W}$	Receiver combiner matrix
$\mathbf{s}$	$(N \times 1)$ vector of transmitted data bits
$\mathbf{y}$	$(L \times 1)$ vector of receiver frontend outputs
$\mathbf{z}$	$(N \times 1)$ vector of receiver decision variables
$f_{tx}(t)$	Impulse response of transmitter pulse-shaping filter
$f_{rx}(t)$	Impulse response of receiver frontend filter
$\mathbf{y_{ss}}$	Vector of the signal-by-signal crossterms of frontend outputs
$\mathbf{y_{ss}}[i]$	Vector of the signal-by-signal crossterms of frontend outputs for the i-th symbol
$y_{ss,D_l}[i]$	Value of the output of the l-th receiver frontend channel considering the signal-by-signal crossterms and the i-th symbol

Contents

1 Introduction

1.1 Motivation

Ultra-wideband (UWB) systems promise to be a cost-effective solution for fields like communications and positioning. This has, for example, led to the release of an alternative physical layer in the IEEE 802.15.4a standard [IEE07] which also allows for non-coherent receivers. These receivers are motivated by their much lower complexity in comparison with coherent architectures. It has to be mentioned that this is accompanied by a performance loss. Nevertheless, their simplicity could make non-coherent UWB receivers the most promising candidate technology for applications like sensor networks or wireless personal area networks (WPAN) where low power and low cost are desirable.

Non-coherent receivers are used to significantly reduce complexity. They can, for example, use an autocorrelation scheme together with a transmitted reference signal to be able to skip the step of an explicit channel estimation [HT02]. This thesis analyses an analog autocorrelation receiver frontend in combination with multichannel signaling and linear combining in the digital receiver backend. One interesting fact it that this receiver does *not* use a transmitted reference signal. This allows for more efficient transmission of the data signal because no signal energy is needed for the reference component.

The use of multichannel signaling opens the possibility for increasing the data rate. There are several signal processing tasks concerning this multichannel signal transmission that are needed to obtain a transmission scheme that is robust with respect to the UWB propagation channel. The design and analysis of such schemes are the focus of this thesis.

1.2 Ultra-Wideband Systems

1.2.1 Motivation and Applications

Wireless communication systems are faced with the challenge of *multipath fading*. The received signal is a linear combination of several copies of the transmitted signals, each one having undergone a certain propagation path to the receiver. As a narrowband or conventional wideband receiver is not able to distinguish these individual signal components, they interfere with each other, which leads to amplitude fluctuations due to constructive and destructive interference [Mol06].

UWB systems face a fundamentally different situation because of their huge signal bandwidth. This bandwidth, in the order of several GHz, and which corresponds to impulses whose duration is in the order of (or below) a nanosecond, allows for the resolution of individual multipath components. Hence the fading effects mentioned above can be largely avoided by coherently adding up each multipath signal copy, which assumes that the receiver knows the phase and amplitude of each component.

One fundamental problem is the allocation of bandwidth, which is a resource that has become increasingly scarce and expensive. Regulatory institutions in different regions have provided UWB with different frequency ranges. In the USA, for example, the FCC [FCC02] has allocated the band from 3.1 GHz to 10.6 GHz to UWB communication systems. In this range of frequencies the average equivalent isotropically radiated power (EIRP) (in the sense of a power spectral density) is limited to -41.3 dBm/MHz which implies that UWB systems overlay existing systems that operate on these frequencies. These limitations restrict the application of UWB to short range usages like indoor positioning, cable replacement, sensor networks or others [Gia03]. It should be noted here that the regulatory situations differ around the world [HW06]. The bandwidth available in the USA is a large contiguous block but this is not the case when combining this block with frequency bands released in other countries. An UWB device that should be usable in different geographical areas has to cope with this and must only use the common bandwidth available in all those areas.

1.2.2 Transceiver Structures

When designing an UWB system, one major task is to define the signaling scheme. Generally there are two popular possibilities for achieving an ultra-wide bandwidth: The first one is to divide the bandwidth in several sub-bands and design a multicarrier system as done in Orthogonal Frequency Division Multiplexing (OFDM) [BBA$^+$04]. The other possibility is to use baseband pulses of ultra-short duration (usually in the order of a nanosecond) that directly use the bandwidth available as done in so-called *Impulse Radio* (IR) schemes [WS98]. Signaling methods representing both of these schemes will be considered in this thesis.

An example for a part of a received signal in an IR scheme can be seen in Figure 1.1. The time extent of the transmitted pulse (T_w) is short with respect to the symbol period T_{sym}. The received pulse, however, can easily extend over several tens of nanoseconds as indicated, determined by the maximum excess delay T_{max} of the UWB radio channel. There are two reasons for choosing a T_w which is much shorter than T_{sym}: First, this can be seen as a zero guard interval protecting subsequent symbols from intersymbol interference (ISI). Secondly, it follows from the regulatory restrictions mentioned above regarding the average power spectral density that the pulse repetition frequency has to be kept low (in the order of several MHz) [HW06].

Due to conceptually easy concepts like IR, the transmitter implementation is generally not considered to be the difficult part of an UWB system design. Designing and implementing a coherent UWB receiver, however, is a challenging task. Due to the fine delay resolution, hundreds of multipath components can be present at the receiver [Mol05]. To achieve a coherent combination of these components it is necessary to determine their amplitude and phase. Receivers that perform this task in order to collect energy from each multipath component are called *rake* receivers [PS08] and will soon become prohibitively complex with increasing bandwidth [Pau07]. Another issue concerning these systems is that the sampling rate required is in the order of several GHz, due to the large signal bandwidth. This might lead to a power consumption that is too high for practical systems.

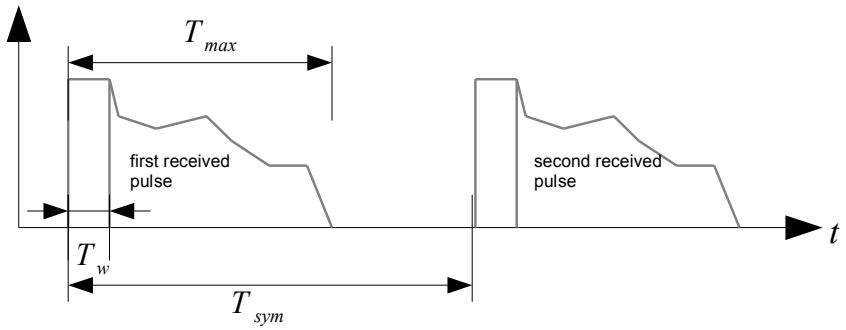

Figure 1.1: Example for impulse radio signaling over the multipath radio channel

1.2.3 Reduction of Complexity - Noncoherent Receivers

From the previous discussion it should be clear that there is a need to reduce the receiver complexity. In essence, if the very high sampling rate was reduced and the step of estimating the amplitude, phase and shape of each multipath component was skipped, one could design a low cost and potentially low power receiver. Taking the latter simplification into account leads us to the common definition of a *noncoherent* receiver which is not able to access the absolute phase information of the received signal [Wit08b]. Instead, it measures the envelope or instantaneous power of the received signal.

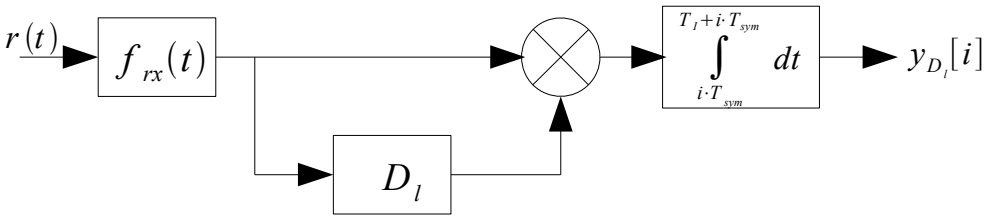

Figure 1.2: Basic scheme of an autocorrelation receiver

One example of a noncoherent receiver is the *autocorrelation receiver* (AcR). Its basic structure is shown in Figure 1.2. The received signal $r(t)$ is filtered by a frontend filter $f_{rx}(t)$ and multiplied with a copy of itself that is delayed in time by D_l seconds. The energy that is obtained in this way is then integrated over a duration of T_I seconds, yielding one output sample $y_{Dl}[i]$ of the AcR, where i denotes the symbol index. It can be seen here that subsequent samples $y_{Dl}[i]$ are delivered at the symbol rate. Thus this receiver frontend effectively despreads the UWB signal and avoids a high sampling rate.

This scheme is often used in conjunction with *transmitted reference* (TR) signaling, where D_l is chosen such that an (unmodulated) reference pulse is aligned in time with the modulated pulse. This is done to avoid the process of channel estimation mentioned

above. The spacing of these two pulses should be no longer than the channel coherence time so that they are both subject to the same propagation conditions. In Figure 1.1, the reference pulse would be the first received pulse and the modulated pulse the second. It should be mentioned here that there are also differential TR schemes in which one modulated pulse serves as a reference for the other [Pau07].

The receiver structure that is analyzed in this thesis will not use the TR concept, though it will use the autocorrelation architecture. Multiple parallel channels of the architecture shown in Figure 1.2 are used, yielding samples of the received pulse autocorrelation function that are further processed by a digital backend. Some of the schemes in Chapter 4 could be interpreted as TR schemes though not in the conventional way. In the context of Figure 1.1, they carry their reference *within* one pulse duration T_w, as will be explained in detail.

1.3 Objective of this Thesis

A noncoherent multichannel UWB receiver was designed in previous work at the institute [Wit08c], [Wit08a]. This receiver works with an OFDM signaling scheme. Due to the nonlinear nature of the autocorrelation operation applied in the receiver frontend, crossterms between the multichannel signals appear. The structure of these terms impose restrictions on the signaling schemes and signal waveforms that can be used with this receiver. An in-depth analysis of the impact of the nonlinear crossterms and the restrictions mentioned is one objective of this thesis.

Furthermore, alternative signaling schemes are investigated where each subchannel uses the full UWB bandwidth of the transmit signal. These signals should provide better fading resistance due to their increased bandwidth. The performance of these alternative schemes should be analyzed in comparison with the OFDM scheme.

The analysis of the receiver was carried out both analytically and by computer simulations.

1.4 Outline

This thesis is organized as follows:

Chapter 2 gives an overview of the multichannel noncoherent receiver that is analyzed in this thesis. It provides a detailed description of the analog receiver frontend and the signaling scheme that is used. The problem of recovering the transmitted data symbols from the received signal samples is formulated as a linear problem. To this end a linear MIMO signal model is introduced and the conditions under which it holds are given. Solving or inverting the linear problem requires the use of backend signal processing schemes that operate on the outputs of the receiver frontend. The backend schemes used in this thesis are also explained in this chapter. A further topic is the choice of several of the system parameters which is discussed here.

It should be made clear that this chapter is heavily based on the work in [Wit08c] and [Wit08a] and constitutes a major part of this thesis in order to make it as self-

explanatory as possible by reviewing the proposed receiver structure and establishing the notation needed for the subsequent chapters.

Chapter 3 deals with the analysis of the OFDM transmission scheme. Performance simulation results for various system parameter settings are provided. These results are analyzed in detail to gain insight in the nonlinear receiver operation. The received signal is decomposed into all its components to define performance measures for the signaling schemes additional to the conventional bit error rate (BER) simulations. These measures include:

- General measures for the problem invertibility.
- Measures for the subchannel signal orthogonality and the channel influence on this orthogonality.
- A signal to Interference Ratio (SIR) for the receiver frontend channels as well as for the decision variables.

Results for these measures are provided with the simulations.

Chapter 4 analyzes the alternative signaling schemes that were found for this receiver structure. It provides the necessary conditions for signals that can be used with the proposed receiver structure. A survey of the elementary bounds for these signal properties is presented. The main part of this chapter introduces and discusses several examples for sub-optimal schemes. It deals with the application of the following pulse waveforms to the signaling scheme:

- Discrete Prolate Spheroidal Sequences
- Orthogonal pulse amplitude modulation using binary codes which carry the information
- Shift-added noise sequences which carry the information directly in their autocorrelation function, and
- Sequences obtained by genetic optimization techniques to optimize the correlation properties of the sequences.

The analysis is carried out in a similar way to the OFDM scheme to provide comparability. It is shown that the problem of designing signals for this receiver is not trivial, at least not for signals that can be synthesized easily in practice. However, the alternative signaling schemes provide additional insight into the operation of the proposed receiver structure.

Chapter 5 finally draws conclusions and provides an outlook to possible future work on this topic.

The appendix is used for the presentation and discussion of additional simulation results. While the main results of these simulations are discussed in the corresponding sections, several images and further notes on them are given here to clarify and support the results in the main text.

2 Noncoherent Autocorrelation Detection of Multichannel UWB Signals

2.1 Motivation

In [Wit08c] and [Wit08a] a noncoherent autocorrelation receiver (AcR) for multicarrier signals is proposed. This receiver has multiple channels, their number is denoted by L, each one at a specific delay lag D_l, which yields an estimate for the sampled received pulse autocorrelation function. Orthogonal frequency-division multiplexing (OFDM) is proposed as the signaling scheme. It is shown that the multichannel AcR is able to estimate (samples of) the power spectral density of the received signal and thus it can detect the energy of the subcarrier signals.

This scheme has several advantages compared with other UWB receiver structures:

- The received UWB signal, having a bandwidth in the order of several GHz, is despread into multiple (L) samples per symbol. Thus a potentially prohibitively high sampling rate is avoided. This is an advantage, of course, over coherent receivers and is shared by other noncoherent autocorrelation and energy detection receivers.

- The data rate is increased proportionally to the number of subcarriers. This of course also applies to other multichannel transmission schemes. The possible simplicity of operations that separate the data in the receiver backend is specific to the system proposed here. The following chapters will discuss the data rates achievable and the possible number of subcarriers.

- In comparison with other noncoherent multichannel receiver architectures (as in [PAU04], for example) the design avoids selective frontend bandpass filters for each subcarrier signal. Only one general frontend filter is used which is designed for the overall signal spectrum. The separation of the channels is achieved by the digital backend processing that operates on the values obtained by the analog frontend architecture, as it will be shown in this section.

- Regarding the OFDM signaling scheme, it will be shown that the digital backend can consist of a simple predefined DFT matrix. Thus a simple post-processing that does not require channel state information is possible.

- In [AW07] it has been shown that this receiver frontend can be used to mitigate narrowband interference that impairs the UWB signal. This aspect is not further discussed in this thesis.

In [Wit08a] this receiver frontend was also successfully applied for the demodulation of the burst position modulated bit in the IEEE 802.15.4a UWB physical layer.

2.2 System Overview and Modeling

Figure 2.1 shows the general design of the multichannel AcR operating at L delay lags. The received signal is filtered by a frontend filter $f_{rx}(t)$ and then multiplied by delayed versions of itself. These products are then integrated over a fixed integration time T_I, reduced by the corresponding channel delay lag D_l [Wit08c].

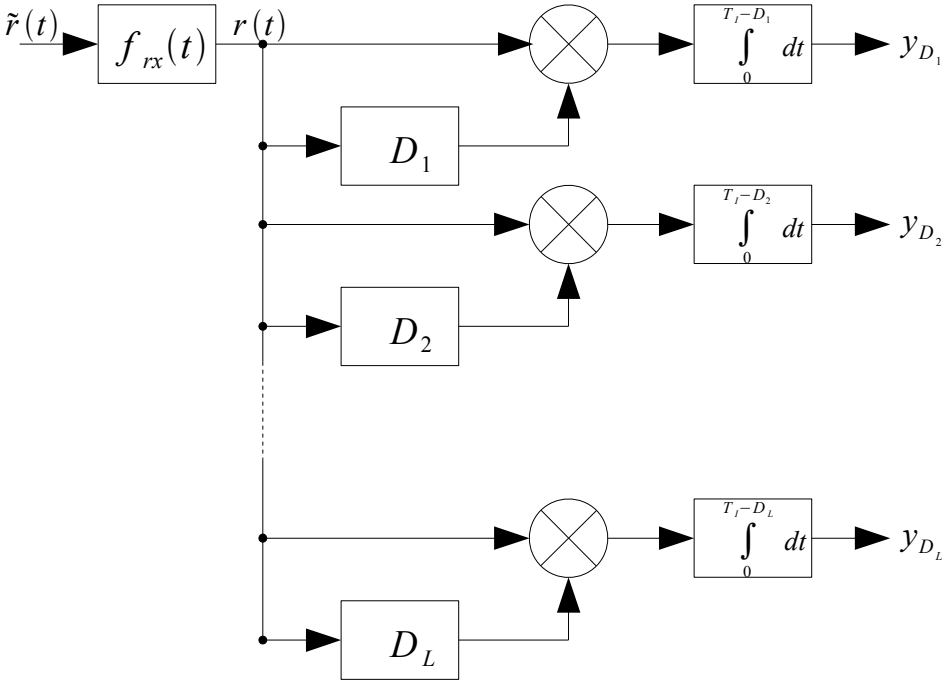

Figure 2.1: The multichannel AcR frontend with L delay lags

The general form of the multichannel transmit signal for one symbol interval is:

$$s(t) = \sum_{n=1}^{N} c_n s_n w_n(t) \tag{2.1}$$

where $s_n \in \{0, 1\}$ are the data symbols and N corresponds to the number of subcarriers. The c_n are equiprobable code symbols from the set $\{-1, 1\}$ that are used to smooth the power spectrum of the transmitted signal. The functions $w_n(t)$ deserve further attention:

- For the OFDM scheme mentioned we have $w_n(t) = w(t)e^{j2\pi n f_c t}$ with the pulse $w(t)$ which has the purpose of shaping the spectrum of the transmit signal. The transmit signal is then (in complex baseband notation):

$$s(t) = w(t) \sum_{n=-N/2}^{N/2} c_n s_n e^{j2\pi n f_c t} \tag{2.2}$$

- Alternative signaling schemes will be introduced later (starting in Chapter 4) which do not use frequency shifts to separate the subcarriers. A set of (orthogonal) pulses will be used that will be denoted by $w_n(t)$ for $n = 1, 2, ..., N$. So the transmit signal will be given by (2.1).

Intersymbol interference is avoided by choosing the length of $w_n(t)$ to be short with respect to the symbol duration T_{sym} (see also Section 1.2.2), so that the restriction to one symbol interval in (2.1) results in no loss of generality.

As a noncoherent receiver is used that can not exploit absolute phase information from the received signal, the choice of modulation schemes is constrained. E.g., phase-shift keying (PSK) is useless, as the information is conveyed in the signal phase there. Looking at the structure of $s(t)$, possible candidate schemes are on-off-keying (OOK) and binary pulse position modulation (PPM). PPM is used throughout this thesis because it allows for a zero threshold to be used in the detector. OOK would require a possibly complex threshold computation [Kay98].

Following the notation of [WP08] and [Wit08c] the multipath radio channel impulse response (CIR) $h(t)$ is modeled as a sum of discrete pulses of the form

$$h(t) = \sum_i \alpha_i \delta(t - t_i) \tag{2.3}$$

where α_i is the (possibly complex) amplitude of the i-th multipath component (MPC) and t_i is its arrival time. The *received pulse* $g_n(t)$ for the n-th subchannel is then written as (with the symbol $*$ denoting convolution):

$$\begin{aligned} g_n(t) &= h(t) * w_n(t) \\ &= \sum_i \alpha_i w_n(t - t_i) \end{aligned} \tag{2.4}$$

This notation for the received pulse will be used in later sections where frequency shifted subcarrier signals are not used. For the OFDM scheme that is analyzed in this section we define a more general function $g_n(t)$:

$$g_n(t) := (h(t)e^{-j2\pi n f_c t}) * w(t) \tag{2.5}$$

as the complex envelope of the channel response to the pulse $w(t)$ at a frequency nf_c. Using this notation the received signal $r(t)$ can be expressed as:

$$r(t) = \sum_n s_n g_n(t) + \nu(t) \tag{2.6}$$

where the code sequence c_n has been omitted for the sake of easier notation. Assuming an ideal transmission scheme (which will be defined later), the sequence c_n has no influence on the demodulation. We will see that that the information-carrying parts of the received signal always carry the *squared* value of the data bit s_n which maps the possible negative values created by c_n back to positive ones. The process $\nu(t)$ is a filtered Gaussian noise process. Now we can take the AcR into account by expressing the output of one channel at delay lag D_l as:

$$y(D_l) = \int_0^{T_I - D_l} r(t) r^*(t + D_l) dt \tag{2.7}$$

where * denotes complex conjugation and D_l corresponds to a positive delay lag. Negative lags can be obtained simply by the Hermitian symmetry of the autocorrelation function ($y(-D_l) = y^*(D_l)$). An inner product notation for integrals as in (2.7) can also be adopted:

$$\langle x(t); y(t) \rangle := \int_{-\infty}^{\infty} x(t) y^*(t) dt \tag{2.8}$$

Together with the rectangular window function $\Pi_{T_I}(t)$ which has a value of one in the interval $[0; T_I]$, the output of one AcR channel is written as

$$y(D_l) = \langle \Pi_{T_I}(t) r(t); \Pi_{T_I}(t + D_l) r(t + D_l) \rangle \tag{2.9}$$

Finally the function $\psi_n(t)$ is introduced as in [Wit08c] with the difference that the frequency shifts are contained in the pulse shapes $w_n(t)$ for the case of OFDM transmission:

$$\psi_n(t) := \Pi_{T_I}(t) g_n(t) \tag{2.10}$$

2.3 Nonlinear Receiver Operation

Noncoherent autocorrelation or energy detection receivers multiply the received signal by itself (with or without a delay, respectively), which is a nonlinear operation. It is a well-known fact (see, e.g., [Wit08b] or [Pau07]) that this results in *crossterms* that appear at the input of the integrator. This is the case because the received signal consists of a sum of the transmitted signal and noise. For the transmission scheme considered here the transmitted signal (2.1) is a sum of N subcarrier signals. Inserting (2.6) in (2.9), expanding the products, using (2.10) and grouping the terms yields:

$$\begin{aligned}
y(D_l) = & \sum_n s_n^2 \langle \psi_n(t); \psi_n(t + D_l) \rangle && \text{(N signal-by-signal terms)} && \text{(2.11a)} \\
& + \sum_n \sum_{\substack{n' \\ n' \neq n}} s_n s_{n'} \langle \psi_n(t); \psi_{n'}(t + D_l) \rangle && \text{(N(N-1) interference terms)} && \text{(2.11b)} \\
& + \sum_n s_n \langle \psi_n(t); \Pi_{T_I}(t + D_l) \nu(t + D_l) \rangle && \text{(N signal-by-noise terms)} && \text{(2.11c)} \\
& + \sum_n s_n \langle \Pi_{T_I}(t) \nu(t); \psi_n(t + D_l) \rangle && \text{(N noise-by-signal terms)} && \text{(2.11d)} \\
& + \langle \Pi_{T_I}(t) \nu(t); \Pi_{T_I}(t + D_l) \nu(t + D_l) \rangle && \text{(1 noise-by-noise term)} && \text{(2.11e)}
\end{aligned}$$

Therefore the output of one AcR channel is a sum of $(N + 1)^2$ crossterms which can be grouped into the following five groups in (2.11a) to (2.11e).

- (2.11a) is the group of signal-by signal terms. These terms form a linear sum over the N squared data symbols multiplied by a scalar product that is the autocorrelation

function (ACF) of $\psi_n(t)$ at the delay lag D_l. This term is written as $h_n(D_l)$ in the following sections:

$$h_n(D_l) = \langle \psi_n(t); \psi_n(t + D_l) \rangle \tag{2.12}$$

- In (2.11b) we find all the crossterms between individual subchannel signals with an *unequal* index. As data symbols from different channels are multiplied here, the presence of these terms leads to useless information that might severely impair receiver operation. We can think of these terms as *interference* between individual subchannels. Inspecting them, one finds out that their structure resembles that of (2.11a) except for the unequal indices and the fact that not the auto-, but the *crosscorrelation* function (CCF) of $\psi_n(t)$ and $\psi_{n'}(t)$ scales the product of the data symbols. It is important to note that the interference terms vanish if *orthogonal* subchannel signals are used. In analogy to (2.12) we define a function $g_{n,n'}(D_l)$ as the crosscorrelation of $\psi_n(t)$ and $\psi_{n'}(t)$ at the lag D_l:

$$g_{n,n'}(D_l) = \langle \psi_n(t); \psi_{n'}(t + D_l) \rangle \tag{2.13}$$

  Thus the performance-impairing terms from (2.11b) will vanish whenever one of the corresponding data bits is zero or if we can guarantee that:

$$\langle \psi_n(t); \psi_{n'}(t + D_l) \rangle = 0 \qquad \forall\ n \neq n' \text{ and } \forall\ D_l \in \{D_l\} \tag{2.14}$$

- (2.11c) contains the data-dependent signal-by-noise terms. Every channel that transmits a bit $s_n = 1$ will result in one such term. Inspecting the structure shows that these terms project the noise process $\nu(t)$ on the data-carrying basis functions $\psi_n(t)$. As in (2.12) we can adopt a simpler notation by writing the scalar product as one term $\nu_n(D_l)$. We obtain:

$$\nu_n(D_l) = \langle \psi_n(t); \Pi_{T_I}(t + D_l)\nu(t + D_l) \rangle \tag{2.15}$$

- (2.11d) is similar to (2.11c), in the simpler notation we can follow (2.15), we just write $\tilde{\nu}_n(D_l)$ for the scalar product.

- (2.11e) is the noise-by-noise term. Reference [Pau07], for example, derives its statistic as a zero-mean Gaussian random variable with variance of approximately

$$\mathrm{var}\{\nu_\nu(D_l)\} \approx \frac{N_0^2}{2} T_I W_{rx} \tag{2.16}$$

  where we introduced the notation $\nu_\nu(D_l)$ for the scalar product denoting the noise-by-noise term. W_{rx} is the equivalent bandwidth of the receiver frontend filter. The zero-mean assumption holds if the delay lag D_l is chosen large enough such that noise samples at different lags are uncorrelated. The existence of this term is considered a drawback of AcRs (and energy detection receivers) because of the squared noise power. We also notice the influence of the integration interval and the bandwidth. This relation should be used when choosing these parameters (see also Section 2.6).

2.4 MIMO Signal Model

Considering the OFDM signaling scheme, we know that the subchannel signals are mutually orthogonal because of the frequency separation. Therefore the interference terms in (2.11b) will vanish and the number of crossterms will be reduced to $3N+1$. By using the simplified notation for the scalar products and the orthogonality assumption the output of one AcR channel becomes:

$$y(D_l) = \sum_n s_n^2 h_n(D_l) + s_n \nu_n(D_l) + s_n \tilde{\nu}_n(D_l) + \nu_\nu(D_l) \tag{2.17}$$

We now turn our attention to the overall output of the AcR which is given by the L samples of the estimated ACF of the received signal. These values $y(D_l)$ are put in an $(L \times 1)$ vector $\mathbf{y}$. The squared transmitted data symbols s_n^2 form the $(N \times 1)$ vector $\mathbf{s}$ and all the noise contributions ((2.11c) - (2.11e)) are stacked in an $(L \times 1)$ vector $\boldsymbol{\nu}$. Finally an $(L \times N)$ matrix $\mathbf{H}$ is introduced by arranging the values of $h_n(D_l)$ from (2.12) in the l-th row and the n-th column. This matrix will be referred to as the *channel matrix*. We can then formulate the linear multiple-input multiple-output (MIMO) relationship:

$$\mathbf{y} = \mathbf{H}\mathbf{s} + \boldsymbol{\nu} \tag{2.18}$$

It is remarkable that the clearly nonlinear AcR operation can be expressed as a linear MIMO model. This has severe implications for the further interpretation of the operation of the receiver and the performance results. With a linear MIMO formulation of the problem, several signal processing backend schemes become applicable [BLM04], [PS08]. Furthermore, the problem can simply be seen as a system of linear equations plus noise contributions. As will be discussed in Section 2.6, we will have $L \geq N$, i.e. the number of receiver channels will be greater than or equal to the number of subchannels. So $\mathbf{H}$ will either be square or have more rows than columns. A matrix that fulfills the latter will be called *skinny* (the opposite will be called a *fat* matrix). In the case of a skinny channel matrix the system of equations will be overdetermined. This means that there will be an infinite number of solutions, requiring us to define a criterion on the solution we want to obtain.

However, it is very important to once again note the assumption of orthogonality that led to this linear model. The case where this assumption is violated must also be considered. There are several reasons for this: Firstly, the orthogonality condition applies to the received signal, whereas we can only control the signal at the transmitter side. So the orthogonality of the subchannels could be impaired by the multipath channel. Secondly, one could want to design sub-optimal signaling schemes (sub-optimal in the sense of orthogonality, as in Chapter 4) that do not provide true orthogonality, but rather a low crosscorrelation of the subchannels. Expressing this in the matrix model and expanding the noise contributions in separate terms yields the complete model:

$$\mathbf{y} = \underbrace{\mathbf{H}\,\mathbf{s}}_{\mathbf{y_{ss}}} + \underbrace{\mathbf{G}(\mathbf{s} \,\tilde{\otimes}\, \mathbf{s})}_{\mathbf{y_{ccf}}} + \underbrace{\mathbf{V}\,\mathbf{s}}_{\mathbf{y_{sv}}} + \underbrace{\tilde{\mathbf{V}}\,\mathbf{s}}_{\mathbf{y_{vs}}} + \underbrace{\boldsymbol{\nu_\nu}}_{\mathbf{y}_{\nu\nu}} \tag{2.19}$$

where the two $(L \times N)$ matrices $\mathbf{V}$ and $\tilde{\mathbf{V}}$ contain the scalar products from (2.11c) and (2.11d) and the $(L \times 1)$ vector $\boldsymbol{\nu_\nu}$ contains the noise-by-noise contributions. The five

summands reflect the information-carrying, the crosscorrelation-induced and the several noise-induced contributions to the overall AcR output. Names have been assigned to them below the equation for further referencing to them as individual $(L \times 1)$ vectors. The symbol $\tilde{\otimes}$ denotes a reduced Kronecker product for two vectors in the sense that it only accounts for those combinations of elements from $\mathbf{s}$ with unequal indices.

The $(N(N-1) \times L)$ matrix $\mathbf{G}$ contains the $g_{n,n'}(D_l)$ from (2.13). This means that it has one row for each delay lag (receiver channel), just like $\mathbf{H}$ and as many columns as there are crosscorrelations between subcarriers. We note that the vector $\mathbf{s}$ that is contained in the crosscorrelation-induced and signal-by-noise terms actually holds the same values as the vector $\mathbf{s}$ that is multiplied by $\mathbf{H}$ and contains the squared values of the s_n. This is due to the fact that the s_n are drawn from the binary alphabet $\{0, 1\}$.

Finally we can also simplify the complete MIMO model notationally by putting all noise contributions together in one $(L \times 1)$ noise vector $\boldsymbol{\nu}$, as it has been done in (2.18):

$$\mathbf{y} = \mathbf{H}\mathbf{s} + \mathbf{G}(\mathbf{s} \,\tilde{\otimes}\, \mathbf{s}) + \boldsymbol{\nu} \tag{2.20}$$

where this noise vector will be referred to as $\mathbf{y}_\nu$. All in all, we have three equations describing the MIMO relationship: (2.18) is used if an ideal signaling scheme with no crosscorrelation between the subchannel signals is used or if the crosscorrelation-induced contributions $\mathbf{y_{ccf}}$ are neglected. (2.19) is the complete and accurate description of the system and (2.20) is used when we want to consider $\mathbf{y_{ccf}}$ but not to distinguish between the noise contributions.

The channel matrix $\mathbf{H}$ represents the mapping between the squared data symbols $\mathbf{s}$ and the AcR output vector $\mathbf{y}$ if we neglect the noise for the moment. Thus the i-th *row* of $\mathbf{H}$ corresponds to the contributions of one receiver channel or one delay lag D_i as it contains the values $h_j(D_i)$ for $j = 1, 2, ..., N$. One *column* of $\mathbf{H}$, say the j-th, depicts one transmit subchannel as its entries are all multiplied by the same s_i^2.

We can judge the mutual crosscorrelation of our channels by the matrix $\mathbf{G}$. It contains all the possible crosstalk between the subcarriers at the delay lags of the receiver, as indicated by (2.13). Again, one *row* corresponds to one specific delay lag but one row now has $N(N-1)$ entries. Assuming a non-ideal transmission scheme with non-zero mutual crosscorrelation between the carriers those *columns* of $\mathbf{G}$ which correspond to the combination of the currently active carriers (those with $s_i = 1$) will have non-zero entries.

It is important to note that the existence of $\mathbf{G}$ is a fundamental difference to conventional MIMO systems. This matrix vanishes for an ideal transmission scheme which fulfills (2.14) but in practical systems it will always deliver contributions to the receiver output. One reason for this is the possible loss of subchannel orthogonality caused by the transmission over the multipath channel which will be addressed in Section 3.3.2.

2.5 Backend Signal Processing

In (2.18) a linear MIMO problem was formulated. Thus all the existing theory on MIMO channel separation can be applied [BLM04], [PS08]. The overall transmission scheme is shown in Figure 2.2. The composite received signal is converted to L samples by the AcR. These samples are the input for a *combiner* which is the $(N \times L)$ matrix $\mathbf{W}$. This matrix computes the N decision variables z_i which are processed by the decision device (DD):

$$\mathbf{z} = \mathbf{W}\mathbf{y} = \mathbf{W}\mathbf{H}\mathbf{s} + \mathbf{W}\boldsymbol{\nu} \tag{2.21}$$

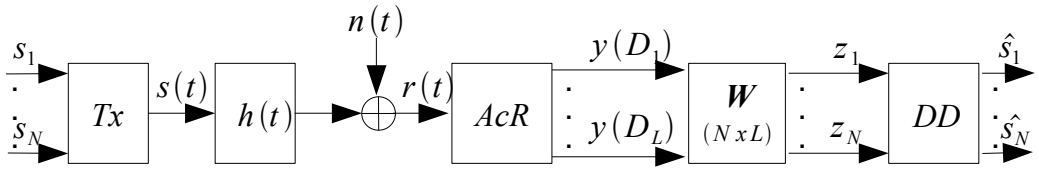

Figure 2.2: Overall transmission system with linear MIMO backend processing

The equivalent MIMO system from (2.18) is shown in Figure 2.3. The channel matrix $\mathbf{H}$ converts the transmitted data vector $\mathbf{s}$ into an $(L \times 1)$ vector $\mathbf{y}$. Together with the definition of the entries of $\mathbf{H}$ from (2.12) we see that the channel matrix contains the transmit pulse shapes, the multipath channel and the whole AcR frontend. The latter fact turns the system into a *memoryless* MIMO system which means that the entries of $\mathbf{H}$ are not functions of time.

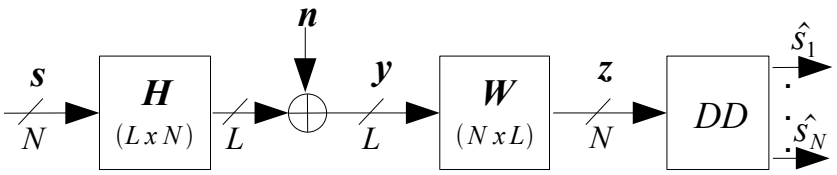

Figure 2.3: Equivalent memoryless MIMO system with linear backend processing

2.5.1 Conventional MIMO combiners

For scalar communication channels we know two important equalization techniques: Zero-forcing (ZF) and minimum-mean-squared error (MMSE) equalizers. They can be generalized to MIMO channels [PS08],[BLM04]. The latter reference also presents an ideal bound for memoryless MIMO channels, the perfect interference cancellation bound.

Zero-Forcing Combiner

The ZF combiner works in analogy to the scalar case which, most importantly, means that it ignores the presence of noise. Moreover, we know that a ZF equalizer for a scalar ISI channel forces the ISI to zero. In the MIMO sense it forces the contributions of the

interfering *columns* of $\mathbf{H}$ (e.g. for the symbol s_i all columns $\mathbf{h}_{j\neq i}$) to zero. Therefore it could throw away useful signal energy. The ZF linear detector chooses the combiner matrix as:

$$\mathbf{W_{zf}} = (\mathbf{H}^*\mathbf{H})^{-\mathbf{1}}\mathbf{H}^* = \mathbf{H}^\dagger \tag{2.22}$$

where $\mathbf{H}^\dagger$ is the *Moore-Penrose* pseudoinverse of $\mathbf{H}$ which implies that $\mathbf{WH} = \mathbf{I}_N$. The symbol * denotes hermitian transposition and $\mathbf{I}_N$ is the identity matrix with N rows and columns. As in the scalar case one can say that the ZF detector inverts the channel. In [PS08] it is also referred to as an *inverse channel detector*. In terms of general linear equations this corresponds to the solution of the system in the least-squares sense without the noise.

The decision variables $\mathbf{z}$ become:

$$\begin{aligned}\mathbf{z_{zf}} &= \mathbf{H}^\dagger\mathbf{Hs} + \mathbf{H}^\dagger\mathbf{G}(\mathbf{s} \,\tilde{\otimes}\, \mathbf{s}) + \mathbf{H}^\dagger\mathbf{W}\boldsymbol{\nu} \\ &= \mathbf{s} + \tilde{\mathbf{y}}_{\mathbf{ccf}} + \tilde{\mathbf{y}}_\nu\end{aligned} \tag{2.23}$$

which recovers the data symbols but transforms the crosscorrelation contributions and the noise terms. If they are present they could of course be severely boosted.

Minimum-mean-square error Combiner

The MMSE combiner also takes the noise into account by choosing the combiner matrix such that the mean square error between the data symbols and the combiner outputs is minimized. This leads to:

$$\mathbf{W_{mmse}} = (\mathbf{H}^*\mathbf{H} + \mathbf{R_{nn}})^{-1}\mathbf{H}^* \tag{2.24}$$

where $\mathbf{R_{nn}}$ is the noise covariance matrix which has to be estimated in practice.

Both the ZF- and the MMSE-combiners determine their combiner matrix by applying calculations on the channel matrix. So $\mathbf{H}$ has to be known to the receiver. The estimation of $\mathbf{H}$ can be accomplished by transmitting training symbols.

Perfect interference cancellation bound

This idea is taken from [BLM04] where it is, amongst others, called the *genie-aided receiver* or the *perfect interference cancellation bound* (PIC). These names are justified by the facts that this hypothetical receiver aims at recovering single data symbols s_i (one channel) and thereby knows all interfering data symbols $s_{j\neq i}$. It can be formulated by the *matrix matched filter* $\mathbf{H}^*$ (MMF) which multiplies the channel output $\mathbf{y}$ to get the output $\tilde{\mathbf{y}}$. The product $\mathbf{H}^*\mathbf{H}$ is an $(N \times N)$ matrix denoted as $\mathbf{R}$. This matrix is decomposed in its diagonal part $\mathbf{R^d}$ and its non-diagonal part $\mathbf{R} - \mathbf{R^d}$. The interference-free decision statistic of the receiver can then be calculated by subtracting the interference terms from the MMF output:

$$\begin{aligned}\mathbf{z_{PIC}} &= \tilde{\mathbf{y}} - (\mathbf{R} - \mathbf{R^d})\mathbf{s} \\ &= \mathbf{R^d s} + \mathbf{R}\nu\end{aligned} \tag{2.25}$$

This bound tells us the hypothetical receiver performance if all the interference concerning the individual symbols can be subtracted. We have to note that this is just the interference coming from the channel matrix $\mathbf{H}$ and has nothing to do with the crosscorrelation-induced interference resulting from the presence of the matrix $\mathbf{G}$. This means that this bound can still indicate a good theoretical receiver performance while the real performance might be bad due to high mutual crosscorrelation.

2.5.2 DFT Combiner

In [Wit08c] it is shown that the Fourier transform of the output samples of the AcR corresponds to the power spectral density (PSD) of the received signal. This can intuitively be understood by reviewing the Wiener-Khinchin-Theorem [Kay93] which states that the autocorrelation function of a process and its PSD form a Fourier transform pair. We can use this fact for the OFDM transmission scheme to estimate the energy of the received signal at certain frequencies, namely the subcarrier center frequencies.

This corresponds to a backend processing scheme where $\mathbf{W}$ is chosen as a discrete Fourier transform (DFT) matrix. The huge advantage of this scheme is that it is completely predefined and does not need channel state information. As we will see in Chapter 3, this scheme is indeed capable of separating the subchannel data and could be used for low-complexity receiver implementations.

2.5.3 Noise and Interference Gain

If $\mathbf{G}$ is present, see (2.20), the backends perform the following operation:

$$\mathbf{z} = \mathbf{WHs} + \mathbf{WG}(\mathbf{s} \,\tilde{\otimes}\, \mathbf{s}) + \boldsymbol{W\nu} \tag{2.26}$$

which means they will introduce interference gain, where interference means the crosscorrelation contributions. We can make this explicit by writing one element of the decision vector $\mathbf{z}$, using one row of the combiner matrix $\mathbf{w}_i^T$:

$$\begin{aligned}z_i &= \mathbf{w}_i^T y \\ &= \mathbf{w}_i^T[\mathbf{y_{ss}} + \mathbf{y_{ccf}} + \mathbf{y_v}] \\ &= z_{i,ss} + z_{i,ccf} + z_{i,v}\end{aligned} \tag{2.27}$$

which decomposes $\mathbf{z}$ into its components. This will be used later to define a signal-to-interference ratio (SIR).

2.6 System Parameters

The following sections discuss several parameters that influence the performance of the proposed system.

Number of channels and data rate

The uncoded data rate of this transmission scheme is given by:

$$R_{b,PPM} = \frac{N}{2} R_s \text{ [bit/s]} \tag{2.28}$$

where the number of subcarriers is N and R_s is the symbol rate of the system. This rate has to be divided by two because binary PPM is used that transmits one bit in two symbol intervals. For a typical symbol duration (including the zero guard interval) of $T_{sym} = 100$ ns and a number of subcarriers of $N = 9$ this results in a bit rate of 45 MBit/s. A strong line-of-sight (LOS) channel with negligible power of the reflected components could allow us to reduce the guard interval and obtain, e.g., $T_{sym} = 10$ ns. We would obtain a gross bit rate of 450 MBit/s. The choice to reduce the guard interval will of course increase the symbol rate but depending on the channel this will introduce intersymbol interference. One other possibility is to use more channels but this makes the receiver more complex because more receiver channels must be implemented.

Bandwidth

We have to distinguish between IR and OFDM schemes regarding the bandwidth:

- With the OFDM scheme each subcarrier has a certain bandwidth and different subcarrier signals are separated in frequency. The receiver performance for different bandwidths will be presented in Chapter 3. We distinguish the cases where each carrier by itself is a UWB signal, meaning that its bandwidth is at least 500 MHz and where the subcarrier bandwidth is less than that. In the latter case we expect a performance penalty because of reduced multipath resolution and, therefore, increased fading.
- In the IR scheme all the subchannels *share* the entire signal bandwidth, which will be 4 GHz for all schemes. A simulation of the best performing scheme at a reduced bandwidth of 2 GHz will also be presented for comparison. The motivation behind the rather high bandwidth is that we expect to have increased fading resistance.

Number of receiver channels

The *generalized Nyquist criterion* for MIMO channels [BLM04] answers the question of under what conditions a receiver employing only linear filtering and symbol rate sampling is able to reconstruct the transmitted data symbols. It relates the number of transmitter (N) and receiver channels (L) as follows:

$$N \leq L \lfloor 2WT_{sym} \rfloor \tag{2.29}$$

where W is the bandwidth of the subchannel signals. Since $1/(2T_{sym})$ is the minimum bandwidth needed for ISI-free transmission, the factor $\lfloor 2WT_{sym} \rfloor$ corresponds to the bandwidth expansion. For impulse radio based UWB systems with a low pulse repetition rate this factor will almost always be quite high because the (ultra-short) pulse representing the data symbol will determine the bandwidth while the actual symbol duration is typically much longer. For the limiting case of UWB transmission at the minimum bandwidth (this means without any guard interval and, therefore, probably severe ISI) (2.29) reduces to $L \geq N$. This case corresponds to the minimum number of receiver channels needed, though for practical systems this bound will be relaxed by the bandwidth expansion. The condition $L \geq N$ can also be intuitively understood by the MIMO-model (2.18). If we had $L < N$, the system of linear equations would be under-determined.

If we want to have symmetric negative and positive delay lags only half of these channels need to be implemented because of the symmetry of the autocorrelation function. For example, this is the case for a baseband OFDM signal like in (2.2). In this case we have to consider that every sample $y_{Dl}[i]$ will be complex-valued.

Integration interval

As [Wit08b] elaborates, choosing the right integration interval T_I for the AcR is a trade-off: On the one hand, we want to capture as much multipath energy as possible which corresponds to a longer T_I, but on the other hand the AcR also accumulates noise energy during T_I. The paper states a rule of thumb which says that T_I should be chosen as approximately twice the RMS delay spread of the channel.

Choosing T_I like that works well for the OFDM scheme, as will be illustrated in the next chapter. The different alternative schemes, however, were ofter seen to benefit from a slightly longer integration interval. This, of course, also boosts the noise terms. The simulation results for several choices will be shown at the end of Chapter 4.

Delay lag spacing

In [Wit08c] it was shown that the delay lag spacing $D = D_{i+1} - D_i$ should be chosen as the inverse of the system bandwidth concerning the criterion that noise samples at adjacent delay lags should be uncorrelated.

Maybe the biggest practical issue in implementing the proposed receiver structure is the required analog ultra-wideband delay line. These filters must have a constant and accurate group delay over the whole signal bandwidth. The multichannel AcR analyzed here, however, has an advantage over other TR-schemes because the required delay values are rather short, in the range of one to several nanoseconds. For example, [BHS+05] propose a structure providing 0.72 ns of delay at a bandwidth of 1 GHz whereas [ZSH06] reports a delay of 60 ps over a bandwidth of 10 GHz.

3 Analysis of the OFDM Scheme

3.1 Overview

The performance of the multichannel AcR presented in Chapter 2 is analyzed in this section with respect to the transmission of the multichannel signal over a multipath radio channel. We want to obtain the performance in terms of the bit error rate (BER) over the signal-to-noise ratio (SNR), defined as the energy used for the transmission of one bit in relation to the noise power (E_b/N_0). The OFDM signal from (2.2) with N subcarriers and L receiver channels was chosen for the transmission. This section also contains the introduction of several other performance measures for this receiver.

We want to characterize the receiver's performance for different settings of system parameters (see Section 2.6), most importantly the number of subcarriers and bandwidth. A simulation of the system at high bit rate, meaning a very short symbol duration, will also be presented.

3.2 Analysis of the Receiver Crossterms

Once again we consider our complete MIMO transmission model from (2.19):

$$\mathbf{y} = \mathbf{H}\mathbf{s} + \mathbf{G}(\mathbf{s} \,\tilde{\otimes}\, \mathbf{s}) + \mathbf{V}\mathbf{s} + \tilde{\mathbf{V}}\mathbf{s} + \boldsymbol{\nu}_{\boldsymbol{\nu}} \tag{3.1}$$

$$= \mathbf{y}_{ss} + \mathbf{y}_{ccf} + \mathbf{y}_{sv} + \mathbf{y}_{vs} + \mathbf{y}_{\nu\nu} \tag{3.2}$$

The combiner matrix is multiplied with the vector $\mathbf{y}$ to get the decision variable vector $\mathbf{z}$. An ideal OFDM signal consists of orthogonal subcarriers because of their frequency separation. Hence the vector $\mathbf{y}_{ccf}$ should be zero. However, the signal is transmitted over the multipath channel with an impulse response $h(t)$ which could cause a loss of this orthogonality. This is further analyzed in Section 3.3.2. The receiver crossterms given in (3.2) will be calculated individually in order to analyze their contributions on the system performance.

Notes on the notation: The five vectors in (3.2) are $(L \times 1)$ vectors reflecting the fact that, on the one hand each crossterm contribution affects all the L delay lags and, on the other hand that we avoid ISI with a guard interval and therefore only consider a single symbol interval. During transmission a stream of N_s symbols will be transmitted, so these vectors can be further indexed with a symbol index. Thus whenever a specific symbol is mentioned this will be done in writing, e.g., $\mathbf{y}_{ss}[n]$, where the square brackets reflect the discrete nature of those outputs. If, finally, a single receiver channel output (one delay lag) of a single symbol is addressed, this will be done by writing $y_{ss,D_l}[n]$.

3.2.1 Multichannel Transmission over the Multipath Channel

Figure 3.1 shows the system that will be used in performance simulations. The multipath channel is commonly modeled as in (2.3) and its impact on the received pulse as in (2.4). This corresponds to physical mechanisms of wave propagation like reflection and time dispersion. The received signal is a *linear* sum of delayed copies of the transmitted signal. This linearity allows for a separate transmission of the subcarrier signals $s_{c,n}(t)$ over the channel and through the frontend filter. Thus the AcR is able to access the individual signals and calculate each crossterm contribution separately.

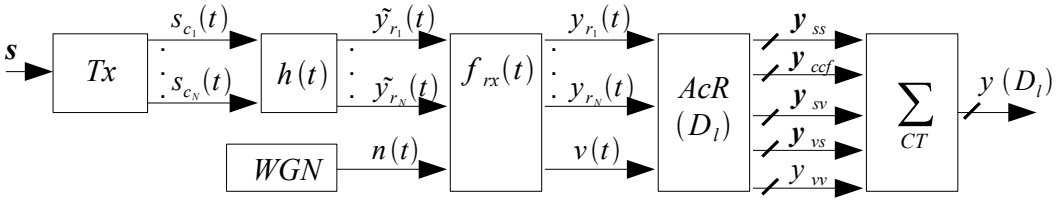

Figure 3.1: Transmission of individual subcarrier signals over the multipath channel

The last block in Figure 3.1 (the sum over all crossterms) is just there to emphasize the fact that this sum corresponds to the conventional AcR output, as in (3.2). We can now simulate the system with or without contributions from specific crossterms. It is assumed that the OFDM scheme provides almost perfect orthogonality due to the frequency separation, hence the contributions from $\mathbf{y_{ccf}}$ will be rather small. For other signaling schemes analyzed in Chapter 4, that are sub-optimal in terms of orthogonality, we can now simply determine impacts on their performance by switching off the crosscorrelation induced crossterms. This allows us to check whether these schemes are limited by their mutual crosscorrelations or not.

3.2.2 Simulation Parameters

Several parameters affect the system simulation and are selectable parameters. They are explained in the following list and the default values are given wherever appropriate. So in the discussions of the following performance results only those parameters that are deviating from their standard values need to be given explicitly.

Signaling : As mentioned in Section 2.2, binary PPM is used for the modulation of the data bits. The pulse shape $w(t)$ is chosen as a root-raised-cosine pulse complying with the receiver frontend filter. This pulse shape is used to control the bandwidth (and effective pulse duration) of the transmit signal. The symbol is extended to a length of 100 ns by inserting a zero guard interval behind the pulse so that ISI is avoided.

Multipath radio channel : In most of the simulations a Rayleigh channel (meaning a Ricean K-factor of zero) with a RMS-delay spread $\tau_{rms} = 10$ns has been used to reflect a worst-case scenario in the sense of a non line-of-sight (NLOS) channel. For the high rate transmission we also consider a LOS channel with a Ricean K-factor of four and $\tau_{rms} = 1$ns. The channel impulse responses are generated as realizations of a statistical channel description for the channel parameters.

Delay lag spacing : As in [Wit08a] this will be chosen as the bandwidth inverse to obtain uncorrelated noise samples.

Backend processing : The following backends, which were described in Section 2.5, are used for the simulations: DFT, ZF and MMSE combiner as well as the PIC-bound. The latter is used to check the different receiver architectures to a reference performance for ideal MIMO backend processing.

3.3 Performance measures for the Multichannel transmission

This section introduces several performance measures for the multichannel AcR. These measures are used in addition to the conventional BER over the SNR in the discussion of the following simulation results. Also the PIC-bound, described in Section 2.5.1, is a useful measure to judge the receiver performance and is thus also included in all performance simulation results.

3.3.1 Measures for the Invertibility of the Problem

Looking at the interpretation of the columns of $\mathbf{H}$ from Section 2.4 it is clear that the columns of the channel matrix should be linearly independent. This is also mentioned in [Boy08]: A matrix whose columns are independent is called *one-to-one*. This means that only the zero-vector is an element of its nullspace which implies that linear mappings with this matrix are always uniquely invertible. As $\mathbf{H}$ is square or skinny (we will always have $L \geq N$) its rank r is then given by N, which is the maximum rank that $\mathbf{H}$ can have. So any rank deficiencies are clear indications of a bad invertibility of the linear problem.

We can check for rank deficiency by a singular value decomposition of $\mathbf{H}$:

$$\mathbf{H} = \mathbf{U}\mathbf{\Sigma}\mathbf{V}^* \tag{3.3}$$

with the orthonormal matrices $\mathbf{U}$ $(L \times L)$ and $\mathbf{V}$ $(N \times N)$ and the $(L \times N)$ diagonal matrix $\mathbf{\Sigma}$ containing the singular values $(\sigma_1, \sigma_2, ..., \sigma_N)$ of $\mathbf{H}$. If we take a look at those singular values we notice that they are zero for values greater than r [BSMM00] where we see a discontinuity in the singular value spread of $\mathbf{H}$ at r. This applies to the case of a rank deficiency. Another interesting case is when $\mathbf{H}$ is full rank but the singular values decrease continuously towards zero and where we have some singular values that are close to zero. This case is referred to as an ill-posed problem [Bra07] for which we also have a bad invertibility.

Both of these cases can be observed via the condition number of $\mathbf{H}$, which is defined as:

$$\text{cond}(\mathbf{H}) = \frac{\max\{\sigma_i\}}{\min\{\sigma_i\}} \tag{3.4}$$

which is the ratio of the largest singular value to the lowest. A condition number in the region of one indicates a good, a very high condition number a bad invertibility. This also complies with the general theory on solving linear equations where the condition number is also a measure for the numerical stability of the solution.

Another measure can be derived when taking into account that linear independence of the columns of $\mathbf{H}$ implies that the following holds for the columns $\mathbf{h_i}$:

$$\mathbf{h_i^* h_j} \stackrel{!}{=} 0 \qquad \forall\, i \neq j \tag{3.5}$$

so the mutual scalar products of columns with unequal index should vanish. In matrix notation we can calculate the matrix $\mathbf{A} = \mathbf{H}^*\mathbf{H}$ and demand that its diagonal entries dominate over the off-diagonal ones. A measure of the diagonality of an $(N \times N)$ matrix $\mathbf{A}$ can be defined by:

$$M_{diag,[dB]}(\mathbf{A}) = 10 \log_{10} \left(\frac{\sum_{i=1}^{N} |A_{i,i}|^2}{\sum_{i=1}^{N} \sum_{j=1, j\neq i}^{N} |A_{i,j}|^2} \right) \tag{3.6}$$

which relates the "energy" of the diagonal elements to that of the off-diagonal ones expressed in dB.

Yet another important observation is that the columns of $\mathbf{H}$ can be interpreted as the sampled autocorrelation function of the received pulse waveform. Taking into account that those columns should be as linearly independent as possible we notice that subchannel signals for this receiver should be designed in a way such that their autocorrelation functions are somewhat different. This will also be shown in Chapter 4, which deals with alternative signaling schemes.

Simulation results for these invertibility measures are provided in the following sections and in Appendix A.1 and A.2.

3.3.2 Measures for the Orthogonality of subchannel signals

The following sections will provide performance results for the OFDM scheme with and without specific receiver crossterms. The signal is transmitted over a simulated multipath channel. This channel is known to seriously influence the transmitted signal in terms of delay dispersion and frequency selectivity. Considering the special case of the multichannel AcR presented here we might ask the question what influence the channel has on our signal concerning our orthogonality condition (2.14). This condition demands orthogonality for the whole set of subchannel signals at *every* delay lag of the receiver. So if this condition is fulfilled at the transmitter which we can assume to be the case for an OFDM scheme, is it still fulfilled at the receiver?

We begin with an easier version of this question: Considering that we transmit a sum of orthogonal pulses as in OFDM, are these waveforms still orthogonal at the receiver? This question neglects the delay lags for now, but we want to know whether the property of orthogonality is impaired by the multipath channel or not.

First of all, one has to define measures for the orthogonality of signals. We know by definition that two signals $x(t)$ and $y(t)$ are orthogonal if their scalar product vanishes:

$$p_{xy} = \int_{-\infty}^{\infty} x(t)y^*(t)dt = \langle x(t); y(t) \rangle = 0 \tag{3.7}$$

which allows us to check for perfect orthogonality. However we will most likely have to deal with *degradations* of orthogonality which occur due to the channel or even at the transmitter due to pulse shaping. Hence we want to establish measures that are between zero and a defined maximum. To this end we first introduce a normalization for the scalar product:

$$\tilde{p}_{xy} = \frac{\langle x(t); y(t) \rangle}{||x(t)||\ ||y(t)||} \tag{3.8}$$

where

$$||x(t)|| := \sqrt{\langle x(t); x(t) \rangle} \tag{3.9}$$

corresponds to the usual definition of the *norm* of $x(t)$. Note that (3.8) is nothing else than the cosine of the *angle* between the two signals. Thus its absolute value ranges between zero (for perfect orthogonality) and one (this would correspond to *collinear* signals). Now we consider the set of our N transmit subchannel signals $\{s_{c,n}(t)\}$ and calculate a matrix $\mathbf{P}$ of each possible scalar product of this set. The entries of this $(N \times N)$ matrix are:

$$P_{i,j} = \frac{\langle s_{c,i}(t); s_{c,j}(t) \rangle}{||s_{c,i}(t)||\ ||s_{c,j}(t)||} \tag{3.10}$$

We note that the entries on the main diagonal correspond to the normalized individual energies of the subchannel signals (so they are equal to one) and the off-diagonal entries are the cosines of the signal angles. The scalar product is commutative, so this matrix is symmetric and contains every angle two times. Therefore we define our *orthogonality matrix* $\mathbf{A}_{orth}$ as its upper triangular part (we write U_Δ for this operation):

$$\mathbf{A}_{orth} := U_\Delta(\mathbf{P}) \tag{3.11}$$

The interpretation of this matrix is of course somewhat cumbersome. It would be better to have a single value that reflects the "mean orthogonality" of the signal set. The first one would be, much in the spirit of (3.6), to relate the energy of the main diagonal to the off-diagonal entries and define:

$$M_{orth,1} := 10 \log_{10} \left(\frac{\sum_{i=1}^{N} |A_{orth;i,i}|^2}{\sum_{i=1}^{N} \sum_{j=1, j \neq i}^{N} |A_{orth;i,j}|^2} \right) [dB] \tag{3.12}$$

An alternative is to use the sum of squares of the off-diagonal entries:

$$M_{orth,2} := \sum_{i=1}^{N} \sum_{j=1, j \neq i}^{N} |A_{orth;i,j}|^2 \tag{3.13}$$

though this measure suffers from bad interpretability as we know no "good" value for it. Another three more intuitive measures can be defined by the mean, the mean-square and the maximum value of the absolute value of the cosine of the angle:

$$M_{orth,3} := \frac{1}{N(N-1)/2} \sum_{i=1}^{N} \sum_{j=1, j\neq i}^{N} |A_{orth;i,j}| \tag{3.14}$$

$$M_{orth,4} := \frac{1}{N(N-1)/2} \sum_{i=1}^{N} \sum_{j=1, j\neq i}^{N} |A_{orth;i,j}|^2 \tag{3.15}$$

$$M_{orth,5} := \max_{A_{orth;i,j,i\neq j}} \{|A_{orth;i,j}|\} \tag{3.16}$$

All these measures are calculated by splitting the subcarrier signals in individual symbols and calculate the mean of the per-symbol measures. This is done because the receiver also makes its decisions on a symbol-per-symbol basis. In the simulations we will calculate the orthogonality measures at the transmitter and the receiver and compare them to each other. This conceptually leads to an *orthogonality loss* that is due to the channel.

The following performance simulation results will also contain results for the orthogonality measures introduced here. Further results showing some orthogonality measures over the channel realizations can be found in Appendix A.3.

3.3.3 Signal to Interference Ratio

The considerations in Section 2.3 and 2.4 have shown that the crosscorrelation-induced crossterms could seriously impair the receiver performance. To be able to quantify this, we want to relate the energy of these terms to the energy of the information-carrying signal-by-signal terms. This leads us to the definition of a Signal to Interference ratio for the composite signal at the receiver delay lags (SIR(D_l)):

$$\mathrm{SIR}(D_l)_{[dB]} := 10 \log_{10} \sum_{n=1}^{N_s} \frac{|y_{ss,D_l}[n]|^2}{|y_{ccf,D_l}[n]|^2} \tag{3.17}$$

where N_s denotes the number of transmitted symbols and n denotes the symbol index. This SIR can be used to check whether there are delay lags (receiver channels) at which the interference energy dominates over the useful signal energy, which will be a useful definition when we consider sub-optimal signaling schemes in Chapter 4. We are also interested in the SIR at the decision device, i.e. SIR(z_i). This can be accomplished by remembering the decomposition of the decision variables in the crossterm contributions from (2.27). The mapping of frontend outputs to the decision variables is linear so the decision variables can also be decomposed into their components. The SIR is defined as:

$$\mathrm{SIR}(z_i)_{[dB]} := 10 \log_{10} \sum_{n=1}^{N_s} \frac{|z_{i,ss}[n]|^2}{|z_{i,ccf}[n]|^2} \tag{3.18}$$

where $i \in [1, ..., N]$ is the index of the decision variable.

Simulation results for the performance of the multichannel AcR concerning the SIR(D_l) and the SIR(z_i) are provided in the following sections. Results that show the SIR(D_l) and the SIR(z_i) over the channel realizations and comparisons with alternative schemes from Chapter 4 can be found in Appendix A.4.

3.4 Performance Results

This section presents the simulation results for the BER performance over the SNR for various parameter settings. Results for the other performance measures that have been introduced are also provided. In the BER plots, solid lines are used for the receiver performance with all the crossterms which corresponds to the real receiver operation. Dashed and dash-dotted lines represent the hypothetical performance if some specific crossterms are not considered in the frontend output. The red solid line is the PIC-bound.

3.4.1 High bandwidth with $N = 9$

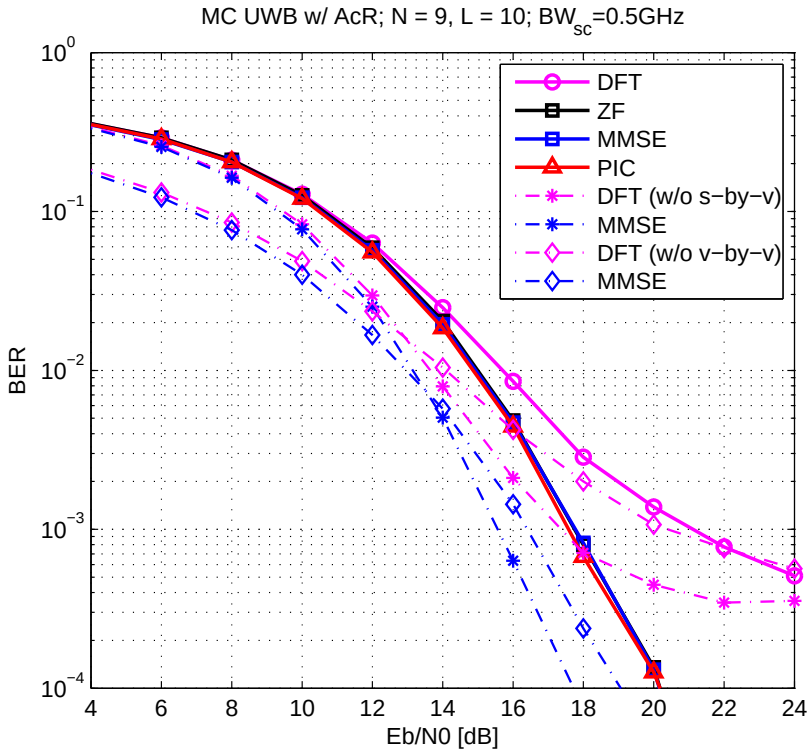

Figure 3.2: Performance for $N = 9, L = 10$ and $BW_{sc} = 0.5$ GHz

The first scenario is the transmission of a transmit signal consisting of $N = 9$ subchannels and a receiver with $L = 10$ autocorrelation channels. For the subcarrier signals we chose an absolute bandwidth $\mathrm{BW_{sc}}$ of 500 MHz which also corresponds to the frequency separation (the distance of their center frequencies) of the signals. This fact implies that the subchannels are orthogonal because there is no overlap in the frequency domain. The overall signal has a bandwidth of about 5 GHz.

Discussion: Figure 3.2 shows the BER performance for the three backends used for this receiver scheme.

- The **crosscorrelation**-induced interference terms do not play a significant role. The BER-curves without the CCF-terms have been omitted because they are visually indistinguishable from those with all the receiver terms. Their influence on all the three backend schemes is negligible which is due to the frequency separation of the OFDM subcarriers. This fact is confirmed by the SIR defined in (3.17) and (3.18). The mean SIR(D_l), averaged over 100 channel realizations and the delay lags, is almost 20dB. Due to the signal combination in the backends, the mean SIR(z_i), averaged over 100 channel realizations and the decision variables, is about 2dB higher than the mean SIR(D_l). Appendix A.4 shows the SIR over the channel realizations.

- Surprisingly, the performance of the **ZF and MMSE** detectors is almost identical which is counterintuitive in the presence of noise. What is particular to this receiver is that all the signal-by-noise terms (see (2.11c) and (2.11d)) are *projections* of the noise waveforms on the signal basis functions. Hence these noise terms are collinear to the data signal terms and can be separated by a linear detector [Wit08c].

  ZF and MMSE backends also performed similarly for limited receiver crossterms which is why just the MMSE backend performance is shown in the plots for these simulations.

- Both the MMSE and the ZF backends reach the **PIC-bound** almost perfectly. This is an indication of a very good invertibility in the sense of our invertibility measures defined in Section 3.3.1. Appendix A.1 provides detailed results for those measures considering this simulation. The mean condition number of $\mathbf{H}$ is 3.44 with only a few outliers that never exceed 7. Also the diagonality measure for $\mathbf{H}^*\mathbf{H}$ defined in (3.6) shows that the energy of the diagonal entries of this matrix dominate with a factor of about 17dB over that of the non-diagonal ones. The PIC-bound, of course, does not change when the crosscorrelation terms are switched off simply because it does not depend on them.

  The fact that the PIC-bound is reached by the ZF-detector can be interpreted using an idea from [BLM04]. There, the ZF-detector is considered for one certain data symbol s_i: As discussed in Section 2.4, this symbol is multiplied by the i-th column of $\mathbf{H}$ which means that the other columns can be seen as *interfering columns*. In the reference we find a definition of an *interference subspace* as the span of all columns $\mathbf{h}_{j\neq i}$. We can decompose $\mathbf{h}_i$ into a part orthogonal to the interference subspace and a part within it. The latter reflects the non-perfect orthogonality of the columns of $\mathbf{H}$ and is denoted by $\hat{\mathbf{h}}_i$.

  [BLM04] also states the mean square error for the ZF-detector and the PIC-detector for the i-th symbol as:

$$\mathrm{MSE}_{i,PIC} = \frac{N_0}{||\mathbf{h}_i||^2} \qquad \text{and} \tag{3.19}$$

$$\mathrm{MSE}_{i,ZF} = \frac{N_0}{||\mathbf{h}_i - \hat{\mathbf{h}}_i||^2} \tag{3.20}$$

  Thus for the BER performance of those two to be equal the MSEs should also be

equal, which is the case if $\hat{\mathbf{h}}_i$ vanishes. This implies that $\mathbf{h}_i$ is orthogonal to the interference subspace. Taking all the data symbols into account we see that all the columns of the channel matrix have to be orthogonal in order to reach the PIC-bound.

Another interpretation of this fact is that there is no need to incorporate a, e.g., non-linear decision feedback MIMO receiver that successively removes interference from the channel matrix from the receiver outputs for each data symbol. As the MMSE and ZF backends already reach the PIC-bound this backend would not be able to perform better. So this receiver is not bounded by the interference contained in $\mathbf{H}$ but both by the CCF contributions which are shown to be negligible and the additional noise terms.

- The **DFT backend** is clearly outperformed by the other, more elaborate ones. One reason for this is of course that the DFT backend can not rely on any form of channel-state information, whereas ZF and MMSE know the channel matrix perfectly. Another reason that limits the performance of the DFT scheme is the well-known leakage effect [OSB98]. If we again interpret the DFT backend as an estimation of the PSD of the received signal at certain discrete frequencies this effect causes energy of DFT bins to "leak" over to neighboring bins. The fact that we implicitly use a rectangular window function on the frontend outputs makes this effect pronounced. In [Wit08c] it is shown that increasing the number of receiver channels and employing a window function that provides side-lope attenuation such as a Hamming window can significantly improve the performance. This is, of course, at the expense of adding complexity to the receiver which contradicts the potential low-complexity of the DFT backend.

- The nonlinear **signal-by-noise** crossterms have a significant influence on the receiver performance. This is intuitively clear if we consider that they only exist when the corresponding subchannel has its current data bit set to one. In this case the corresponding subchannel causes an additional noise term in the receiver.

- The influence of the **noise-by-noise** crossterms is significant at lower values of the SNR where the noise dominates the performance. This is why the influence of the signal-by-noise terms becomes more important at higher SNRs.

- The fact that the influence of the crosscorrelation-induced terms is vanishingly small, but not completely zero, is due to non-ideal **subchannel orthogonality** at the transmitter caused by pulse-shaping and a slight loss of orthogonality due to the channel. Simulation results of the orthogonality measures defined in Section 3.3.2 show that the orthogonality loss caused by the multipath channel is small. For example, the mean absolute per-symbol cosine of the signal angle is at about 0.02 which is negligible. Figure A.4 in Appendix A.3 contains results for these measures.

3.4.2 High bandwidth with $N = 3$

We decrease the number of carriers to $N = 3$, giving an overall bandwidth of about 1.5 GHz. The results for this simulation are shown in Figure 3.3.

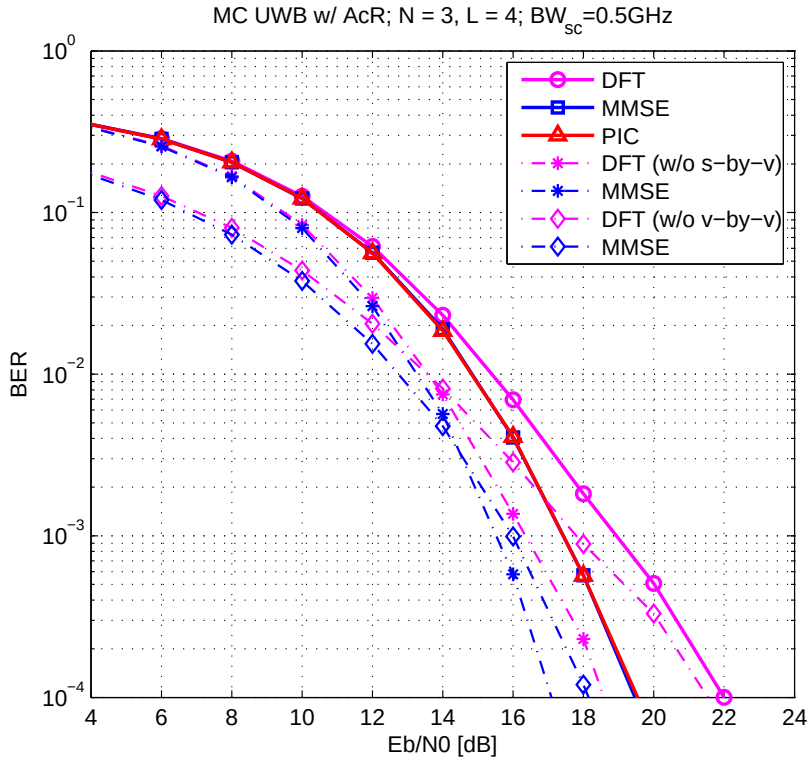

Figure 3.3: Performance for $N = 3, L = 4$ and $BW_{sc} = 0.5$ GHz

Discussion: Here we have three transmit signal subchannels and four receiver channels. The bandwidth of the subchannels is again 500 MHz. Solid lines correspond to the receiver operation including all terms. The ZF backend has been omitted because its performance is again equal to the MMSE backend. We can observe:

- The influence of the **crosscorrelation**-induced terms is again negligible, meaning that the BER-curves for DFT and MMSE with and without these terms are almost the same. For $N = 3$, the influence of these terms has to be quite small because the number of CCF-induces terms scales with N^2.

- The second important result is that the **DFT backend** is now able to separate the subchannel data simply because the leakage effect is reduced. The performance of this low-complexity backend is not much behind the backend that perform an estimation of the channel matrix though the variance of the BER with respect to the channel realization is still slightly higher for the DFT backend.

- Concerning the **problem invertibility**, we can observe a mean condition number of $\mathbf{H}$ over 100 channel realizations of 2.2 and the diagonal entries of $\mathbf{H}^*\mathbf{H}$ dominate with almost 20dB over the non-diagonal ones, which confirms an even better invertibility with a lower number of channels.

- The **noise-by-noise** term which is shown here for the DFT backend, has a dominant influence on the performance for low SNR because it contains the noise terms with the squared noise power (see (2.16)). The influence of the signal-by-noise terms is more apparent at higher SNRs, as they decrease linearly with the SNR, while the noise-by-noise term decreases quadratically.

3.4.3 Low bandwidth with $N = 9$

The bandwidth of the individual subcarrier signals is now changed to $BW_{sc} = 100$ MHz, which implies that each subchannel is now no longer an UWB signal by itself. The overall signal has a bandwidth of about 1 GHz. The results for this simulation are shown in Figure 3.4.

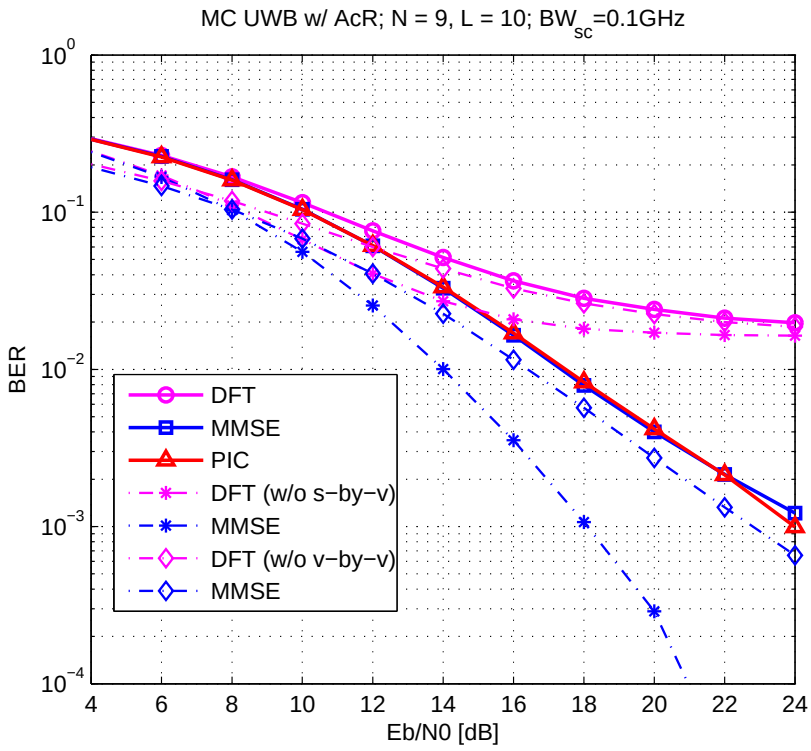

Figure 3.4: Performance for $N = 9, L = 10$ and $BW_{sc} = 0.1$ GHz

Discussion: We see a general performance degradation in all the backend schemes, which is due to reduced fading resistance.

- Again, the **CCF-induced crossterms** have a negligible influence on the BER. This is confirmed by the mean SIR(D_l), averaged over 100 channel realizations and the delay lags, which is about 18dB. The mean SIR(z_i), averaged over 100 channel

realizations and the decision variables, is again about 2dB higher than the mean $\mathrm{SIR}(D_l)$ for all backend schemes.

- For the DFT scheme, the **error floor** already seen in Figure 3.2 is now higher. It is also even more apparent that this error floor is not due to any of the receiver crossterms. This confirms that the DFT is not an optimal backend for this scheme though for some applications the performance of the higher bandwidth scheme might be sufficient.

- The influence of the **noise-by-noise** term is less than for the higher bandwidth which is due to the fact that its variance is reduced at a lower bandwidth. It is clearly not the performance limiting term for this scenario, as confirmed by the fact that the value of the SNR at which the signal-by-noise terms become more important is now reached much earlier.

- The fact that the system at this bandwidth lags behind the higher bandwidth scheme is further illustrated by the **invertibility measures**: The mean condition number of the channel matrix has increased to about 13 whereas the diagonality measure for $\mathbf{H}^*\mathbf{H}$ is still very good at about 19dB. We take the former fact as an indication of the increased fading, and the latter confirms that the channel autocorrelation functions are still sufficiently different from each other for the OFDM scheme.

- The subchannel **orthogonality loss** caused by the multipath channel is more severe than for the higher bandwidth scheme. This is shown in Figure A.5 in Appendix A.3. The reason for this is again the reduced multipath resilience. Nevertheless, the worse subcarrier orthogonality at the receiver is of course not the main problem of this scheme. This is confirmed by the fact that there is still no influence of the crosscorrelation-induced terms.

There is an additional important benefit with the higher bandwidth: As the delay lag spacing is chosen as the bandwidth inverse, a higher bandwidth leads to much lower values of the delays that are needed. From an implementation point of view this leads to much more relaxed requirements on the RF circuit design. However, a lower bandwidth will allow for a narrower front-end filter which will reduce the noise power but the advantage of increased fading resistance seems to more than outweigh this.

3.4.4 High data rate transmission with $N = 15$ and high bandwidth

The number of subcarriers is increased to $N = 15$, each one having a bandwidth of $BW_{sc} = 500$ MHz. This results in an overall bandwidth of about 7.5 GHz which is the maximum contiguous bandwidth any UWB system could possibly have due to the FCC regulations [FCC02]. The overall symbol period is reduced to a tenth of its original value, which is only 10ns. This results in a gross data rate (see Section 2.6) of 750 MBit/s. Simulation results are presented that use both a LOS channel ($K = 4$ and $\tau_{rms} = 1$ns) without intersymbol-interference (ISI) and a longer NLOS channel ($K = 0$ and $\tau_{rms} = 4$ns) that shows the influence of ISI on the performance. The results of this simulation are shown in Figure 3.5.

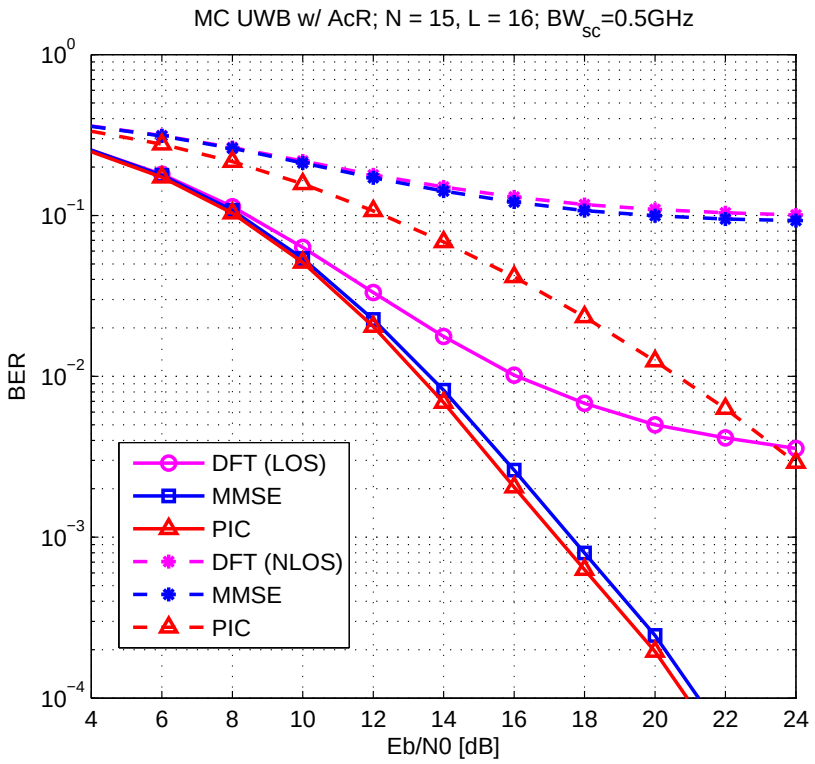

Figure 3.5: Performance for $N = 15, L = 16$ and $BW_{sc} = 0.5$ GHz, simulation of a short symbol interval with and without ISI

- Using the LOS channel for the **ISI-free** transmission the performance of this high-data rate scheme is surprisingly good regarding the high number of channels. Again, the influence of the CCF-terms is negligible (without ISI) and MMSE and ZF (not shown) backends operate almost at the PIC-bound for the LOS channel. The DFT backend, however, is greatly impaired by the leakage effect.

- For the NLOS channel the performance is severely deteriorated by the presence of **ISI**. All the backends reach about the same high error floor because no ISI-mitigation technique is applied. Hence ISI has to be avoided for a low-complexity receiver by the choice of a zero guard interval long enough to prevent ISI.

- Concerning the **invertibility measures** ISI of course leads to an increased ill-conditioning of the problem. For the ISI-free LOS channel we have a mean condition number over 100 channel realizations of about 5.8 which fits well with the results at this subchannel bandwidth until now. This mean condition number rises to over 51 when ISI is present. Interestingly, the diagonality measure of $\mathbf{H}^*\mathbf{H}$ only falls from about 13dB to 11dB. Hence the received subcarrier autocorrelation functions are still distinguishable, but this is outweighed by the bad invertibility.

4 Alternative Signaling Schemes

4.1 Motivation

So far we have considered an OFDM-based signaling scheme. Simulations of the AcR performance showed that this transmission scheme works well, meaning that we can obtain steep BER curves. We also observed an influence of the subcarrier bandwidth on the performance. Increasing the bandwidth led to better multipath resistance and a lower BER. The question is: Can we come up with a signaling scheme that fulfills our orthogonality conditions from (2.14) *without* separating the subchannel signals in the frequency domain?

We assume that such a set of pulses could possibly lead to an easier implementation of the transmitter because no carrier modulation stage would be needed. The system would be a multichannel impulse radio (IR) scheme without frequency separation. Furthermore, the bandwidth available for the transmit signal has to be split up for the OFDM scheme. Hence, there is a trade-off between multipath resistance and number of carriers. In a multichannel IR scheme, however, *each* of the subchannel signals could exploit the full bandwidth. So when we want to increase the subchannel bandwidth in the OFDM scheme, the AcR frontends noise bandwidth will increase proportional to N, which will probably boost the noise-by-noise term. In the IR scheme we have to consider this bandwidth increase only once for all channels.

The transmit signal can be modeled in the same way as in Chapter 2.2:

$$s(t) = \sum_{n=1}^{N} s_n w_n(t) \tag{4.1}$$

where we again skipped the random code sequence c_n for simplicity. The following chapters will investigate several signaling schemes which consist of a set of N pulses $w_n(t)$ that are modulated by the data symbols.

4.2 Definitions

The multichannel autocorrelation receiver measures samples of the received signal autocorrelation function. Hence some alternative signaling schemes could possibly be found by not designing the signal shapes themselves but rather the second order statistics of the signaling waveforms. As we will make use of the correlation properties of signals we need to define the auto- and crosscorrelation functions (ACF and CCF).

For two deterministic discrete-time sequences $x[m]$ and $y[m]$ of length M the CCF at time lag d is:

$$\Phi_{xy}[d] := \frac{1}{||x[m]||\ ||y[m]||} \sum_{m=0}^{M-1} x[m]y^*[m+d] \tag{4.2}$$

where (4.2) is the ACF when $x[m] = y[m]$ and $||x[m]||$ is the norm of the sequence $x[m]$ defined as the square-root of the scalar product of the sequence with itself (see also (3.9)). The normalization by the product of the norms is of course optional but it is useful, because the Cauchy-Schwarz-inequality guarantees that $|\Phi_{xy}[d]| \leq 1$. This greatly helps when comparing correlation properties throughout this chapter. In the case that the sequence $x[m]$ is a realization of a wide-sense-stationary (WSS) stochastic process we have to perform the ensemble average (with $E\{\cdot\}$ denoting expectation) and replace the signal norms by the standard deviations of the processes:

$$\Phi_{xy}[d] := \frac{1}{\sigma_x \sigma_y} E\left\{x[m] y^*[m+d]\right\} \tag{4.3}$$

For two deterministic continuous-time signals $x(t)$ and $y(t)$ of length T_s the CCF at time lag τ is:

$$\Phi_{xy}(\tau) := \frac{1}{||x(t)||\ ||y(t)||} \int_{t=0}^{T_s} x(t) y^*(t+\tau) dt \tag{4.4}$$

where (4.4) is the ACF when $x(t) = y(t)$. For stochastic WSS processes we perform the expectation analog to (4.3).

For the discussion of binary spreading codes we also need the definition of the *periodic* ACF and CCF (PACF and PCCF). For two sequences $x[m]$ and $y[m]$ of length M the PCCF is:

$$\tilde{\Phi}_{xy}[d] := \sum_{m=0}^{M-1} x[m] y^*[m+d] \tag{4.5}$$

where the shift of the sequence $y[m]$ is circular, thus $\tilde{\Phi}_{xy}[d]$ will be periodic with the period M. Again, when $x[m] = y[m]$ (4.5) will be the PACF. The periodic correlation functions are often found without normalization which we will adopt here.

4.3 General Requirements on the Signaling Scheme

This section provides a short summary of the requirements on the signaling scheme for the multichannel AcR. It also contains a short survey on bounds that exist for ACF and CCF properties of signals, which shows that we are not free do design both of these properties independently.

4.3.1 Correlation and Orthogonality Properties

The most basic condition that applies for our subchannel signals is of course given by our orthogonality condition in (2.14) and repeated here:

$$\langle \psi_n(t); \psi_{n'}(t + D_l) \rangle = 0 \qquad \forall\ n \neq n' \text{ and } \forall\ D_l \in \{D_l\} \tag{4.6}$$

The importance of this condition is that, if we can fulfill it, then our MIMO signal model from (2.18) holds because the matrix $\mathbf{G}$ will vanish. It was shown that the OFDM scheme is resilient concerning these CCF-induced interference terms which is of course due to the

frequency separation of its subchannel signals. Every signaling scheme with sub-optimal CCF properties in the sense of (4.6) faces the challenge that there are always $N(N-1)$ CCF-induced receiver crossterms, whereas there are only N information carrying signal-by-signal terms. This explains why the performance of alternative schemes with non-zero mutual crosscorrelations degrades with an increasing number of subchannels which will be shown in this chapter.

The fact that the multichannel AcR calculates samples of the received signal ACF, requires to put some effort in the design of the subchannel ACFs. This chapter will also show schemes that fail to do so, which results in bad performance. In Section 3.3.1, several invertibility measures were introduced where, e.g., $M_{diag}(\mathbf{H}^*\mathbf{H})$ was interpreted as the degree of distinguishability of the received subchannels ACFs. As this measure was high for the well-performing OFDM scheme we expect it to be also a criterion for other signaling schemes.

4.3.2 Channel Influence on the Correlation Functions

In general an intuitive interpretation of transmission schemes designed for this multichannel AcR is that all the usable signal sets have to somehow carry the information in their autocorrelation function as this is measured by the receiver frontend. So we attempt to transmit information in the signal ACF. Such an attempt has also been made in [ND03] but with filters matched to the signal ACFs in the receiver and with frequency-separated pulses. This reference states that the shape of a pulses ACF is relatively robust to the multipath propagation, whereas the pulse shape is not.

An elaborate discussion of the statistics of the correlation functions of UWB channels can be found in [WP08] where, e.g., the expected value of the received pulse autocorrelation function is derived as:

$$E\{\Phi_{gg}^{T_I}(\tau)\} \approx \Phi_{ww}(\tau) \int_0^{T_I} P_h(t)dt \tag{4.7}$$

where the function $P_h(t)$ is the *average power delay profile* (APDP) of the multipath channel and the correlation function $\Phi_{gg}^{T_I}(\tau)$ is the ACF of the received pulse

$$g(t) = h(t) * w(t) \tag{4.8}$$

as it is calculated in the receiver frontend (cf. Section 2.2) for the integration interval $[0, T_I]$. Hence (4.7) is the expected value of the ACF of the received signal. This equation tells us that this received signal ACF is a scaled version of the transmitted ACF which also motivates the concept of transmitting a specially designed ACF over the multipath channel.

Especially for noncoherent receivers which often perform autocorrelation operations this is useful: The *pulse-shape* of an UWB signal is severely distorted by the multipath channel, whereas the shape of its autocorrelation function is not. A noncoherent receiver will have difficulties coping with the signal distortions as no channel estimation is performed, but it might be able to exploit the information that is put in the shape of the ACF.

4.3.3 Elementary Bounds on the Correlation Properties

Welch [Wel74] derived a lower bound on the maximum crosscorrelation of signals. He considered the periodic and aperiodic correlation functions, the latter being the more important here. The Welch-bound for a set of M signals of length N is given as:

$$\Phi_{\max} = \sqrt{\frac{M-1}{M(2N-1)-1}} \tag{4.9}$$

where $\Phi_{\max}$ denotes the maximum value of the set of the values of the aperiodic auto- and crosscorrelation functions for all delay lags of the signal set. Welch derived this bounds for vectors of length N, not explicitly for continuous-time signals. He however refers to the fact that with the use of the sampling theorem the problem of designing (band-limited) continuous-time signals can always be reduced to the design of discrete-time signals or vectors.

Sarwate [Sar79] also gives a bound for how small the ACF and CCF of a set of signals can be simultaneously. His work considers the periodic correlation functions and gives the tightest bound [Goi98] for families of M sequences of length L where $M < L$. The usefulness of the Sarwate-bound is founded on the fact that it relates ACF and CCF maxima with each other:

$$\frac{1}{N}\tilde{\Phi}_{xy_{max}} + \frac{N-1}{N^2(M-1)}\tilde{\Phi}_{xx_{max}} \geq 1 \tag{4.10}$$

where this bound on the maxima of the periodic correlation functions can be related to those of the aperiodic correlation functions as will be further shown in Section 4.5.

There is also a contribution from Saporta [Sap64] in which the average crosscorrelation of a set of N continuous-time signals is related to their average energy. The latter lower-bounds the average CCF values. However no treatment of delay lags greater than zero in the correlation functions is performed.

These and more bounds and properties of periodic and aperiodic correlation functions can also be found in [SP80].

4.4 Discrete Prolate Spheroidal Sequences

4.4.1 Properties and Usage

Discrete Prolate Spheroidal Sequences (DPSS) are the discrete-time equivalent to Prolate Spheroidal Wave Functions (PSWF) [SP61], [Sle78]. They are interesting pulse waveforms, because of their unique property of being those functions with the highest possible energy concentration to an interval in time domain while simultaneously being band-limited. They have been proposed by some authors for UWB signaling (see [UZN04], just to give one example) but mostly for M-ary orthogonal signaling with coherent Rake reception. Their applicability to UWB signaling is due to the fact that a set of DPSS is orthogonal and that they have controllable bandwidth and time concentration.

The PSWF also play an important role in several fields of theory. They can be found for example in the dimensionality theorem (also known as the Landau-Pollak-Theorem) [PS08], which relates a set of time-limited signals that are approximately band-limited (or

vice-versa) to the minimal dimensionality needed to represent those signals. There the PSWF are the orthogonal basis functions for the representation of the signal set.

One drawback of the DPSS is that no closed-form solution exists. As we are interested in their general applicability to the multichannel AcR, we will resort to a simple algorithm for their generation [GH94], [ZM05]. The continuous-time PSWF can be formulated in terms of a second order differential equation and can be found as a combination of Legendre polynomials. Their discrete-time versions, the DPSS, can be obtained by the solution of an eigenvalue problem.

4.4.2 Signal Generation and Modulation

A DPSS with index limitation to the range $m = 0, ..., M-1$, denoted by $u_i[m]$ or by an $(M \times 1)$ vector $\mathbf{u}_i$ satisfies:

$$\mathbf{C}\mathbf{u}_i = \lambda_i \mathbf{u}_i \tag{4.11}$$

where an $(M \times M)$ matrix $\mathbf{C}$ was introduced whose elements are given as:

$$c_{i,j} = \frac{\sin(2\pi W[j-i])}{\pi[j-i]} \qquad \text{for } i, j = 1, ..., M \tag{4.12}$$

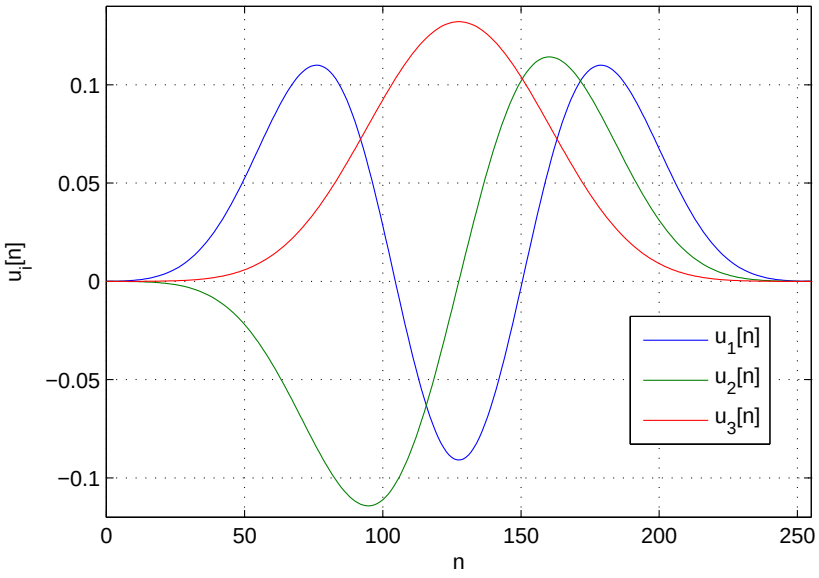

Figure 4.1: Example of a set of three DPSS

Here the factor W relates to the bandwidth of the (band-limited) DPSS and the amount of their energy concentration in time domain is given by the corresponding eigenvalue, which is in the range of $[0, 1]$. The eigenvalue spread of $\mathbf{C}$, however, indicates that this method of DPSS construction is very ill-conditioned. There are some eigenvalues that are

close to one and (depending on the choice of W, see [ZM05] for details) many that rapidly decay towards zero. The eigenvectors corresponding to the latter are not usable as signals. So when constructing DPPS this way one has to be careful which eigenvectors are selected as signals.

Figure 4.1 shows an example set of three DPSS constructed using (4.11). This is a set of orthogonal sequences with respect to the index set $[0, ..., M-1]$ and also $[-\infty, ..., \infty]$. Due to the controllable bandwidth and the inherent band-limitation no additional pulse-shaping is needed that might harm orthogonality. We also observe that the DPSS have a constant pulse-width independent of their order i.

4.4.3 Performance Results

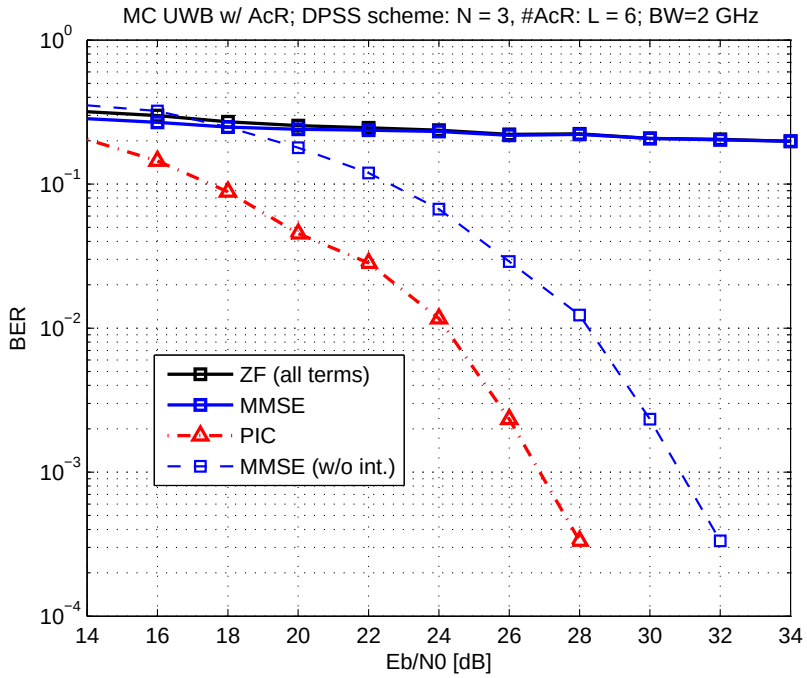

Figure 4.2: BER performance for the DPSS scheme with 3 subchannels and 6 receiver channels

Figure 4.2 shows the performance for a DPSS scheme with a bandwidth of 2 GHz, three subchannels and six receiver channels. A Ricean multipath channel model with a K-factor of $K = 4$ and $\tau_{rms} = 4$ns has been used. We see that a high error floor is reached considering the solid lines that represent the receiver operation including all the crossterms. The blue dashed line indicates the hypothetical performance without all contributions caused by the crosscorrelation-terms. For this case a discrimination of the signals is possible although this result clearly lags behind the PIC-bound, which indicates that the problem invertibility concerning the conditioning of the channel matrix is also worse than for the OFDM scheme.

This scheme suffers from the fact the a set of DPSS is only orthogonal if the sequences are not shifted with respect to each other. Taking our orthogonality condition from (2.14) into consideration we required the subchannel signals to be orthogonal for all delay lags of the AcR. These are again chosen as the bandwidth inverse, which is one nanosecond in this case.

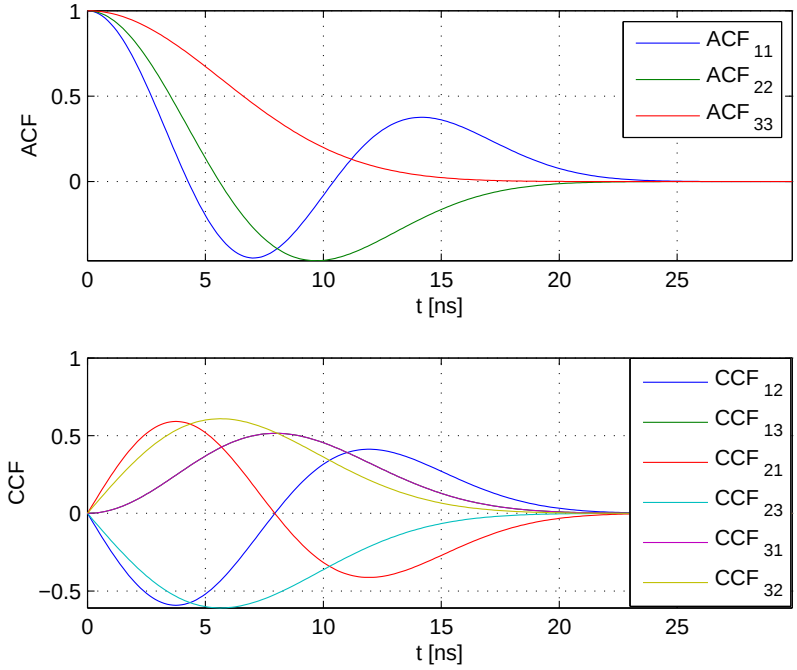

Figure 4.3: Auto- (top) and crosscorrelation (bottom) functions of a set of three DPSS

Figure 4.3 shows auto- and crosscorrelation functions for the used signal set, where only positive lags are shown. We see that orthogonality is given for lag zero but the CCF is clearly non-zero for lags $|D_l| > 0$. Taking into account that the AcR measures the sum of the CCFs of all the channel combinations, the energy of $\mathbf{y}_{ccf}$ will dominate over the useful signal energies contained in $\mathbf{y}_{ss}$ which was also confirmed by simulations calculating the SIR defined in (3.17) and (3.18).

Simulations have been done with frequency-separated DPSS. Here the channel separation was possible, though such a scheme has no apparent advantage to the conventional OFDM scheme.

4.5 OPAM Scheme with binary Codes

4.5.1 Motivation

The previous section dealt with using Discrete Prolate Spheroidal Sequences as a signal set for the multichannel AcR. This concept failed due to the significant crosscorrelation

contributions for delay lags $D_l \neq 0$ or, in other words, the violation of the orthogonality condition (2.14). We still want to obtain a set of signals that is not separated in frequency but satisfies this condition, while we do not expect to be able to *exactly* provide zero CCF levels. In general we want to obtain a set of signals usable for our pulse shapes $w_n(t)$ that provides low mutual crosscorrelation. A modulation scheme, in which a set of orthogonal pulses is used to represent the data symbols is generally referred to as *Orthogonal Pulse Amplitude Modulation* (OPAM) [BLM04]. The idea presented in this section is to use binary code sequences with well-known correlation properties and use them for signaling.

4.5.2 Binary spreading Sequences

We borrow the idea of binary spreading sequences from Code Division Multiple Access (CDMA) schemes. There, binary sequences are used which are designed for enabling receivers to sort out individual users by correlating the received signal with the users *spreading sequence*. The spreading sequences that are used in such systems should have high autocorrelation peaks for delay lag zero and low mutual crosscorrelation, such that the multi-user interference is suppressed.

Lots of research has been conducted concerning these sequences or codes (see [Dix76], [Goi98], [DJ98] for example). We only want to wrap up the most important points for this thesis here. In the field of binary sequence design the *periodic* discrete correlation functions play an important role. Their definition can be found in (4.5). The values of the sequences are confined to the binary alphabet $\{-1, 1\}$. We hope to be able to exploit the correlation properties also in the sense of non-periodic correlation functions as they are more applicable to the AcR signaling scheme. However we need the definitions of the PACF and the PCCF for the discussion of the commonly used binary sequences:

M-sequences: These are also called pseudo-noise (PN) sequences. They are generated using binary feedback shift-registers that have a certain feedback pattern. This pattern is also referred to as the *generator polynomial*. If certain conditions concerning these polynomials are met [Goi98], the register outputs lead to sequences of maximum length, hence the name. For a shift register with n bits this maximum length is given as $M = 2^n - 1$. This value denotes the number of bits after which the sequence repeats itself. We will continue to denote the sequence length with M. Tables for the generator polynomials can be found for example in [Dix76].

Their PACF has a value of M at lag zero and is -1 for all other lags. However, M-sequences are not designed to directly provide low mutual CCFs, so they do not seem directly usable for our scheme. Their importance comes from the fact that they are used for the generation of Gold- and Kasami-codes.

Gold sequences: Gold [Gol67] found a set of sequences that have the desirable property of a *bounded* periodic CCF that assumes three defined values. They are generated using the modulo-2-addition of phase-shifted versions of so-called *preferred* pairs of M-sequences [Goi98]. These M-sequences have to have the same length M which is also the length of the individual Gold-sequences. They create an amount of $M + 2$ Gold-sequences which corresponds to the modulo-2-addition of one M-sequence to all (cyclical) phase shifts of the other one plus the two original M-sequences themselves.

At delay-lag zero a set of Gold-sequences has a non-zero PCCF but they can also be made completely orthogonal for lag zero by using a method mentioned in [DO99], that also increases their length by one.

Kasami sequences: The sequences found by Kasami [Kas66] have four-valued PCCFs. They come in different sets: There is a large set of Kasami-sequences which has the advantage of providing a huge supply of codes which is important in multiuser CDMA-systems. However their PCCF properties are slightly worse than those of the small set of Kasami-sequences. These reach the well-known *Welch-bound* [Wel74] that lower-bounds the mutual crosscorrelation of a set of signals (see also Section 4.3.3). This bound is missed by the Gold-sequences by a factor of at best $\sqrt{2}$ for large sets of sequences. Kasami sequences are not orthogonal to each other.

Walsh-Hadamard-codes: These are used in conjunction with other codes in some CDMA systems. They are orthogonal by default and are used for user separation. However, CDMA systems that are using them are synchronous and they do not provide orthogonality when shifted with respect to each other [Mol06].

These sequences have very regular bit patterns which lead to very messy PSDs of the transmit signal which makes their direct usefulness for OPAM doubtful.

We note that both the Gold- and Kasami- and possibly the Walsh-Hadamard codes could be candidates for our signaling scheme because the motivation behind them is based on the fact that they provide low mutual crosscorrelation. There is one other possibly important point: The binary sequences have fixed lengths, always given by powers of two. Only for these lengths they have their defined correlation properties which means that their flexibility is limited in this sense.

4.5.3 Signal Generation and Modulation

The basic idea is to assign the well-known correlation properties of the binary sequences to continuous-time signals that we can use as our set of N pulses $w_n(t)$. The sum of these pulses will be our composite multichannel transmit signal like in (4.1). For the generation of this continuous-time signal we choose the above mentioned OPAM-approach [BLM04]. In this scheme the transmit signal for one symbol period is written as:

$$s(t) = \sum_{n=1}^{N} s_n w_n(t) \tag{4.13}$$

where we recognize the similarity to our multichannel signal from (4.1). The pulses $w_n(t)$ can be generated with the help of a binary sequence $x_n[m]$ and a *chip-waveform* $h_c(t)$ of length T_h:

$$w_n(t) = \sum_{m=0}^{M-1} x_n[m] h_c(t - mT_c) \tag{4.14}$$

It is well-known [BLM04] that if we make the translates of $h_c(t)$ mutually orthogonal then the pulses $w_n(t)$ can be made orthogonal to each other by the choice of the spreading

sequences $x_n[m]$. The individual binary values of $x_n[m]$ will be called *chips* in the following. This tells us that we can carry over the property of orthogonality from binary codes to continuous-time pulses created with them. Another fundamental result that motivates the assignment of the overall correlation properties in the same way is stated by Sarwate in [SP80]. For *any* choice of $h_c(t)$ the PCCF and CCF maxima can be related as:

$$\max\{|\Phi_{xy}(\tau)| : 0 \leq \tau \leq T\} = \lambda \max\{|\tilde{\Phi}_{xy}[d]| : 0 \leq m \leq M-1\} \tag{4.15}$$

where the constant λ is the energy of the pulse waveform $h_c(t)$, such that $\lambda = \int_0^{T_h} h_c^2(t)dt$. Sarwate considers periodic signals $x(t)$ and $y(t)$ with a period of T seconds, which we could generalize to be our symbol period for each subchannel signal.

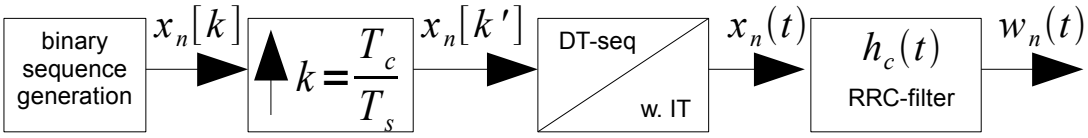

Figure 4.4: Generation of one subchannel pulse for the OPAM/CDMA scheme

An overview of the signal generation for the n-th pulse $w_n(t)$ is shown in Figure 4.4. The first block generates one of the binary spreading sequences mentioned above. A continuous-time signal is obtained by converting the discrete-time sequence into a weighted impulse train which is done by the third block in the system. The bandwidth B of this signal is controlled by the chip-waveform $h_c(t)$, which we choose as a root-raised-cosine (RRC) filter with the pulse duration T_p. Thus the bandwidth is given by:

$$B = \frac{1}{2T_p} \tag{4.16}$$

We will design the RRC filter such that the overall raised-cosine filter (the concatenation of transmit and receiver front-end filter) has its zero-crossings equal to the duration of the chips of $x_n[m]$ after their conversion to a continuous-time impulse train. Therefore consecutive chips will not interfere with each other in the signal $w_n(t)$. This explains the purpose of the upsampler in Figure 4.4. Zeros are placed in-between the chips to allow for values of $h_c(t)$ at these sampling instants which is needed for the simulations. The upsampling ratio is chosen as $k = T_c/T_s$ where T_c is the time between individual chips and T_s is the inverse of the sampling frequency f_s. If we want the zero-crossings of the overall raised-cosine filter to be aligned with the chips, we have to choose $T_p = T_c$. In terms of the bandwidth we can write

$$B = \frac{1}{2T_c} = \frac{f_s}{2k} \tag{4.17}$$

Figure 4.5 shows an example for a pulse generated with the scheme mentioned above using a chip-sequence from an orthogonalized set of Gold-sequences of length 31.

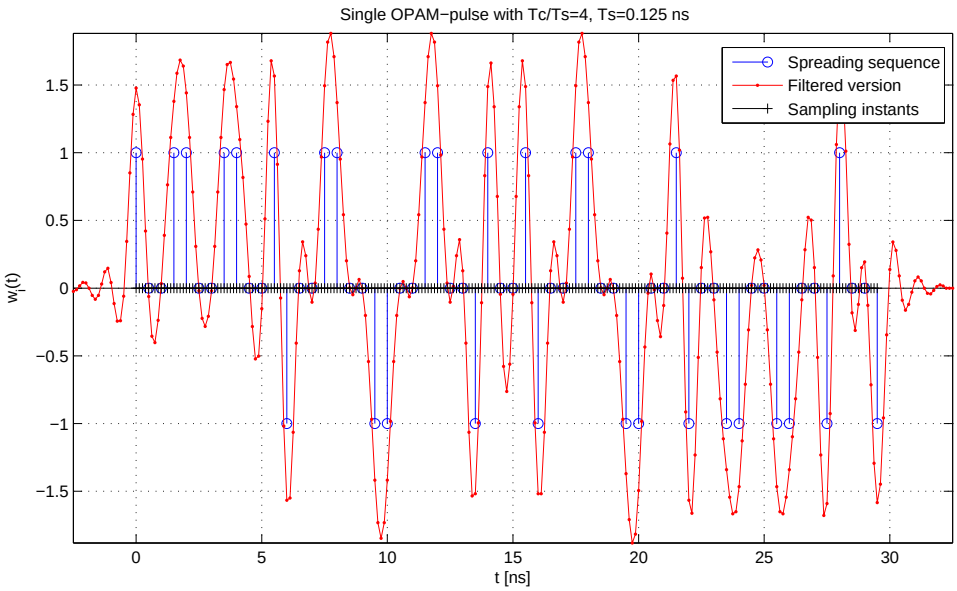

Figure 4.5: Example for one pulse $w_i(t)$ generated with the OPAM/CDMA scheme

Note: The use of the term *OPAM* is a slight abuse of notation here as it is somewhat misleading: Only for orthogonal spreading sequences the pulses $w_n(t)$ of our signal set will be orthogonal to each other. For codes like the ordinary Gold- or Kasami-codes this will not be the case.

4.5.4 Performance Results

Several performance simulations of the OPAM-scheme with CDMA spreading codes have been done. In general they show rather non-satisfying results. Despite the fact that we designed signal sets with the help of binary sequences having optimized mutual cross-correlation properties, the performance is not much better than for the DPSS-scheme presented in the previous section. The reasons behind this are discussed below by means of an example using Kasami sequences as they provide the best crosscorrelation properties.

Discussion: Figure 4.6 shows the performance of the OPAM/CDMA-scheme with the use of Kasami sequences of length 63, 3 transmit signal subchannels and 4 receiver channels. The overall bandwidth of the system is 2 GHz. Again the solid lines correspond to the AcR operation including all crossterms and the blue dashed line is the MMSE-performance without the CCF-induced interference terms. The PIC-bound is shown by the red dashed line. The result shows a high BER-floor, which has several reasons:

- The mean condition number of the channel matrix $\mathbf{H}$ averaged over 100 channel realizations was about 38 (see also Section 3.3.1). Singular value decompositions

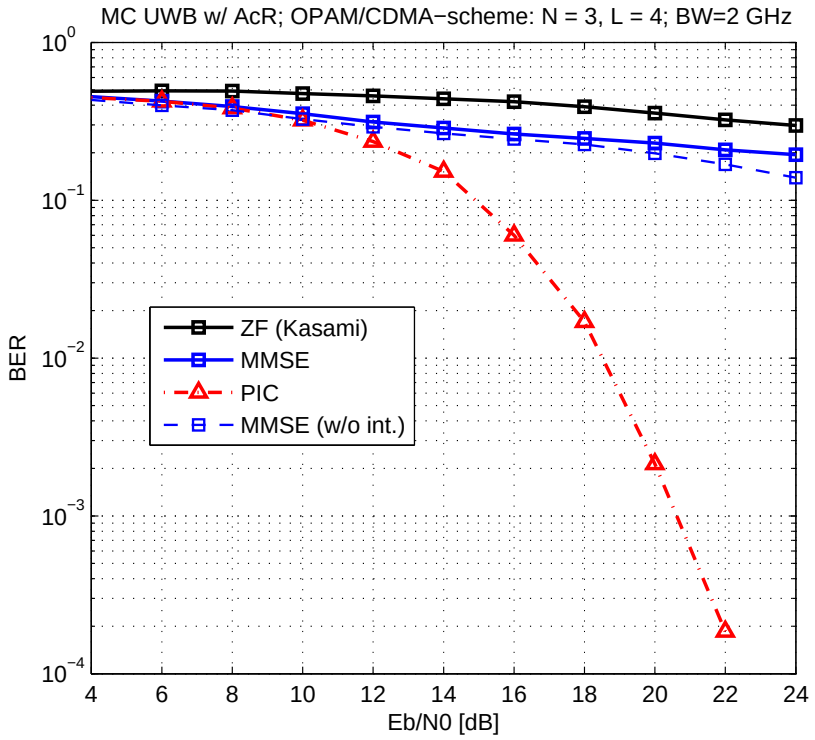

Figure 4.6: BER performance for the OPAM/CDMA scheme with 3 subchannels and 4 receiver channels and OPAM-pulses contructed with Kasami sequences

of $\mathbf{H}$ show that the singular value spread contained at least one rather small entry. This causes an increased ill-conditionedness of the problem.

- The reason for this ill-conditionedness is found easily by looking at Figure 4.7 which shows ACF and CCF properties of the signal set at the receiver. The blue dash-dotted lines represent the positive delay lags of the AcR. We see that the absolute value of the mutual crosscorrelation functions is indeed much less than in the DPSS scheme, which is due to the use of Kasami sequences. Nevertheless the autocorrelation functions show a fundamental problem: Comparing them we find that they share a common shape. Quantitatively this can be expressed by the diagonality of $\mathbf{H}^*\mathbf{H}$ (see (3.6) for example). Evaluating our matrix diagonality measure for this matrix product we find that the diagonal entries are at about the same level as the off-diagonal ones. In other words, the autocorrelation functions of the received signal are not fundamentally different, which does not allow for subchannel data separation at the receiver.

- The previous point is also the reason why the PIC-bound is not very meaningful in this scenario: It only considers the diagonal values of $\mathbf{H}^*\mathbf{H}$ (see (2.25)) and ignores the off-diagonal ones which we already know to be high.

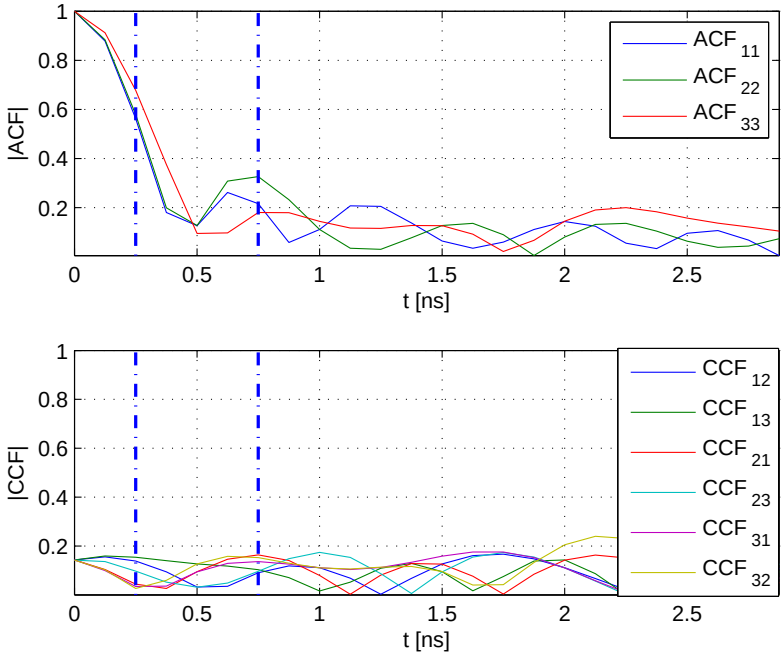

Figure 4.7: Auto- (top) and crosscorrelation (bottom) functions at the receiver of a set of three OPAM-pulses contructed with Kasami sequences; dash-dotted lines correspond to positive AcR delay lags

- It is not surprising that turning off the CCF-induced interference terms in the AcR does not improve the situation much. The set of signaling pulses provide rather good crosscorrelation properties although the OFDM scheme with its frequency separation can not be reached. The presence of small interference terms is not the main reason for the bad performance. However, if we had more transmit signal subchannels the overall level of CCF-induced interference of course would increase with the square of N. The latter fact is generally a limiting problem of sub-optimal signal sets in the sense of mutual crosscorrelation.
- Simulation results of the SIR are shown in Figure 4.8 where we notice that just the two smaller delay lags deliver signal energy that has a level that is significantly greater than the interference level. For the two channels with longer delays these levels are about the same. Although the SIR for the decision variables z_i is on average positive, though small, this useful signal-by-signal energy can not be used to separate the channels as discussed above.

Concluding remarks: All in all the non-satisfying performance of the OPAM/CDMA scheme is due to the fact of *not suitable* correlation properties. The binary spreading sequences were designed for providing low crosscorrelation (at least Gold-, Kasami and

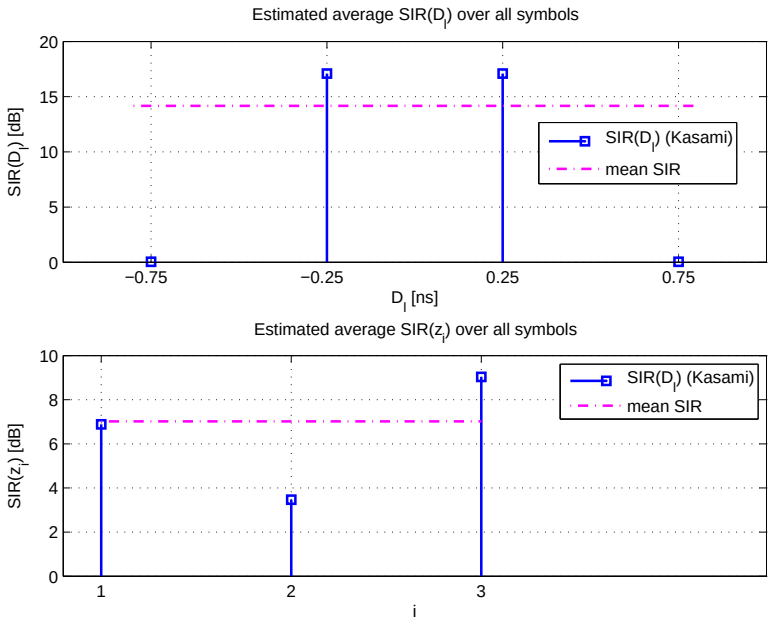

Figure 4.8: SIR(D_l) (top) and SIR(z_i) (bottom, for the MMSE backend) of a set of three OPAM-pulses contructed with Kasami sequences

Walsh-Hadamard-sequences). One simple problem is that they were also designed for having a noise-like autocorrelation function which means a peak at lag zero and lowest possible correlation elsewhere. The multichannel AcR is however dependent on significant and discriminable autocorrelation functions of the subchannel signals. The remainder of this thesis will deal with more specifically designed signal sets.

4.6 OPAM Scheme with Noise Waveforms

The previous two sections have shown that the design of an OPAM-like signaling set for the multichannel AcR is a non trivial problem when we attempt to use "off-the-shelf signals" like DPSS or CDMA-spreading codes and convert them to continuous-time signals. Both of these schemes provide *some* of the necessary properties but not *all*. OPAM signals with CDMA-codes like Kasami-sequences for example provide an *overall* low level of the CCF but their autocorrelation properties are not suitable due to their optimization for other applications.

However, we do not need to constrain the CCF values for *arbitrary* delay lags. The OFDM scheme provides this by its frequency separation but for a multichannel IR-like signaling scheme this is a strong limitation of the degrees of freedom in the signal design. Looking at our orthogonality condition in (2.14) we notice that the CCF values just have to be low or ideally zero near or at the set of the receivers delay lags $\{D_l\}$. Thus it could make sense to design a customized set of signals that attempts to fulfill (2.14), rather than

providing globally low CCF values. This set of signals should also convey the information sent by each subchannel *directly* in the ACF of that channel which has not been done by the schemes until now.

Note: Of course the term OPAM is misused notation also here as these signal sets will not be designed for having perfect orthogonality in the common sense either.

4.6.1 Possible schemes and their Properties

The operation of the multichannel AcR can be understood for the OFDM scheme via the fact that it is able to estimate the PSD of the received signal (see Section 2.5.2) or via the validity of the MIMO signal model from (2.18). When we look at the entries of the channel matrix $\mathbf{H}$ we see that they are the $h_n(D_l)$ from (2.12) which are the samples of the autocorrelation function of the received signal at the delay lags $\{D_l\}$. This leads to the interpretation of the operation of the AcR as a measurement of the received signal ACF which we will use here.

Suppose we have $N = L$ meaning that the number of subchannel signal equals the number of receiver channels. One column of $\mathbf{H}$, say the i-th, corresponds to the contributions of the i-th subchannel signal to all of the receivers channels. We could now design a signaling scheme for which each off-diagonal entry in $\mathbf{H}$ is as small as possible. The way to do this to create signals with the desired ACF properties. Those signals should be designed in a way that the i-th subchannel signal maximizes its diagonal entry in $\mathbf{H}$, $h_i(D_i)$ which requires a square channel matrix. So we need signals that have a high value or a peak in their ACF at their corresponding receiver delay lag and whose ACF is zero otherwise. The latter requirement can of course be relaxed by just demanding a zero ACF at the delay lags that correspond to the other channels in the system. Additionally, the *set* of those signals should have low mutual CCF values, at least at or around the receiver delay lags.

Considering the construction of one subchannel signal pulse $w_n(t)$ for the moment, we can create a peak in its ACF by adding it to a shifted version of itself. If we take a sample function of a Gaussian white noise process $n_n(t)$ and a time shift of d_n we can calculate one pulse $w_n(t)$ of our signal set:

$$w_n(t) = n_n(t) + n_n(t + d_n) \tag{4.18}$$

The sum transmit signal is then given by:

$$s(t) = \sum_{n=1}^{N} s_n \left[n_n(t) + n_n(t + d_n) \right] \tag{4.19}$$

In terms of a system of linear equations the case with a square system matrix corresponds to a system with one unique solution, assuming no rank deficiency. If we can diagonalize $\mathbf{H}$, we would even have the possibility of skipping the backend processing step altogether which we will try in the following. The scheme of (4.19) can be seen as a transmitted reference scheme because each subchannel consists of a superposition of two *identical* waveforms that carry the information of one modulating data bit s_n. Because each channel has its own reference noise waveform we will call this scheme *per-channel-reference* noise scheme. Its properties are discussed in the following section.

Per-channel-reference noise scheme

One subchannel pulse $w_n(t)$ generated by (4.18) has an ACF of:

$$\Phi_{w_n w_n}(\tau) = \delta(\tau) + \frac{1}{2}\left[\delta(\tau + d_n) + \delta(\tau - d_n)\right] \tag{4.20}$$

where $\delta(t)$ is the Dirac-delta function.

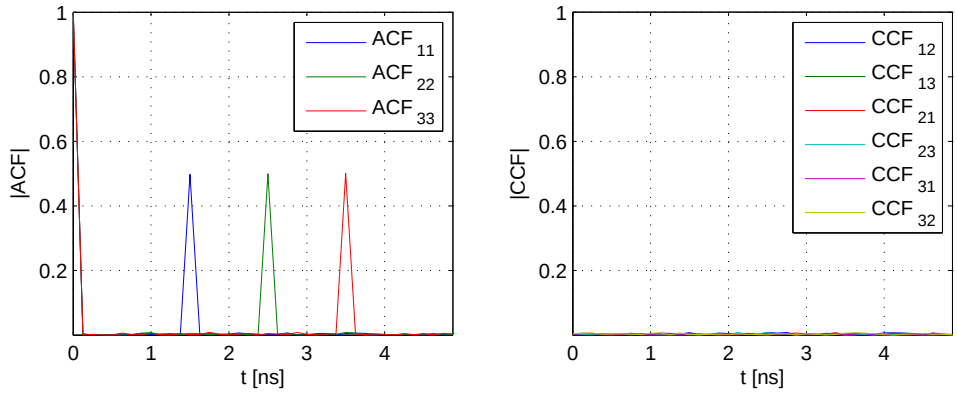

Figure 4.9: Ideal correlation properties of shift-added noise sequence with very long sequence lengths, left: ACFs of *individual* signals, right: Mutual CCFs

The ACFs and CCFs of an example set of such waveforms is shown in Figure 4.9. We see that each channel for itself has a peak that is one half of the magnitude of its ACF at lag zero. The latter corresponds to the pulse energy which implies that we can not make the peak at the delay lag d_n arbitrarily high because the pulse energy will always be constrained. The mutual CCFs of this signal set show very low values which is due to the fact that the noise processes are uncorrelated.

However we are interested in the ACF of the overall transmit signal as this will be sent over the channel and processed by the receiver. Additionally, we have to face the fact that the noise signals we can use will only be time-limited snapshots of the noise process that has the desired correlation properties. This very much hampers those properties as illustrated in Figure 4.10, which shows the ACF of the sum transmit signal (with $s_n = 1 \,\forall\, n$ corresponding to a symbol where all subchannel data bits are set to one) and the mutual CCFs of a set of pulses that have a length that corresponds to the parameters of the UWB system. In this case this was an effective pulse length of 25 ns at a sampling frequency of 8 GHz resulting in 200 samples per pulse. We see that the overall CCF-level rises to a non-zero level due to the finite length and also that the ACF looks non-ideal as the peaks are considerably decreased.

The essential problem is that due to the nonlinearity of the autocorrelation operation, the ACF of the sum signal is not the sum of the individual channel ACFs. The ACF of the sum signal $s(t)$ can be written as:

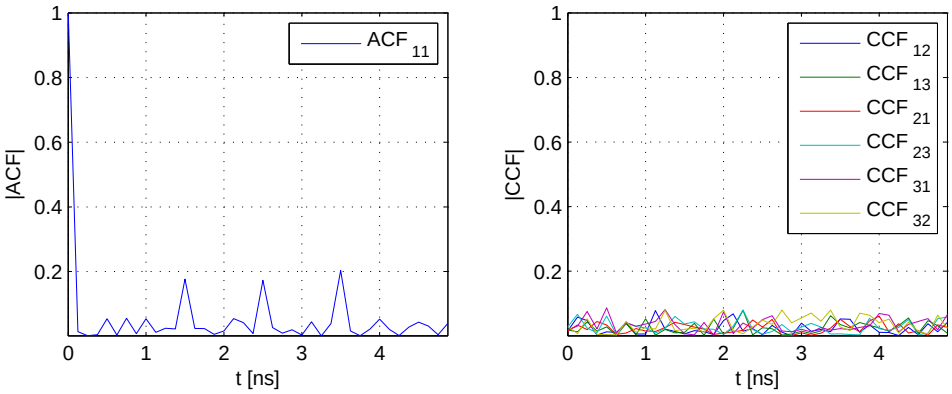

Figure 4.10: More realistic correlation properties of shift-added noise sequences with short sequence length (N=200), left: ACF of *sum* signal, right: Mutual CCFs

$$\Phi_{ss}(\tau) = 2N\delta(\tau) + \sum_{n=1}^{N} [\delta(\tau + d_n) + \delta(\tau - d_n)] \tag{4.21}$$

We notice that the lag-zero contribution scales with the factor $2N$ which is also viewable in Figure 4.10. Note that this is the "worst-case" in which all data bits s_n are set to one. So on average we have to deal with a reference power that will not be usable but will dominate over the usable signal power with a factor of roughly N. This and the increasing overall level of CCFs will be the limiting factors for this scheme for an increasing number of subchannels.

Common-reference noise scheme

The problem that the "reference" signal component in (4.21) is scaled with $2N$ in the sum signal ACF motivates another possible scheme using shift-added noise sequences. Looking at (4.19) we identify the problem: Each channel has its own distinct reference noise waveform that is added to the respective shifted noise sequences. Each of these references components needs transmit signal energy to be generated but is by itself not measured by a receiver delay lag.

We can however reduce this relative reference power in the signal by just using one *common* reference noise waveform and shifting each subchannel waveform with respect to it:

$$s(t) = n(t) + \sum_{n=1}^{N} s_n n(t + d_n) \tag{4.22}$$

where again $n(t)$ is a sample function of a white Gaussian noise process. This scheme is not as intuitive as the previous as the correlation properties of the transmit signal are only observable in the sum transmit signal and not in the subchannels. So it corresponds to the idea of designing the overall signal ACF and not the subchannel ACFs.

The overall ACF of a signal generated by (4.22) can be written as (again with $s_n = 1 \; \forall \; n$ to reflect the "worst-case" with the largest number of peaks):

$$\Phi_{ss}(\tau) = (N+1)\delta(\tau) + \sum_{n=1}^{N} [\delta(\tau + d_n) + \delta(\tau - d_n)] + \sum_{i=1}^{N} \sum_{\substack{j=1 \\ j \neq i}}^{N} \delta(\tau + d_j - d_i) \tag{4.23}$$

hence it consists of the same terms as the ACF for the per-channel-reference scheme, but with the scaling of the peak at $\tau = 0$ reduced to $N + 1$. The last term in (4.23) is a mixed term that consists of peaks at all the differences of delays, which are caused by using the same reference waveform. For now, we want to use all the ACF terms but the mixed term to create a signaling scheme that works just like the per-channel-reference scheme but with increased relative height of the ACF peaks at the AcR delays. That means we have to choose the delays of each channel such that the mixed terms do not coincide with them.

For the sake of an easier notation we consider the symmetry of an ACF and restrict ourselves to positive delay lags. First we choose equidistant delay lags and require that:

$$j > i \Rightarrow d_j - d_i > 0 \; \forall \; i, j \in \{1, ..., N\} \tag{4.24}$$

which just means that the delays increase with their respective index. We can write the "positive-lag" part $\Phi_{ss,\text{pos}}(\tau)$ of the ACF as:

$$\Phi_{ss,\text{pos}}(\tau) = (N+1)\delta(\tau) + \sum_{n=1}^{N} \delta(\tau + d_n) + \sum_{i=1}^{N} \sum_{j=i+1}^{N} \delta(\tau + d_j - d_i) \tag{4.25}$$

We will denote the last term, which is a simplified mixed term, as $\Phi_{ss,\text{mix}}(\tau)$. The choice of equidistant delay lags constrains the locations of the peaks in the ACF caused by the mixed term to a few locations that are given by integer multiples of the delay lag spacing. We denote this spacing by

$$\begin{aligned} d_{i+1} - d_i &=: c_{d,1} \\ d_{i+2} - d_i &=: c_{d,2} \\ &\vdots \\ d_{i+N-1} - d_i &=: c_{d,N-1} \end{aligned} \tag{4.26}$$

Now we can group the peaks in the ACF by their $c_{d,i}$ and obtain the simplified mixed term:

$$\Phi_{ss,\text{mix}}(\tau) = \sum_{i=1}^{N-1} (N-i)\delta(\tau + c_{d,i}) \tag{4.27}$$

where we note that this term put in (4.25) together with the symmetry of an ACF yields a complete description of the sum-signal ACF for the case that we have equidistant lags for all channels and a white noise signal $n(t)$. The $N(N-1)$ peaks from the mixed term

in (4.23) are converted to $N-1$ *effective* peak locations to which the mixed terms can contribute. We see that we have to choose the delay spacing such that it is not equal to the first peak location in the ACF. For example we will choose in the following $c_{d,1} = 1\text{ns}$ and $d_1 = 1.5\text{ns}$.

4.6.2 Signal Generation and Modulation

Per-channel-reference scheme

An overview of the signal generation for this scheme is given in Figure 4.11. One subchannel is generated by adding a WGN signal and a time-shifted version of itself. The resulting signal is filtered by a transmit pulse shaping filter $f_{tx}(t)$ that limits the signal bandwidth. The insertion of the zero guard interval for avoiding ISI is not shown here. Selecting the "prototype" signal as a WGN signal has the advantage that this signal is spectrally white and the power spectrum of the transmit signal can be completely determined by the squared magnitude of the transmit filter transfer function. The pulse is switched on or off by the corresponding data bit s_i.

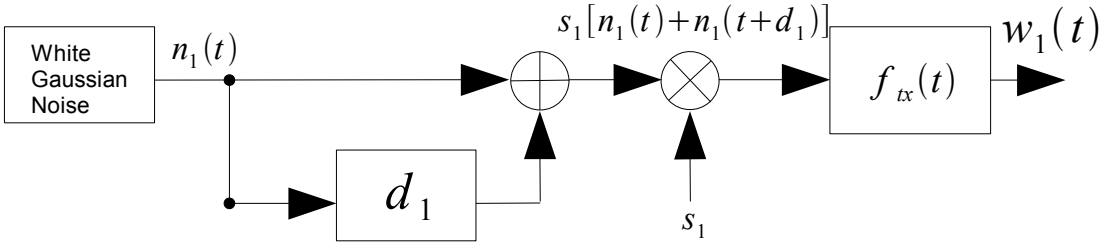

Figure 4.11: General scheme of the OPAM-noise modulator for the generation of one subchannel pulse of the signal set $\{w_n(t)\}$ for the per-channel-reference scheme

However the transmit filter transfer function has to be chosen with care. The ACF of the sum of the shift-added noise sequences $\tilde{w}_i(t)$ before the filter carries the information. We design this ACF such that it has peaks at the receivers delay lags as discussed before. Passing a signal through a linear time invariant system like $f_{tx}(t)$ of course influences its ACF. Denoting the sum signal (over all N subchannels) before the filter as $\tilde{s}(t)$ and the filtered sum signal as $s(t)$, we have the well-known identity (see, e.g., [BLM04]):

$$\Phi_{ss}(\tau) = f_{tx}(\tau) * f_{tx}(-\tau) * \Phi_{\tilde{s}\tilde{s}}(\tau) \tag{4.28}$$

We also have to consider the receiver frontend filter $f_{rx}(t)$ (see Figure 2.1). For the moment we neglect the channel in between to find a criterion to design this cascade of filters. This of course is much like the Nyquist criterion on pulse-shaping filters that is used to avoid ISI at the symbol instants, only that here we have to apply it to the ACF. The signal $s(t)$ is filtered by $f_{rx}(t)$, giving the received signal $r(t)$ that has an ACF of:

$$\begin{aligned}\Phi_{rr}(\tau) &= f_{rx}(\tau) * f_{rx}(-\tau) * \Phi_{ss}(\tau) \\ &= f_{tx}(\tau) * f_{tx}(-\tau) * f_{rx}(\tau) * f_{rx}(-\tau) * \Phi_{\tilde{s}\tilde{s}}(\tau)\end{aligned} \tag{4.29}$$

which can be interpreted as filtering the *ACF* of $\tilde{s}(t)$ by a cascade of four linear filters. This ACF is given in (4.21) as a sum of impulses. Linear filtering of Delta-impulses places copies of the filters impulse response at the locations of the impulses. This implies that the impulse response of the overall filter cascade has to have its zeros at integer multiples of the receiver delay lag spacing (assuming equidistant delay lags which we have here).

Looking at (4.29) we have two possibilities of achieving this: The first one is, looking at the second line, design the ACF of $\tilde{s}(t)$ and choose $f_{tx}(t)$ and $f_{rx}(t)$ as *fourth*-root raised cosine filters such that the cascade has a pulse width that is an integer multiple of the delay lag spacing. The second possibility comes from looking at the first line of (4.29) and is to directly design the ACF of $s(t)$ (including the transmit filters influence) and choose $f_{tx}(t)$ and $f_{rx}(t)$ as conventional square-root raised cosine filters. Both possibilities have been tested and show similar results which means that the ACF-properties at the receiver delay lags are not influenced by linear filtering. The performance results here are created using the second method because of its easier implementation.

A further complication arises from the time-limitation of the snapshots of the Gaussian noise process, which leads to a considerable variance of the correlation properties. Therefore it is not advisable to just generate one noise waveform per channel and perform the shift-add operation. The very random correlation properties will probably not meet the signaling requirements. The generated signals $w_n(t)$ have to be checked for their ACF and CCF properties before employing them as subchannel pulse waveforms. Therefore, a stochastic search algorithm is introduced which performs these checks. This algorithm will be explained in the next section but before, we shortly discuss the signal generation for the common-reference scheme.

Common-reference scheme

Figure 4.12 shows the signal generation and modulation for the common-reference scheme.

Each subchannel is a delayed version of the *same* noise process but for itself contains no peaks in its respective ACF. Not until the reference signal is added to *all* channels the ACF of the sum signal is generated. The signal is filtered by a transmit pulse-shaping filter for which the same considerations as for the per-channel reference scheme hold. If a data symbol consists of only zero bits then no reference component is transmitted.

The specific feature of this scheme is that it does not make sense to decompose the sum signal in subchannels and view their influence on the receiver. Another issue that has to be mentioned is that in this scheme the random code sequence from (2.1) can not be used because it alters the peaks in the ACF randomly. This is not the case for the per-channel-reference scheme in which the random sequence multiplies *both* the shifted signal and its respective reference. Hence the power spectrum of a signal generated with this method will show spectral lines and spectral smoothing will have to be accomplished by some other means such as random time hopping [HW06]. This will make the system more complex to implement and is omitted here because we only want to check the performance in comparison to the per-channel-reference scheme.

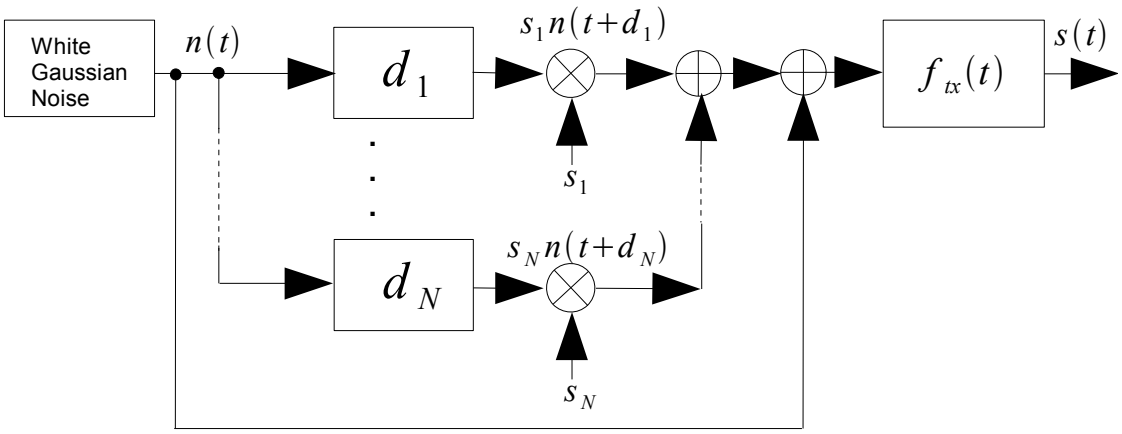

Figure 4.12: General scheme of the OPAM-noise modulator for the generation of the sum transmit signal for the common-reference scheme

4.6.3 Stochastic Search Algorithm and Measures of Correlation

We want to make the per-channel-reference signaling scheme robust by rejecting waveforms that do not meet certain correlation properties that we require from the scheme. A stochastic search algorithm is used that has the following iterative structure:

1. A candidate waveform $w_i(t)$ is generated for the i-th channel, just as in Figure 4.11, including the filtering step.

2. For $w_i(t)$ the following properties are calculated:

   a) ACF of the channel at delay lag d_i corresponding to the same delay lag of the receiver.

   b) ACF of the channel at the delay lags of the *other* $N-1$ transmit subchannels. These two steps are taken to make the channel matrix as diagonal as possible.

   c) CCFs of the channel with respect to all the other $w_j(t),\ j \in \{1, ..., i-1\}$ that are already calculated by the previous iterations. The CCFs are calculated for all the receiver delay lags. This step is done to make the influence of the CCF-induced interference matrix $\mathbf{G}$ as small as possible such that the linear MIMO signal model holds.

   The computational complexity of the last step of course scales exponentially with each overall iteration (with each new channel) so one could want to omit it. As the number of CCFs between the subchannels is $N(N-1)$ the overall CCF level will also grow roughly with N^2, thus skipping this step is not advisable.

3. After a specified number of iterations the algorithm chooses the best waveform that was found and proceeds to the next subchannel waveform $w_{i+1}(t)$.

This is done for all the N subchannels and the resulting set of waveforms $\{w_n(t)\}$ is used for the modulation. We now want to further specify the correlation measures that are calculated in step two of the algorithm. Generally a *mean-square-correlation*-measure is used for the CCF like it is also used with some variations in [DO99] for example. So in the i-th iteration, corresponding to the i-th subchannel signal, the mean-square CCF value for the current candidate signal $w_i(t)$ with respect to the other previously found subchannel signals $w_j(t),\ j \in \{1, ..., i-1\}$ is defined as:

$$\mu_{ccf,i} := \sum_{j=1}^{i-1} \sum_{D_l \in \{D_l\}} |\Phi_{w_i w_j}(D_l)|^2 \tag{4.30}$$

where $\{D_l\}$ is the set of all receiver delay lags and $\mu_{ccf,1}$ is zero per definition. For the ACF properties we calculate values of the (normalized) ACF at each of the D_l from $\{D_l\}$ and calculate for $w_i(t)$ the measures:

$$\mu_{acf,i} := \begin{cases} 1/2 - |\Phi_{w_i w_i}(D_i)| & \text{for } |\Phi_{w_i w_i}(D_i)| < 1/2 \\ 0 & \text{otherwise} \end{cases} \tag{4.31}$$

and

$$\overline{\mu}_{acf,i} := \frac{1}{N-1} \sum_{D_l \in \{D_l\} \setminus D_i} |\Phi_{w_i w_i}(D_l)|^2 \tag{4.32}$$

Hence (4.31) is a measure for the ACF of $w_i(t)$ at its corresponding AcR delay lag (it is zero for ACF values greater than its theoretical maximum and decreases towards zero for non-optimal values) and (4.32) is the mean-square value of the ACF of $w_i(t)$ at all the other channels delay lags. All in all, we can formulate an objective function that our search algorithm uses as a measure for the correlation properties of the pulse $w_i(t)$:

$$\mathcal{C}(w_i(t)) = \mu_{ccf,i} + \mu_{acf,i} + \overline{\mu}_{acf,i} \tag{4.33}$$

The search algorithm now performs a search over a predefined number of maximum runs and selects those $w_i(t)$ as subchannel pulse waveforms that minimize their respective $\mathcal{C}(w_i(t))$.

Figure 4.13 shows the correlation properties of a set of 3 pulses generated with the stochastic search algorithm. We see that at the respective receiver delay lags only the pulse of the corresponding channels has an ACF peak and all the others have a significantly low level there. The level of the mutual CCFs is also low at these lags. Comparing the overall level of the CCFs qualitatively with the OPAM/CDMA scheme from Section 4.5 (see Figure 4.7) that was using Kasami codes we see a similar level of the CCFs which is considered to be a good result, because the Kasami codes reach the Welch-bound for their CCFs.

Common-reference scheme: For this scheme the search algorithm is not suitable. We just perform a simple check on the candidate noise sequence here. The "worst-case" ACF (meaning a symbol with all data bits s_n set to one) is calculated for the candidate noise waveform. The peaks at the receivers delay lags should theoretically (see (4.23)) be $1/(N+1)$ times the peak at lag zero. This is checked with a simple threshold.

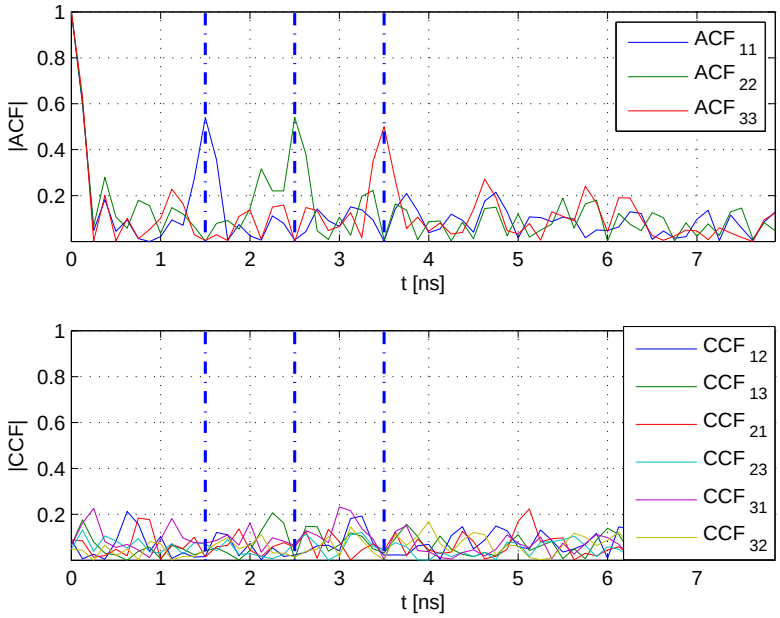

Figure 4.13: Individual ACFs and CCFs of 3 shift-added noise subchannel signals using the stochastic search algorithm with ACF and CCF criteria; Vertical lines denote receiver delay lags

4.6.4 Performance Results

This section provides performance results for several example scenarios and both the signaling schemes explained.

Influence of the search algorithm

Figure 4.14 shows the performance of a signal set of the per-channel-reference noise scheme generated with the search algorithm discussed above over an additive white Gaussian noise channel (AWGN) in comparison with a randomly generated set of pulses. We see that in general the transmission of the ACF works, even *without* any backend processing (indicated by "skipped" backend).

Discussion: It is shown that the search algorithm is essential for the per-channel-reference noise scheme. For the optimized signal set we get a performance close to the PIC-bound even when no backend processing is used on the frontend outputs. The latter as well as the MMSE backend show a rather high error floor for the randomly chosen signal set mostly due to high mutual CCF contributions. Finally even the PIC-bound for this scheme lags behind the optimized one which indicates a generally worse invertibility.

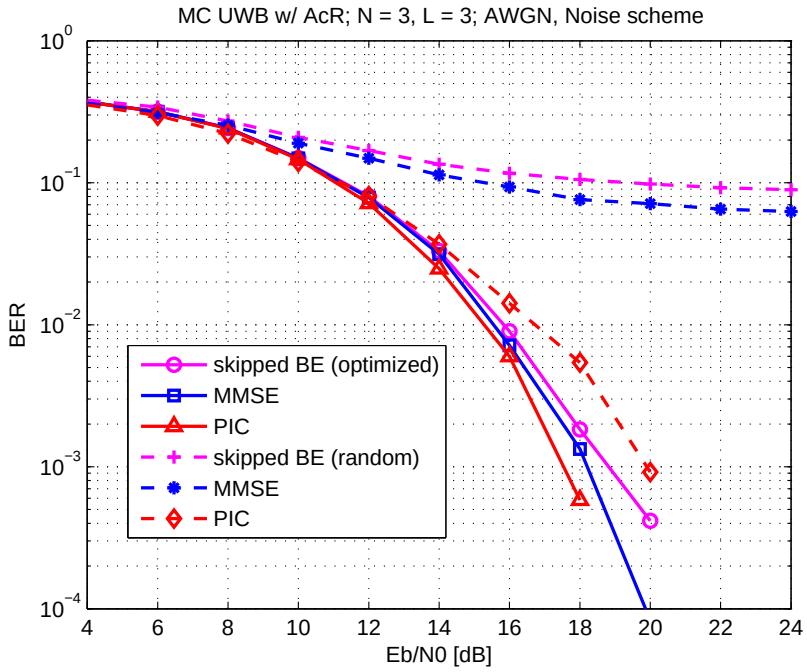

Figure 4.14: BER Performance for the noise scheme, $N = 3$, $L = 3$ for three backends and a signal bandwidth of 4GHz. Shown are an optimized scheme (solid lines) and a randomly chosen sheme (dashed lines) over AWGN

Transmission with $N = 3$ over an LOS channel

Figure 4.15 shows the performance for the noise scheme with three subchannels using the optimized signal set from above as well as one example for the common-reference scheme. An LOS radio channel model has been used with an rms-delay-spread $\tau_{rms} = 5$ns and a Ricean K-factor of $K = 4$.

Discussion:

- The transmission over the multipath channel works for the MMSE backend that performs channel estimation although the performance degradation due to multipath propagation is apparent. Concerning the skipped backend scheme that for the AWGN channel was able to almost reach the MMSE backend, this degradation is even more severe. This is, of course, due to the fact that no channel compensation is performed. Comparing this with the DFT backend from the OFDM scheme we notice that the latter was more robust concerning the multipath channel although also no channel estimation was performed. The reason for this is that still signal properties were exploited by analyzing the received signal ACF in frequency domain which corresponds to a PSD estimation (see also 2.5.2).

- If we look at the **SIR** (see also Appendix A.4) and compare it to the OFDM scheme

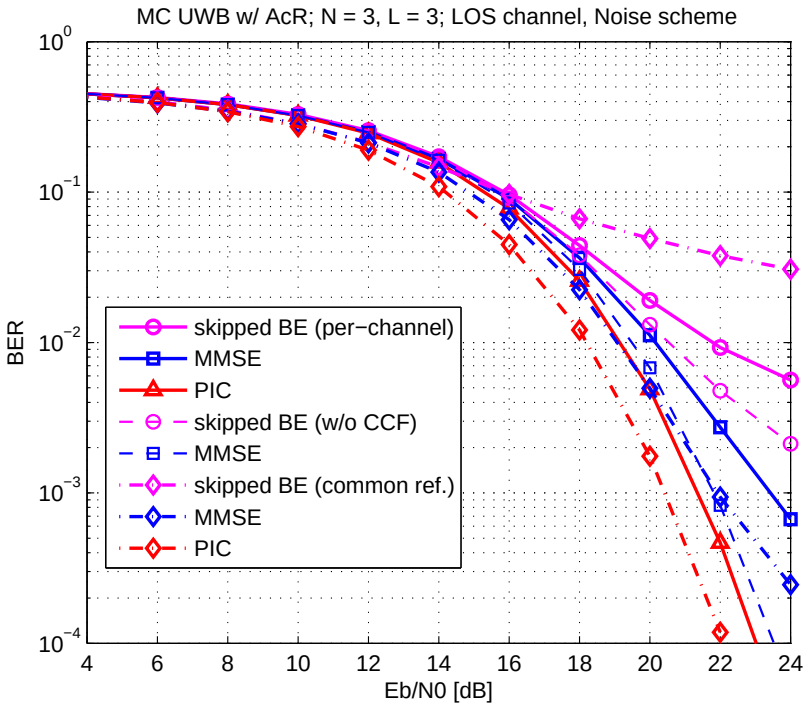

Figure 4.15: BER Performance for the noise scheme, $N = 3$, $L = 3$ for three backends and a signal bandwidth of 4 GHz, transmission over a Ricean channel with $\tau_{rms} = 5$ns and $K = 4$; solid and dashed lines are the per-channel-ref. scheme, dash-dotted lines for the common-ref. scheme

we see another advantage of the latter: There the mean SIR (even using nine subchannels) over 100 channel realizations was about 22dB for the MMSE backend, whereas here it is down to about 15dB here. The fact that for the OFDM scheme we could observe a *gain* in the SIR caused by the backend can not be observed here where the SIR at the delay lags and the decision variables are at about the same level. Hence the frequency separation of the OFDM subcarriers still outperforms the CCF properties of the noise waveforms.

In the BER curves this is apparent if we look at the dashed lines that indicate the performance without the CCF-induced terms. The performance is significantly increased here and the MMSE backend operates almost at the PIC-bound.

- The **common-reference** scheme using the MMSE backend slightly outperforms the per-channel scheme which is also the case for the corresponding PIC-bounds. Interestingly the skipped backend scheme is far behind the per-channel reference scheme. This is due to the fact that the common-reference scheme is not explicitly designed to diagonalize $\mathbf{H}$. Concerning our invertibility measures we have much better values for the per-channel scheme: The mean condition number cond($\mathbf{H}$) is about 1.8 and the diagonality measure for $\mathbf{H}^*\mathbf{H}$ (see (3.6)) is about 10dB. For the

common-reference scheme the mean of cond($\mathbf{H}$) is about 3.2 and the diagonality measure is even down to only 1.2dB.

- Comparing the **invertibility measures** for the per-channel scheme to those of the OFDM scheme with nine channels we find that cond($\mathbf{H}$) was about 3.6 there. This can be explained by the fact that the noise scheme is designed to diagonalize the channel matrix. On the other hand the diagonality measure $M_{diag,[dB]}(\mathbf{H}^*\mathbf{H})$ defined in (3.6) is about 10dB for the noise scheme and almost 17dB for the OFDM scenario which could be due to the fact that the frequency separation of OFDM also creates very distinguishable ACFs of the subchannel signals.

Transmission with $N = 5$ over an NLOS channel

Figure 4.16 shows the performance for the noise scheme with five subchannels using the stochastic search algorithm from above as well as one example for the common-reference scheme. An NLOS radio channel model has been used with an rms-delay-spread $\tau_{rms} = 8$ns and a Ricean K-factor of $K = 0$ such that this corresponds to the channel models used for the simulations of the OFDM scheme. The rms-delay spread has been chosen a little shorter to avoid ISI because for the noise scheme the pulses themselves are longer than for the OFDM scheme. Note that the y-axis is scaled to have its minimum at a BER of 10^{-3} which is one order of magnitude more than until now. This is done to better show the differences between the curves.

Discussion:

- Generally the separation of data symbols conveyed in multiple ACFs sent over the multipath channel seems to be challenging. The previous simulation with $N = 3$ has shown that it works in principle but with an increasing number of subchannels the overall level of CCF-induced contributions of course increases. Turning off the CCF-terms in this scenario (not shown in the figure) leads to a BER-curve for the MMSE backend that approaches the PIC-bound.

- A comparison of the per-channel and common-reference noise scheme shows an interesting behavior: Compared with the previous scenario the skipped-backend scheme works much better now which might be due to good correlation properties of the selected noise reference. But for the MMSE backend it is slightly outperformed by the per-channel scheme at high SNRs. Again this is due to the low diagonality measure of $\mathbf{H}^*\mathbf{H}$ for the common-reference scheme which is again at just around 1dB. The PIC-bound is neglecting this bad problem invertibility and nicely shows the benefit of just using one common reference waveform instead of N.

Concluding remarks: All in all the noise schemes are the first alternative schemes that provides a possible discrimination of the subchannel signals at the AcR. However, the BER performance lags behind the OFDM scheme, especially over the multipath channel. The limiting factor of the per-channel-reference scheme is the influence of the CCF-induced interference. The other possible limiting factor which was the influence of the number of subchannels on the possible height of the ACF peaks of each channel (see (4.21)) was

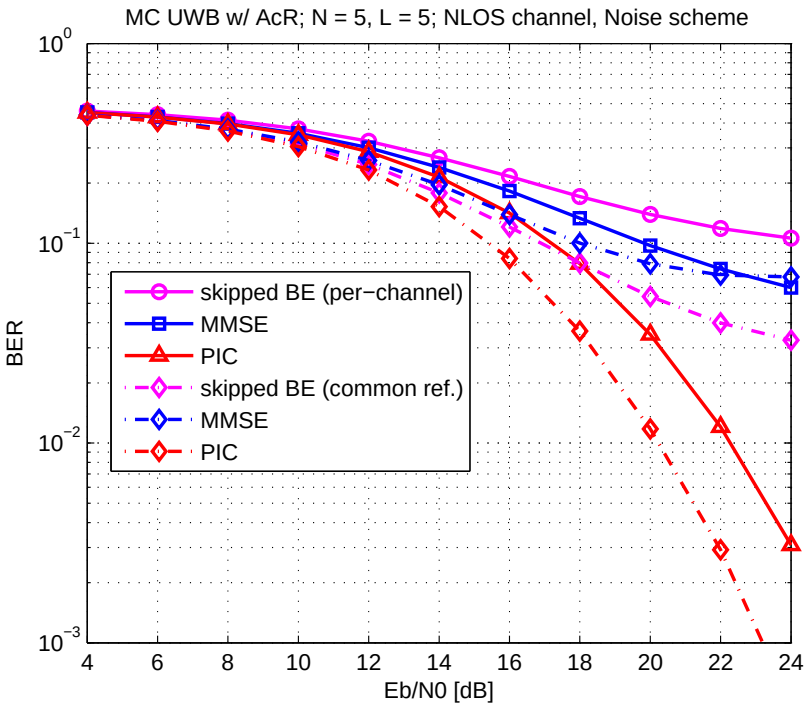

Figure 4.16: BER Performance for the noise scheme, $N = 5$, $L = 5$ for three backends and a signal bandwidth of 4 GHz, transmission over a Rayleigh channel with $\tau_{rms} = 10$ns and $K = 0$; solid lines are the per-channel-ref. scheme, dash-dotted lines for the common-ref. scheme

also considered in simulations. In a scenario with $N = 6$ the modulating bit sequence was altered such that for each symbol no more than three bits were set to one. This showed a positive influence on the performance but the influence of turning off the CCF-interference terms was significantly higher, so the latter is considered to limit the performance of this scheme most severely.

This problem of the scaling of the ACF peaks was addressed by the design of the common-reference scheme which was shown to improve the performance by increasing the relative height of the channels peaks in the transmit signal ACF. The problem with this scheme is that the off-diagonal entries of the channel matrix can not be kept low as with the per-channel scheme.

4.7 Sequence Design using Genetic Optimization

The last section dealt with the generation of waveforms for the subchannel signals that carry the information directly in their autocorrelation function. We have seen that due to practical considerations such as limited length of the signals, the correlation properties can not be made arbitrarily good in the sense of the orthogonality condition (2.14). In

Section 4.6.3 measures for the ACF and CCF properties of subchannel signals designed for the multichannel AcR were presented. The problem of the huge variance of those properties in candidate signals was addressed with a stochastic search algorithm. This algorithm however shows no form of convergence: If a signal is found with good, but not the best properties it is thrown away without exploiting its properties any further.

This drawback is addressed in this section with the use of a stochastic optimization algorithm, namely the genetic optimization. We still want the same correlation properties as for the shift-added noise sequences, so the cost function $\mathcal{C}(w_i(t))$ from (4.33) will largely be the same, only the optimization algorithm will change.

4.7.1 The Genetic Optimization Algorithm

We want to use an optimization algorithm that minimizes our cost function $\mathcal{C}(w_i(t))$, that is based on a sum of several ACF and also mutual CCF properties of the current signal $w_i(t)$. Assume we aim to design a pulse of 25 ns length at a sample rate of 8 GHz, hence one discretized version of a candidate $w_i(t)$ will consist of 200 samples. So the optimization algorithm works on a problem with 200 variables and a cost function, about whose structure nothing is known to us. This cost function could probably have a lot of local minima and also has to consider all previously designed signals for the CCF-measures.

In such circumstances, the use of stochastic optimization algorithms is worthwhile [BEM08]. Such an algorithm accepts an increase of the cost function during its iterations which helps to escape local minima. One other problem of the search algorithm from Section 4.6.3 mentioned earlier is that it throws away possibly useful signal candidates and does not further exploit their properties. This is addressed by the use of the *genetic algorithm* [Hol75] that has many similarities to biological evolution. In [CMR05] the genetic algorithm is used to generate CDMA-spreading codes with good correlation properties which also motivates its use here.

Here we just want to give a very basic overview of the genetic algorithm and refer to the literature for further details [BEM08], [Hol75]. The algorithm first creates a *population*, in our case this is a randomly generated set of candidate sequences. For all of them, the cost function $\mathcal{C}(w_i(t))$ is evaluated, resulting in a so-called *fitness*-value of each member of the population. The set of sequences then creates a descendant generation with the help of genetic operators:

- *Recombination:* Certain individuals of the population exchange randomly selected values with each other (also called cross-over).
- *Reproduction:* A parent individual can be passed to a descendant generation without changes. This is usually done for a set of individuals that already have a good fitness. This set is sometimes called the *elite*.
- *Mutation:* A few values of each sequence are changed randomly, e.g. by the addition of small random numbers.

All of these operators have an associated probability with which they are applied, e.g., mutation is usually done with a low probability. The algorithm iterates until the fitness function converges or a maximum number of iterations is reached.

4.7.2 Signal Generation and Modulation

For the actual optimization we used the genetic optimization toolbox provided by Matlab. An overview of the selected optimization parameters can be found in the next subsection. Here, the general approach to the optimization problem is discussed.

The design of the subchannel signal waveforms is carried out sequentially: The first channel is optimized just by taking into account its ACF properties. This means that its fitness function $\mathcal{C}(w_i(t))$ just consists of the ACF terms. The peak at its own delay lag should be as high as possible whereas the values of the ACF at the other delays should be as low as possible. One difference to the cost function of the noise scheme as defined in (4.33) is that we can increase the maximum ACF peak height defined as 0.5 in (4.31). This is due to the fact that we are not shift-adding sequences which constrains this peak.

Starting with the second channel's pulse waveform we also take the CCF properties into account. Every additional channel's pulse is checked concerning its CCF to all the previously found pulses. This is done in the same way as in the stochastic search algorithm. Once again we choose to directly design the *filtered* waveforms, hence the transmit pulse shaping filter is a root-raised cosine filter as explained in Section 4.6.2.

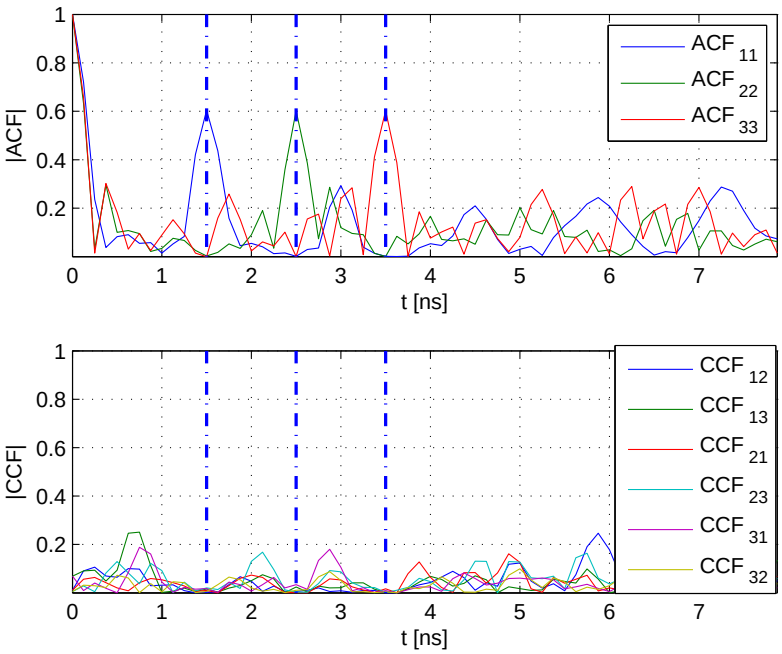

Figure 4.17: Individual ACFs and CCFs of 3 subchannel signals generated with the genetic optimization algorithm; Vertical lines denote receiver delay lags

Figure 4.17 shows the correlation properties of an example set of three pulses generated with the genetic optimization algorithm. Comparing with Figure 4.13 that shows the similar case for the per-channel-reference noise scheme we observe that the peaks at the respective delay lags are increased and that the CCF properties around the receiver delay

lags are also significantly improved.

The process of signal generation and modulation is very similar to that of the common-reference noise scheme from Section 4.6.2 (see also Figure 4.12). The pulse shapes found by the optimization are already filtered so they are just modulated by the data bit sequence and the sum signal over all channels is the transmit signal.

4.7.3 Optimization Parameters

This section contains an overview of the most important optimization parameters.

- *Number of variables:* In this case, this is just the number of samples in the sequences, which is given by 200 (see Section 4.7.1).
- *Initial population:* The initial number of sequences was chosen to be 100 individuals (sequences). Their values are random numbers drawn from a Gaussian distribution.
- *Elite count:* This is the number of individuals that are passed to the next generation without any modification. These are the sequences with the best value of the fitness function. The elite count was set to two.
- *Crossover fraction:* This is the fraction of individuals of the descendant generation which is created by a combination of values (samples) of two individuals from the parent generation. The value was set to 0.8.
- *Mutation fraction:* This fraction of the descendant generation is created by random mutation of values (samples) of one individual from the parent generation. This mutation is done by adding Gaussian random numbers to some of the samples. The mutation fraction is given implicitly by all individuals not created by crossover and not being the elite of the parent generation.
- *Stopping criterion:* The genetic algorithm stops if the number of iterations exceeds 200 or if the value of the fitness function for the best individual does not change by more than 10^{-6} from one iteration to the next.

The values for elite count and crossover fraction are the standard values provided by the Matlab genetic optimization toolbox. Tuning them to slightly different values did not change the results drastically.

4.7.4 Performance Results

As the correlation properties of the sequences obtained from genetic optimization are in principle similar to those of the noise schemes we use the same scenarios for the performance simulations for the sake of comparability. For the case of the LOS channel we also present a comparison of a system at a bandwidth of 4 GHz and one at 2 GHz.

Transmission with $N = 3$ over an LOS channel at different bandwidths

Figure 4.18 shows the BER performance over the same LOS channel model that was used for the noise schemes.

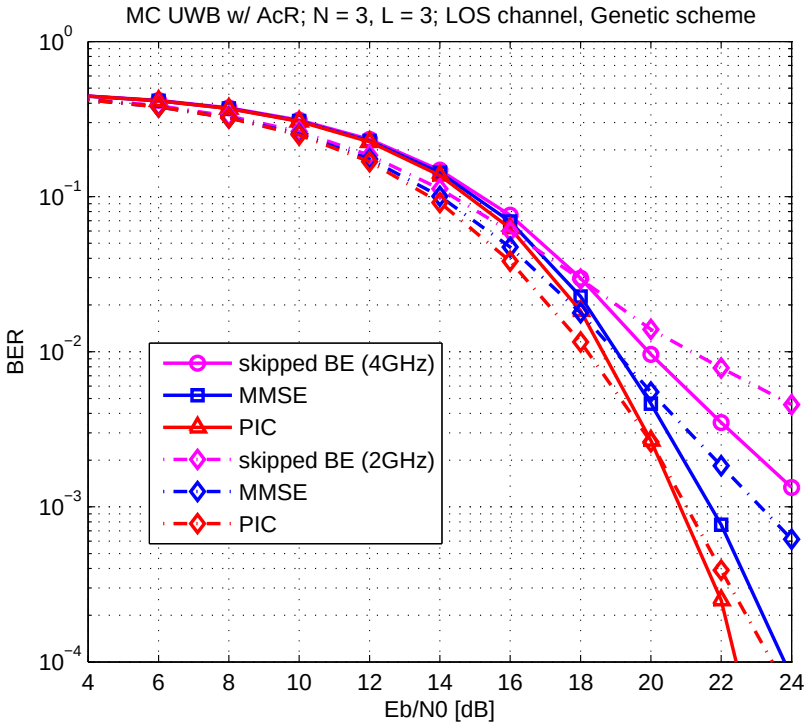

Figure 4.18: BER Performance for the genetically optimized scheme, $N = 3$, $L = 3$ for three backends and signal bandwidths of 4 GHz (solid lines) and 2 GHz (dash-dotted lines), transmission over a Ricean channel with $\tau_{rms} = 5$ns and $K = 4$

- Comparing the performance with those from Figure 4.15, we observe that the genetically optimized waveforms at a bandwidth of 4GHz outperform the corresponding shift-added noise waveforms, only the PIC-bound of the common-reference noise scheme has a similar performance.

- Concerning the **invertibility measures** for the better performing 4-GHz-case, the performance is a little better than for the per-channel reference noise scheme: The mean condition number of $\mathbf{H}$ is about 1.7 and the mean diagonality measure for $\mathbf{H}^*\mathbf{H}$ is about 12dB. The latter may be an indication why the performance of the OFDM scheme (there this measure was at almost 20dB) is still not achievable.

- One goal of designing alternative signaling schemes was to exploit the benefits regarding fading resistance by using the full UWB **bandwidth** for each subchannel. This benefit is observable in Figure 4.18 when comparing the two systems at different bandwidths. A system at higher bandwidth performs slightly worse at low SNRs where the noise-by-noise term dominates the behavior. This term is of course boosted by the higher noise bandwidth of the receiver front-end filter (see also (2.16)). Comparing to the performance that is gained by the higher bandwidth at high SNRs this

performance penalty is not important.

However, comparing with the OFDM scheme at comparable bandwidth (see Section 3.4.1 and Figure 3.2) it is obvious that the BER curve for the OFDM scheme reaches its steep region much earlier. Even the genetically optimized scheme with only three channels needs a considerable higher SNR to be in the steep region of the BER curve.

- The performance in terms of the **SIR** is for the first time similar to the OFDM scheme. The mean SIR(D_l) over 100 channel realizations was about 20dB which is almost the same as for the OFDM schemes. Again a gain in the SIR(z_i) as it was the case for the OFDM scheme can not be observed. SIR(D_l) and SIR(z_i) are at about the same level. The high SIR is also the reason that no performance curves without the CCF-terms are shown as these are not much different to the performance with all the crossterms.

Transmission with $N = 5$ over an NLOS channel

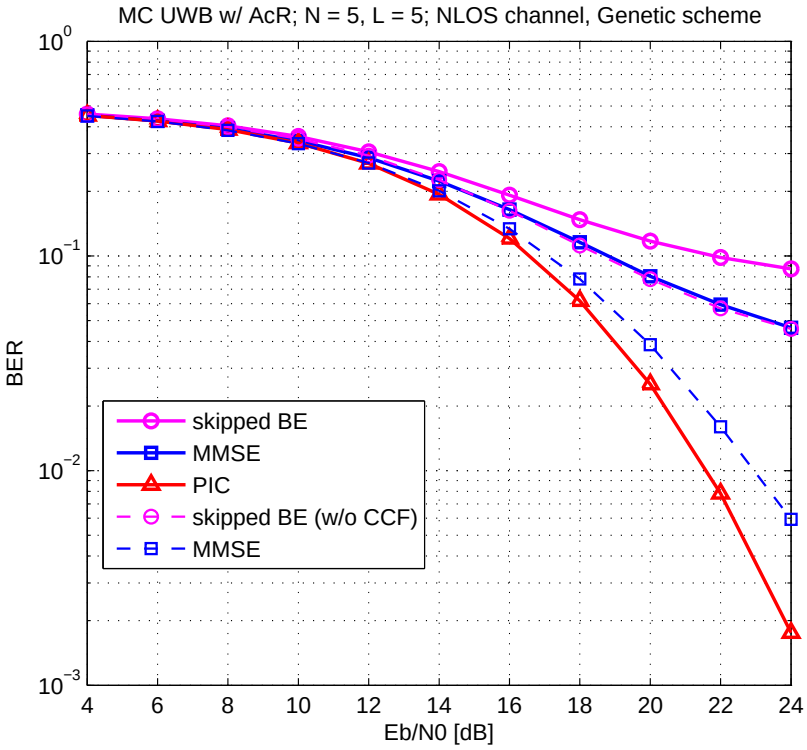

Figure 4.19: BER Performance for the genetically optimized scheme, $N = 5$, $L = 5$ for three backends and a signal bandwidth of 4 GHz; Shown is the performance with all terms (solid lines) and without CCF terms (dash-dotted lines); Transmission over a Rayleigh channel with $\tau_{rms} = 8$ns and $K = 0$

Figure 4.19 shows the BER performance over the same NLOS channel model that was

used for the noise schemes, again the BER-axis is scaled to have its minimum at 10^{-3}. The signal bandwidth is fixed at 4 GHz which was shown to yield better results in the previous section.

- The overall performance is only slightly better than for the corresponding noise schemes (see Figure 4.16). Again the main reason are the increased **CCF-terms** due to the longer NLOS channel. This is shown by the dashed lines that indicate the hypothetical performance without these terms. The skipped backend scheme is not improved that much in the sense that its BER-curve does not get steep by turning off the CCF terms. For the MMSE backend we observe that it approaches the PIC-bound where the latter itself is raised significantly by the longer NLOS channel and the higher number of channels.
- Concerning the **invertibility measures** we can observe a mean condition number of $\mathbf{H}$ of almost 5 and maybe more importantly the diagonality measure for $\mathbf{H}^*\mathbf{H}$ has dropped to only 4dB which indicates that the distinguishability of the received signal ACF is severely deteriorated.

Influence of Noise and Integration Interval

Figure 4.20 shows the BER-performance for the genetically optimized scheme at a bandwidth of 4 GHz with five subchannels over an NLOS channel. Only the MMSE backend is shown with different groups of receiver crossterms switched off and at two different integration intervals of the AcR.

- Simulations using different values for the **integration interval** T_I (30 ns and 60 ns compared to 23 ns for the 500 MHz OFDM scenario) have been done which have shown that, concerning the steepness of the BER curves in regions of high SNRs, an integration interval much higher than that of the OFDM scheme is beneficial. This of course also boosts the noise-by-noise term (see also (2.16)) which we expect to flatten the curves at lower SNRs. However, this effect is barely visible in the curves that correspond to the performance using all terms.

  The beneficial effect of a longer T_I was also observed for the noise schemes though it was weaker there. The reason for it might be that a longer integration interval is needed to actually yield a better estimate of the ACF of the received signal.

- The **noise behavior** is interesting: The noise-by-noise terms have a significantly larger influence on the scheme using a longer T_I which is supported by (2.16). Concerning the signal-by-noise terms we observe that the influence on the performance is less significant for the longer T_I scheme at low SNR where the noise-by-noise term is more important. This effect is reversed for the scheme with shorter T_I. In general, the noise-by-noise term governs the noise behavior at low SNR and its influence diminishes quadratically for high SNR. The signal-by-noise terms only decrease linearly with the SNR.

- Figure 4.20 shows again that the **CCF-terms** are the reason for the error floor. Without those terms, a rather steep BER-curve can be obtained.

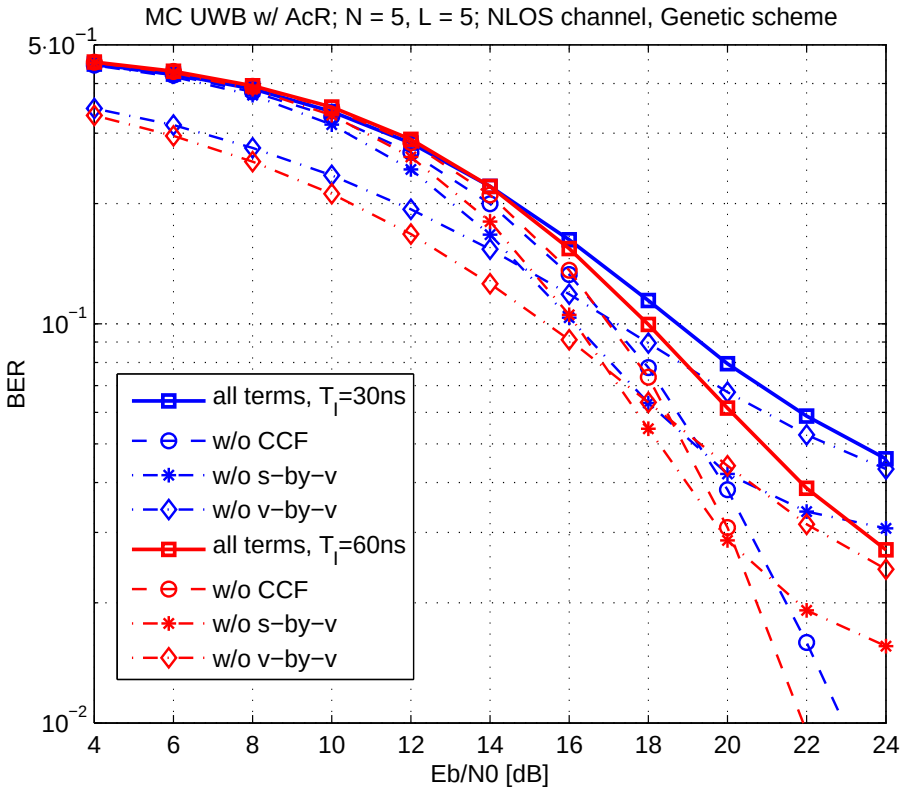

Figure 4.20: BER Performance for the genetically optimized scheme, $N = 5$, $L = 5$ for the MMSE backend and a signal bandwidth of 4 GHz; Shown is the performance with all terms (solid lines) and without specific crossterms terms (dashed and dash-dotted lines); Transmission over a NLOS channel with $\tau_{rms} = 8$ns and $K = 0$. Blue lines correspond to $T_I = 30$ns, red lines to $T_I = 60$ns

Concluding remarks: All in all the performance that is achievable with genetically optimized sequences is not dramatically different compared to the noise schemes. This is due to the fact that the noise and genetically optimized schemes still overall have the same correlation properties and work in a similar way. The difference is that the latter scheme achieves its properties better through the use of an optimization technique and may be used to check for the bounds of a scheme that tries to achieve certain correlation properties. Finally the OFDM scheme is still the signaling scheme that provides the best performance results in particular due to its much better robustness with respect to the multipath channel.

As it already was the case for the noise schemes one big practical problem is the constrained length of the sequences. When trying to fulfill the orthogonality condition (2.14) the restriction to a rather small set of samples imposes a huge reduction of the available degrees of freedom in the signal design. A tradeoff has to be found between the pulse length and the achievable correlation properties. Another important point which argues

	Corr. properties	**Invertibility**	**Comments**
OFDM	CCFs very low due to frequency separation, ACFs distinguishable	**H** generally well conditioned and robust with respect to channel	Most suitable and robust scheme
DPSS	CCF level high for $D_l > 0$	Irrelevant due to much too high CCF level	CCF terms dominate by far, therefore unusable
OPAM with binary codes	CCF level can be kept low, but ACF properties not suited	Bad due to the ACF properties	Not usable with common codes, maybe with customized codes
Noise schemes	ACF controllable, but overall CCF level is limiting	Very good but not robust with respect to channel	SIR decreases with N^2, practical problems
Genetic optimization	Optimized but still CCF is limiting	Very good but not robust with respect to channel	SIR decreases with N^2, practical problems

Table 4.1: Comparison of the signaling schemes for the multichannel AcR

for shorter pulse length is of course the impulse radio concept itself and the regulatory issues which constrain the transmit power spectral density.

4.8 Comparison of the Signaling Schemes

Table 4.1 shows an overview of the signaling schemes that have been used. The OFDM scheme is clearly the most suitable scheme for the multichannel AcR. Although other schemes like the noise schemes or the sequences obtained from genetic optimization achieve similar or even better results in terms of the condition number of the channel matrix, the OFDM scheme is the only one that provides steep BER curves for a higher number of channels and an NLOS channel.

We can identify the most important aspects concerning signaling schemes for the multichannel AcR:

- The most important criterion on a robust scheme is still the **mutual orthogonality** condition (2.14). This is also the reason for the dominance of the OFDM scheme which fulfills this by the frequency separation of its subchannel signals. A low overall CCF-level is essential because the number of CCF-induced interference terms scales with N^2 whereas the number of signal-by-signal terms only scales with N. Another interesting observation is that only for the OFDM scheme the ZF and MMSE backends were able to actually *increase* the SIR from the delay lags to the decision variables by around 2dB on average. For all the other schemes a *loss* of SIR could be observed caused by the operation of the backends.

- The **practical problems** indicated in the comparison table for the noise- and the genetically optimized schemes are the following: Firstly, the time limitation of the

pulse shapes makes the design of a suitable ACF challenging. To this end, several optimization steps had to be performed. Also, the pulses have to have a certain length in order to have specified correlation properties. This might lead to implementation problems in practical, energy-limited transceivers.

- There are also problems at the receiver related to the previous point: The AcR integration interval T_I is on the one hand confined by the noise variance (see (2.16)). On the other hand a longer T_I enables a better estimation of the signal's ACF. This influences the steepness of the BER curves in certain SNR regions as it was confirmed by the simulations for the genetically optimized scheme.

- It is also worthwhile to discuss the **measures of invertibility** from Section 3.3.1, namely the condition number of $\mathbf{H}$ and the diagonality measure of $\mathbf{H}^*\mathbf{H}$. We were able to improve the former with respect to the OFDM scheme by designing the subchannel ACFs but the latter measure provided by OFDM was out of reach for the alternative schemes. For example the mean diagonality measure over 100 channel realizations for an nine-channel OFDM scheme over the NLOS channel was about 17dB whereas it was only about 11dB even for the *three*-channel scheme that used genetically optimized sequences. We take this as an indication that the ACFs of the OFDM subcarrier signals still provide better separability of the subchannel signals than all the alternative schemes.

So the performance of the OFDM scheme could not be reached by other signaling schemes. The schemes that tried to use off-the-shelf signals (DPSS and CDMA codes) failed due to the fact that in the common applications of sequences that impose requirements on the correlation functions one of the requirements is often that the ACF should be noise-like. While being favorable for radar, ranging or CDMA, this is unusable for the multichannel AcR as we have seen in Section 4.5.

Section 4.3.3 has shown that the values of ACF and CCF of a set of signals are bounded. One can not arbitrarily choose them *simultaneously* and *independently*. However it is possible to make one property "better" by making the other one worse, depending on the definition of the criterion. Thus it could be possible to formulate an optimization problem for the problem of an IR-like signaling set for this multichannel AcR. It is questionable though if a scheme can be found that outperforms the OFDM scheme which has the additional benefit of being a tried and tested scheme with a possible low-complex implementation.

5 Conclusion and Outlook

An analysis of a multichannel autocorrelation receiver (AcR) is presented in this thesis. This section provides a short summary of the most important outcomes of this analysis together with an outlook regarding possible future work on this topic.

Conclusion

In its original conception the multichannel AcR works with an UWB-OFDM signaling scheme. The nonlinear operation of the multichannel AcR on the multichannel received signal leads to crossterms between signal and noise and between the subchannel signals themselves. It has been shown that the latter terms can largely be avoided for the OFDM scheme which allows for a considerable number of subchannels to be used and, therefore, an increased data rate. To this end, simulations of the BER-performance of the AcR with various parameter settings have been presented which have also shown the influence of the several groups of crossterms.

OFDM with subcarriers at ultra-wide bandwidth was found to be the most suitable signaling scheme for the multichannel autocorrelation receiver regarding BER performance and robustness with respect to the multipath channel.

The reason for this is the very low level of the mutual crosscorrelation functions (CCF) of the OFDM subchannel signals which is due to their separation in the frequency domain. No deterioration of the BER-performance due to their presence was observed, which is a remarkable result concerning the number of CCF-induced crossterms that is roughly the square of the number of information-carrying terms. Furthermore an OFDM signal can be separated with a predefined DFT backend scheme that does not require any channel state information.

Every signaling scheme that is taken into consideration for this receiver is required to have very low mutual crosscorrelations at least at the receivers delay lags.

It has been shown through examples that the violation of this condition leads to a dominance of the CCF-induced crossterms even for a moderate number of channels. To this end a signal-to-interference ratio (SIR) has been defined for the subchannel signals after the receiver frontend and for the decision variables. Alternative signaling schemes have been introduced that do not rely on frequency separation of their subchannels.

Alternative signaling schemes can improve the invertibility of the problem to some extent but they do not achieve the performance of the OFDM signaling scheme.

Several measures of the problem invertibility have been defined. In general the OFDM scheme performs very well in terms of all these measures while alternative signaling schemes can provide some good individual measures but are not optimal for all the measures described.

In addition to the non-ideal correlation properties, practical considerations such as the pulse length also limit the use of the alternative schemes.

Fulfilling the conditions that apply for the signaling scheme is increasingly difficult when considering practically usable waveforms that are only of short duration. Longer pulses are needed for achieving certain correlation properties while the OFDM scheme inherently provides a good orthogonalization of the channel matrix.

Outlook

The UWB-OFDM scheme together with the multichannel AcR is a promising candidate scheme for channel-robust communication also at high data rates as has been shown by the performance simulations. Some simplifying assumptions made in these simulations motivate further research on this topic.

The effects of non-perfect knowledge of the channel matrix should be further analyzed.

In practice we will not be able to perfectly estimate the channel matrix. As the best-performing backend schemes rely on such knowledge, estimation techniques should be surveyed and their effects on the receiver performance should be analyzed.

A further analysis of the effects of orthogonality loss by a time-varying channel imposing a Doppler spread is necessary.

The orthogonality loss imposed by a linear multipath channel was stated to be not severe in this thesis. However an analysis should be done also for time-varying channels which could impair the OFDM scheme by frequency shifts. Such an additional loss of orthogonality might raise the CCF-induced crossterms.

The design and implementation of UWB delay lines is still a challenging task.

Integrated circuitry for delay lines working at ultra-wide bandwidth is necessary to be able to realize a low-cost low-power receiver. As we can not expect perfect performance from such circuits, an analysis including the tolerance of such parts might be useful to observe possible degradations in the performance of a practical receiver.

As correlation properties can in principle be carried over from binary codes to continuous-time signals, further optimization of these codes might be worthwhile.

Although the widely used binary codes from CDMA systems can not be used directly with this receiver, the design of a set of sequences with certain correlation properties might be possible. Such a set of sequences can in principle be used as the basis of signaling waveforms.

A Appendix - Additional simulation results

A.1 Simulation results for the Invertibility Measures

Figure A.1 shows simulation results for the invertibility measures defined in section 3.3.1 for the OFDM scheme at $BW_{sc} = 0.5$ GHz, $N = 9$, $L = 10$ and an NLOS channel. In general the conditioning of $\mathbf{H}$ is very good with a few outliers. We neither have the case of a rank deficiency nor a really ill-posed case with one very small singular value.

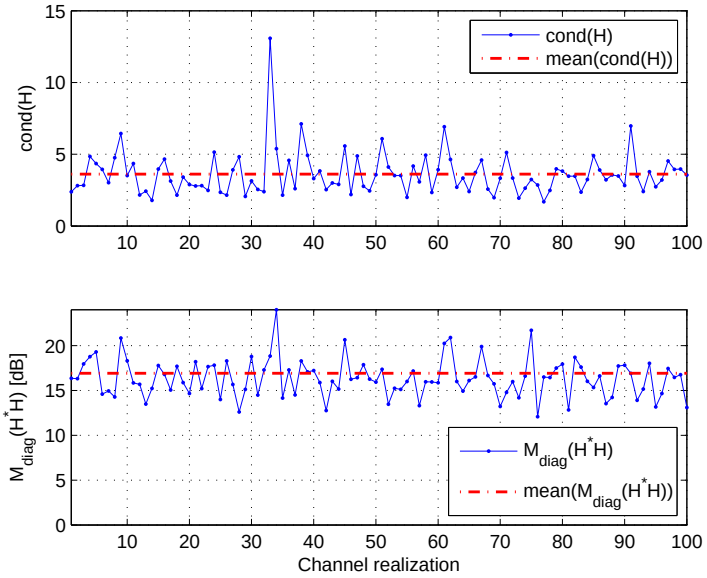

Figure A.1: Measures for the MIMO problem invertibility for the OFDM scheme at $BW_{sc} = 0.5$ GHz and $N = 9$ over 100 channel realizations

Figure A.2 shows the results of the same simulations for the genetically optimized scheme with $N = 5$ and an LOS channel. Interestingly the mean condition number is lower than for the OFDM scheme which is partly due to the LOS channel and the specifically designed ACFs. The diagonality of $\mathbf{H}^*\mathbf{H}$ however is significantly lower than for OFDM which was generally observed to be a big benefit of the OFDM signaling scheme. As it has been discussed in section 3.3.1 this measure can be understood as the degree of distinguishability of the subchannels ACFs.

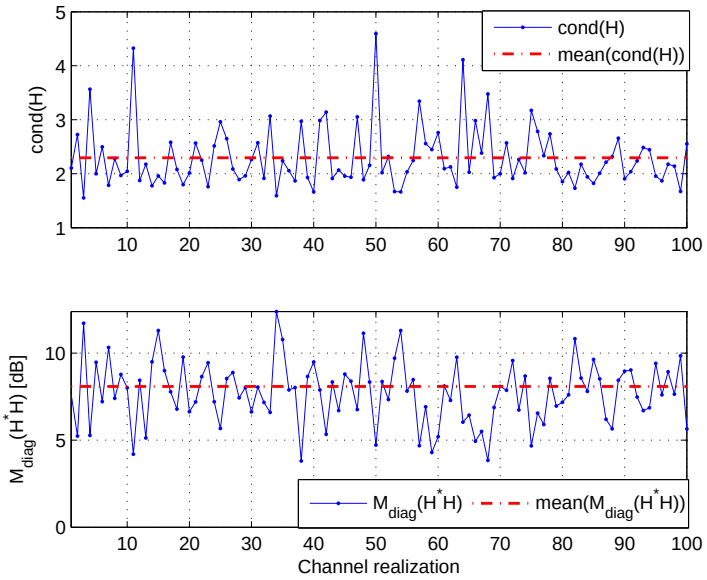

Figure A.2: Measures for the MIMO problem invertibility for the genetically optimized scheme at $BW = 4$ GHz and $N = 5$ over 100 channel realizations

A.2 Influence of the Invertibility Measure on the Performance

Figure A.3 shows the influence of the invertibility measure, here the channel matrix condition number on the receiver performance. We see that for the best conditioned channel realization, the DFT backend almost reaches the PIC bound which is clearly not the case on average. For an increasingly ill-conditioned channel also the PIC bound has an error floor which might be due to the fact that $\mathbf{H}^*\mathbf{H}$ is ill-conditioned and has one almost zero diagonal entry. Not shown are ZF and MMSE backend as they nearly always perform between DFT and PIC.

All in all the simulation results of all the schemes that work in principle (OFDM, Noise and genetically optimized sequences) have shown significant correlations of the invertibility measures according to the channel realization and the respective BER that could be achieved at a certain E_b/N_0. This correlation was highest for the OFDM scheme but was also observable for the other schemes mentioned. This confirms the usability of these measures to quantify the problem invertibility for this receiver. It has to be mentioned that for the alternative schemes often the influence of the degraded SIR caused by the non-ideal CCF-properties was more significant than that of the invertibility measures.

A.3 Channel Influence on the Orthogonality

Figure A.4 shows the influence of the simulated linear multipath channel on two of the the per-symbol orthogonality measures which were defined in section 3.3.2. Shown is the mean

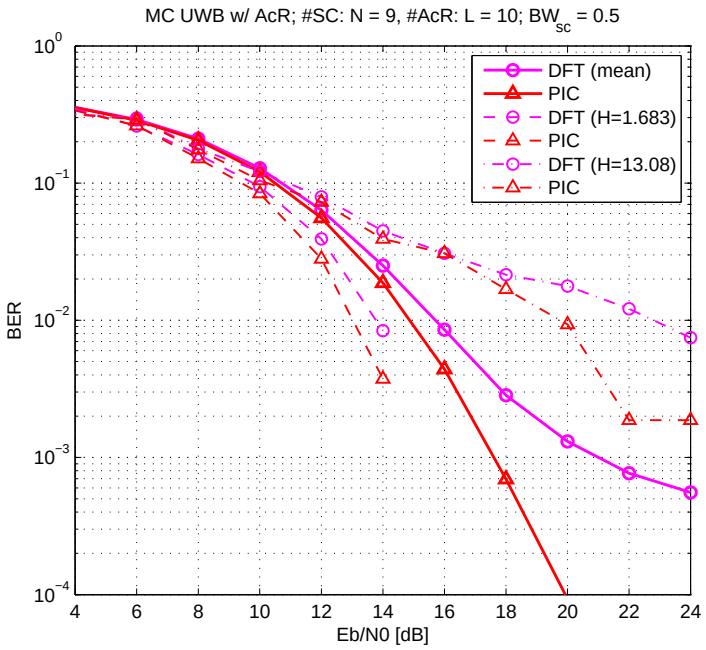

Figure A.3: BER performance for the scenario from section 3.4 with high bandwidth, $N = 9$ and $L = 10$; Shown is the mean BER over all simulations and the BERs for the best and worst conditioned channels for DFT and PIC Backend

absolute cosine of the signals angle ($M_{orth,3}$) and the maximum of the cosine of the angle ($M_{orth,5}$). The scenario is the nine-channel OFDM scheme with 500-MHz-wide subcarriers and an NLOS channel. It is shown that the linear channel does not cause a significant loss of the subchannel orthogonality. The small deviation from zero in the orthogonality at the transmitter is caused by the pulse shaping filter.

Figure A.4 shows the same for the nine channel OFDM scenario at a subcarrier bandwidth of 100 MHz. The orthogonality measure at the transmitter is at about the same level as for the higher bandwidth scheme. It is shown that the orthogonality loss is significantly higher due to the lower bandwidth which is an additional reason for the worse performance of the lower bandwidth scheme.

We see that the channel causes the signal orthogonality to degrade but the resulting orthogonality loss is not severe. It is important to note here that in the multipath channel simulation the channel is modeled as linear and time-invariant. Simulations where a very weak nonlinear transfer function was added to the channel simulation showed a more severe loss of orthogonality. Linearity of the channel will be important for the OFDM signaling scheme, just like in conventional OFDM systems. Nonlinearity causes intermodulation products between the subcarriers and additional loss of orthogonality due to inter-carrier-interference [PS08].

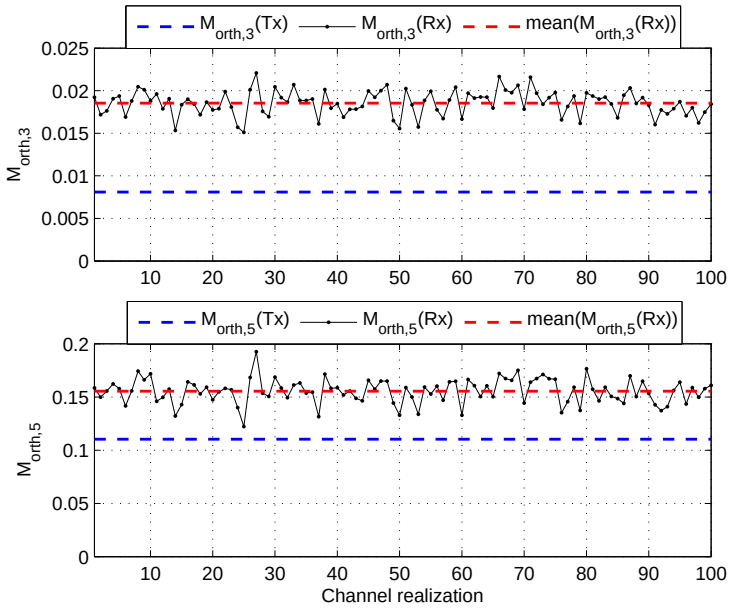

Figure A.4: Orthogonality measure $M_{orth,3}$ at Tx and Rx (top) and $M_{orth,5}$ at Tx and Rx (bottom) for OFDM at $BW_{sc} = 0.5$ GHz and $N = 9$ over 100 channel realizations

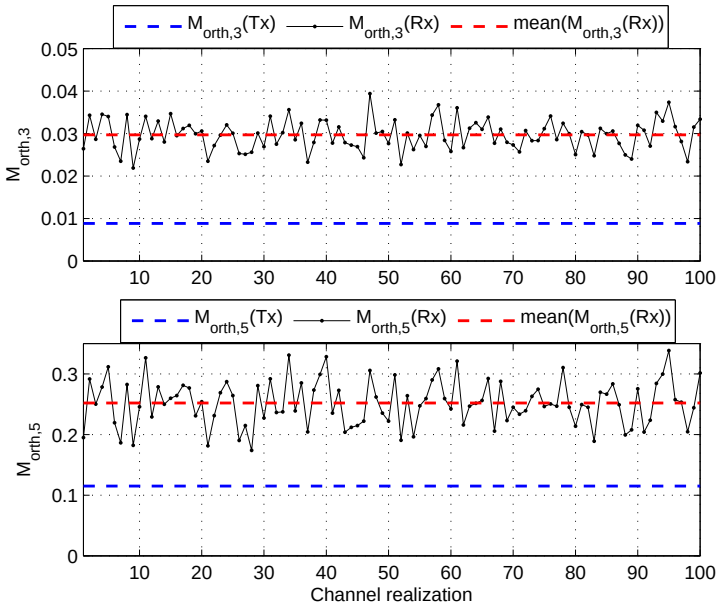

Figure A.5: Orthogonality measure $M_{orth,3}$ at Tx and Rx (top) and $M_{orth,5}$ at Tx and Rx (bottom) for OFDM at $BW_{sc} = 0.1$ GHz and $N = 9$ over 100 channel realizations

A.4 Simulations of the SIR and SIR gain

Figure A.6 shows the mean SIR(D_l) (averaged over D_l) together with the mean SIR(z_i) (averaged over z_i) for the DFT, the ZF and the MMSE backends for OFDM and the scenario with $N = 9$ subcarriers and a subcarrier bandwidth of 500 MHz. The SIR at the decision device is almost always higher than at the delay lags for all backend schemes. This means that not only none of the backends boosts the crosscorrelation-induced interference terms, they are even further suppressed or the useful signal energy is boosted more than that of the interference terms.

Figure A.7 shows a comparison of the SIR(D_l) (averaged over D_l) and mean SIR(z_i) (averaged over z_i) for the MMSE backend and the scenarios with $N = 3$ from the 500 MHz OFDM scheme, the per-channel-reference noise scheme and the genetically optimized scheme. It shows that the enhancement of the SIR by the backend processing is unique to the OFDM signaling scheme. Furthermore, only the genetically optimized sequences have a mean SIR(D_l) similar to the corresponding OFDM scheme but since only the MMSE backend for the OFDM scheme can increase this SIR, OFDM is superior to the genetically optimized sequences. This is also a special case, since for higher numbers of channels the OFDM scheme always has a clearly greater SIR(D_l) than any other scheme.

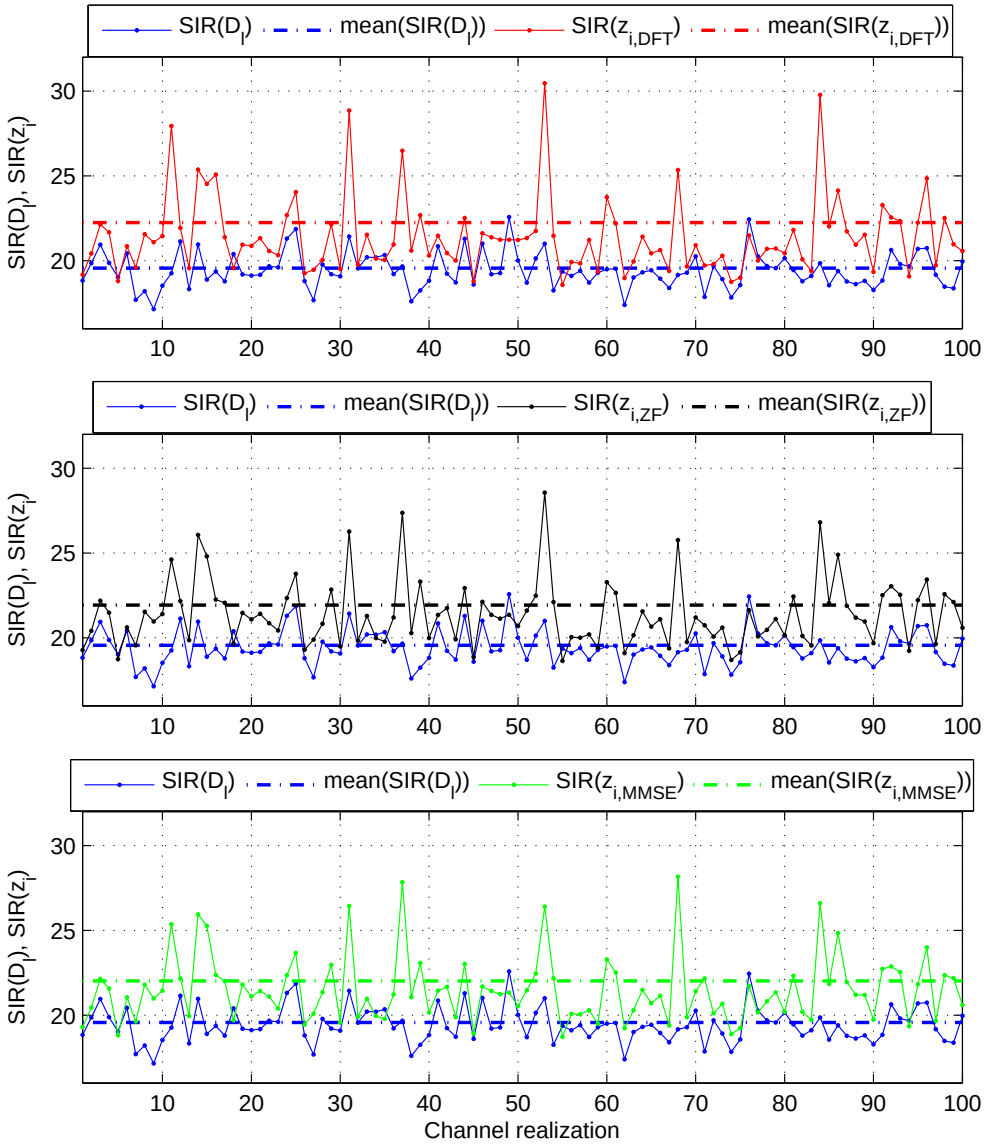

Figure A.6: Mean SIR at the AcR frontend and after the combiner for the OFDM scheme at $BW_{sc} = 0.5$ GHz and $N = 9$ over 100 channel realizations. Shown are the DFT- (top), the ZF- (middle) and MMSE-backends (bottom).

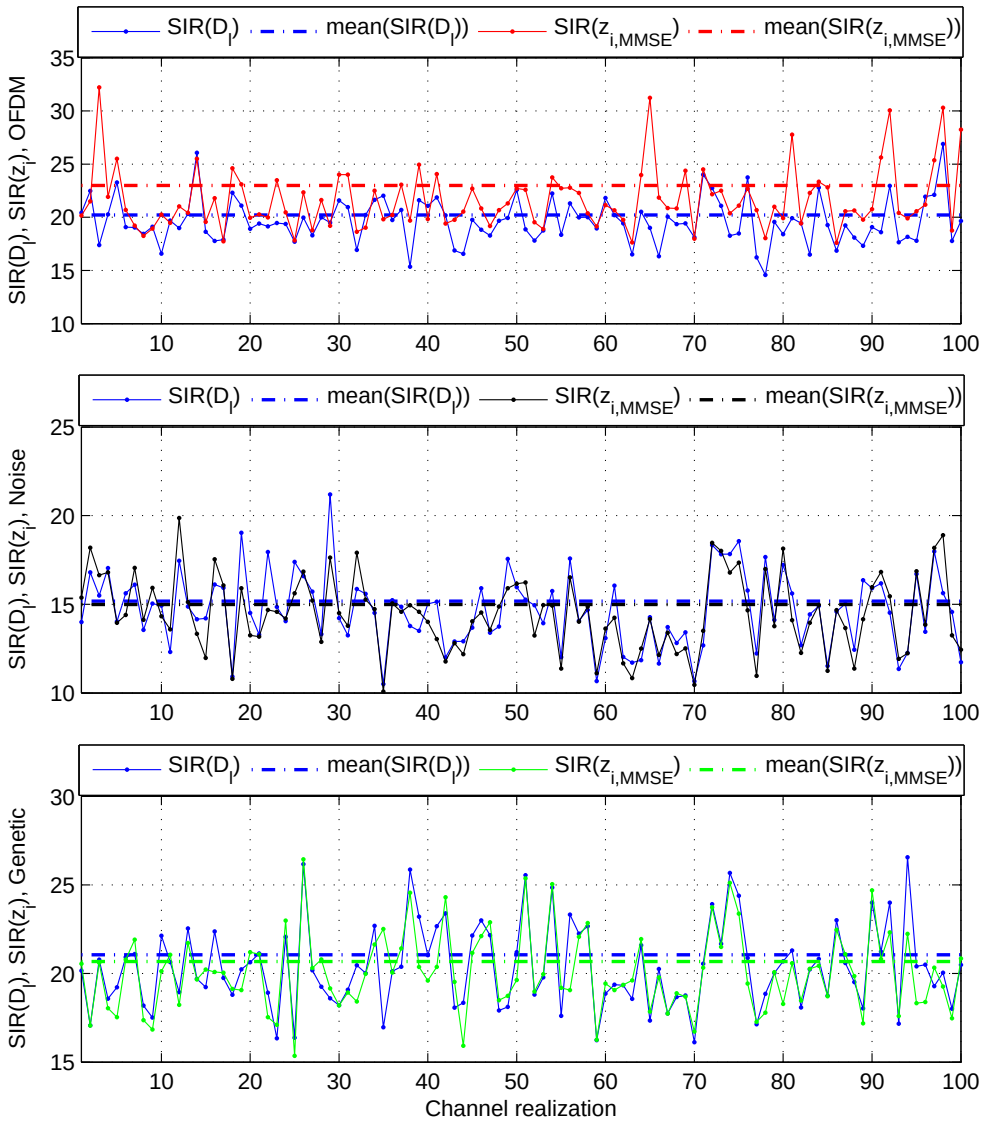

Figure A.7: Mean SIR at the AcR frontend and after the combiner for the $N = 3$ scenarios of OFDM (top), per-channel reference Noise scheme (center) and genetically optimized scheme (bottom).

Bibliography

[AW07] Y. D. Alemseged and K. Witrisal. Modeling and mitigation of narrowband interference for transmitted-reference uwb systems. *IEEE Journal of Selected Topics in Signal Processing*, 1(3):456–469, Oct. 2007.

[BBA+04] A. Batra, J. Balakrishnan, G. R. Aiello, J. R. Foerster, and A. Dabak. Design of a multiband OFDM system for realistic UWB channel environments. *IEEE Transactions on Microwave Theory and Techniques*, 52(9):2123–2138, Sept. 2004.

[BEM08] U. Baumgartner, T. Ebner, and C. Magele. Optimization in electrical engineering. Lecture Notes for Numerical Optimization, Graz University of Technology., 2008.

[BHS+05] S. Bagga, S. A. P. Haddad, W. A. Serdijn, J. R. Long, and E. B. Busking. A delay filter for an ir-UWB front-end. In *Proc. IEEE International Conference on Ultra-Wideband ICU 2005*, pages 323–327, Sept. 2005.

[BLM04] J. R. Barry, E. A. Lee, and D. G. Messerschmitt. *Digital Communication*. Kluwer Academic Publishing, Third edition, 2004.

[Boy08] S. Boyd. Lecture Notes for EE263 (Introduction to linear dynamical Systems). Stanford University, 2008.

[Bra07] B. Brandstaetter. Inverse Problems, Ill-posedness and regularization - an illustrative example. *Elektrotechnik und Informationstechnik*, 124/7/8:224–231, 2007.

[BSMM00] I. N. Bronstein, K. A. Semendjajew, G. Musiol, and H. Muehlig. *Taschenbuch der Mathematik*. Verlag Harri Deutsch, Fifth edition, 2000. (in German).

[CMR05] M. Cinteza, I. Marghescu, and T. Radulescu. Design of PN Sequence Families with Bounded Correlation Properties, Using Genetic Algorithms. In *Proc. EUROCON 2005.The International Conference on Computer as a Tool*, volume 2, pages 1818–1821, Nov. 2005.

[Dix76] R. C. Dixon. *Spread Spectrum Systems*. Wiley Interscience, 1976.

[DJ98] E. H. Dinan and B. Jabbari. Spreading codes for direct sequence CDMA and wideband CDMA cellular networks. *IEEE Communications Magazine*, 36(9):48–54, Sept. 1998.

[DO99] H. Donelan and T. O'Farrell. A new Method for generating Sets of Orthogonal Sequences for a Synchronous CDMA System. *Lecture Notes in Computer Science, Springer Berlin / Heidelberg*, 1746/1999:799, 1999.

[FCC02] FCC. Revision of part 15 of the commission's rules regarding ultra-wideband transmission systems. First Report and Order ET-Docket 98-153, FCC 02-48, Federal Communications Commission, Feb. 2002.

[GH94] D. M. Gruenbacher and D. R. Hummels. A simple algorithm for generating Discrete Prolate Spheroidal Sequences. *IEEE Transactions on Signal Processing*, 42(11):3276–3278, Nov. 1994.

[Gia03] G. B. Giannakis. Ultra-wideband communications: An idea whose time has come. In *Proc. IEEE International Conference on Acoustics, Speech, and Signal Processing (ICASSP 2003)*, volume 1, pages I–3, 6–10 April 2003.

[Goi98] A. J. Goiser. *Handbuch der Spread-Spectrum Technik*. Springer Wien New York, 1998. (in German).

[Gol67] R. Gold. Optimal binary sequences for spread spectrum multiplexing (Corresp.). *IEEE Transactions on Information Theory*, 13(4):619–621, Oct. 1967.

[Hol75] J. H. Holland. *Adaption in Natural and Artificial Systems*. Ann Arbor: University of Michigan Press, 1975.

[HT02] R. Hoctor and H. Tomlinson. Delay-hopped transmitted-reference RF communications. In *Proc. Digest of Papers Ultra Wideband Systems and Technologies 2002 IEEE Conference on*, pages 265–269, 21–23 May 2002.

[HW06] W. Hirt and M. Weisenhorn. Overview and Implications of the Emerging Global UWB Radio Regulatory Framework. In *Proc. IEEE 2006 International Conference on Ultra-Wideband*, pages 581–586, 24–27 Sept. 2006.

[IEE07] IEEE. 802.15.4a-2007 (Amendment 1), 802.15.4: Wireless Medium Access Control (MAC) and Physical Layer (PHY) Specifications for Low-Rate Wireless PANs, 2007.

[Kas66] T. Kasami. Weight Distribution Formula for Some Class of Cyclic Codes. Technical Report R-285, Coordinated Science Lab, Univ. IL, Urbana, April 1966.

[Kay93] S. Kay. *Fundamentals of Statistical Signal Processing: Estimation Theory*. Prentice Hall Signal Processing Series, 1993.

[Kay98] S. Kay. *Fundamentals of Statistical Signal Processing: Detection Theory*. Prentice Hall Signal Processing Series, 1998.

[Mol05] A. F. Molisch. Ultrawideband propagation channels-theory, measurement, and modeling. *IEEE Transactions on Vehicular Technology*, 54(5):1528–1545, Sept. 2005.

[Mol06] A. F. Molisch. *Wireless Communications*. John Wiley and Sons, 2006.

[ND03] F. Nekoogar and F. Dowla. Performance of multiple pulse multiple delay modulated UWB signals in a multiple access indoor wireless channel. In *Proc. PACRIM Communications, Computers and signal Processing 2003*, volume 2, pages 545–548, Aug. 2003.

[OSB98] A. V. Oppenheim, R. W. Schafer, and J. R. Buck. *Discrete-Time Signal Processing*. New Jersey, USA: Prentice-Hall, Second edition, 1998.

[PAU04] S. Paquelet, L. M. Aubert, and B. Uguen. An impulse radio asynchronous transceiver for high data rates. In *International Workshop on UWB Systems joint with Conf. UWB Syst. and Techn., UWBST & IWUWBS, Kyoto, Japan*, pages 1–5, May 2004.

[Pau07] M. Pausini. *Autocorrelation Receivers for Ultra Wideband Wireless Communications*. PhD thesis, Delft University of Technology, 2007.

[PS08] J. G. Proakis and M. Salehi. *Digital Communications*. McGraw-Hill, Fifth edition, 2008.

[PSB04] J. G. Proakis, M. Salehi, and G. Bauch. *Contemporary Communication Systems using MATLAB* ©. Bookware Companion Series, Second edition, 2004.

[SA05] M. K. Simon and M.-S. Alouini. *Digital Communication over Fading Channels*. Wiley Series in Telecommunications and Signal Processing, Second edition, 2005.

[Sap64] L. Saporta. A Lower Bound on the Cross Correlation Between Signals of Prescribed Energy. *IEEE Transactions on Communications Systems*, 12(2):251–251, June 1964.

[Sar79] D. Sarwate. Bounds on crosscorrelation and autocorrelation of sequences (Corresp.). *IEEE Transactions on Information Theory*, 25(6):720–724, Nov 1979.

[Sle78] D. Slepian. Prolate Spheroidal Wave Functions, Fourier Analysis and Uncertainty - V: The discrete case. *Bell Systems Technical Journal*, 57:1317–1430, 1978.

[SP61] D. Slepian and H. O. Pollak. Prolate Spheroidal Wave Functions, Fourier Analysis and Uncertainty - I. *Bell Systems Technical Journal*, 40:43–64, 1961.

[SP80] D. Sarwate and M. B. Pursley. Crosscorrelation properties of pseudorandom and related sequences. *Proceedings of the IEEE*, 68(5):593–619, May 1980.

[UZN04] K. Usuda, Honggang Zhang, and M. Nakagawa. M-ary pulse shape modulation for PSWF-based UWB systems in multipath fading environment. In *Proc. IEEE Global Telecommunications Conference GLOBECOM '04*, volume 6, pages 3498–3504, 29 Nov.–3 Dec. 2004.

[Wel74] L. Welch. Lower bounds on the maximum cross correlation of signals (Corresp.). *IEEE Transactions on Information Theory*, 20(3):397–399, May 1974.

[Wit08a] K. Witrisal. A Noncoherent Multiband Receiver for IEEE802.15.4a UWB Signals. In *Proc. COST 2100 Management Committee Meeting, Trondheim, Norway*, 2008.

[Wit08b] K. Witrisal. A Tutorial on Noncoherent UWB Systems. Ch. 1 in Proc. Design and Analysis of Noncoherent UWB Transceivers, Habilitation Thesis, Graz University of Technology, Sep. 2008.

[Wit08c] K. Witrisal. Noncoherent autocorrelation detection of orthogonal multicarrier UWB signals. In *Proc. IEEE International Conference on Ultra-Wideband ICUWB 2008*, volume 2, pages 161–164, 10–12 Sept. 2008.

[WP05] K. Witrisal and M. Pausini. Impact of multipath propagation on impulse radio UWB autocorrelation receivers. In *Proc. IEEE International Conference on Ultra-Wideband ICU 2005*, pages 485–490, 5–8 Sept. 2005.

[WP08] K. Witrisal and M. Pausini. Statistical Analysis of UWB Channel Correlation Functions. *IEEE Transactions on Vehicular Technology*, 57(3):1359–1373, May 2008.

[WS98] M. Z. Win and R. A. Scholtz. Impulse radio: How it works. *IEEE Communications Letters*, 2(2):36–38, Feb. 1998.

[ZM05] T. Zemen and C. F. Mecklenbrauker. Time-Variant Channel Estimation Using Discrete Prolate Spheroidal Sequences. *IEEE Transactions on Signal Processing*, 53(9):3597–3607, 2005.

[ZSH06] L. Zhou, A. Safarian, and P. Heydari. CMOS wideband analogue delay stage. *Electronics Letters*, 42(21):1213–1214, Oct. 2006.